



Technische Universität München
TUM School of Medicine and Health

**Inhibition of SARS-CoV-2 infection by vaccine-induced antibodies and
small-interfering RNAs**

Cho-Chin Cheng

Vollständiger Abdruck der von der TUM School of Medicine and Health der
Technischen Universität München zur Erlangung des akademischen Grades eines

Doctor of Philosophy (Ph.D.)

genehmigten Dissertation.

Vorsitzende: Prof. Dr. Agnes Görlach

Betreuerin: Prof. Dr. Ulrike Protzer

Prüfer*innen der Dissertation:

1. Prof. Dr. Radu Roland Rad
2. Priv.-Doz. Dr. Ursula Ehmer
3. Prof. Dr. Oliver T. Keppler

Die Dissertation wurde am 24.07.2023 bei der Technischen Universität München eingereicht
und durch die TUM School of Medicine and Health am 16.10.2023 angenommen.

Table of contents

Abstract	6
Zusammenfassung	8
1 Introduction	10
1.1 Severe acute respiratory syndrome coronavirus 2	10
1.1.1 Structure and the replication cycle of SARS-CoV-2.....	10
1.1.1.1 Structure of viral particles	10
1.1.1.2 Genome organization of SARS-CoV-2	10
1.1.1.3 Viral life cycle	12
1.1.2 SARS-CoV-2 pathogenesis and clinical features	13
1.1.2.1 Major infection route and symptoms	13
1.1.2.2 SARS-CoV-2 multi-organ tropism and manifestation	14
1.1.2.3 Long COVID.....	15
1.1.3 Evolution of SARS-CoV-2.....	16
1.2 Epidemiology of SARS-CoV-2.....	18
1.2.1 The unfolding and development of the pandemic.....	18
1.2.2 SARS-CoV-2 transmission.....	19
1.2.3 Diagnostics for SARS-CoV-2 infections.....	19
1.2.3.1 Swab test for diagnosing active infections.....	19
1.2.3.2 Serological antibody test for monitoring infected individuals....	20
1.3 Prophylaxis and therapeutics against SARS-CoV-2	20
1.3.1 Prophylaxis strategies for COVID-19.....	21
1.3.1.1 Restrictions for preventing virus spread	21
1.3.1.2 Prophylactic vaccinations development.....	21
1.3.2 Therapeutics for SARS-CoV-2 infection	23

1.3.2.1 Antiviral drugs: chemical compounds and monoclonal antibodies	23
1.3.2.2 Immunomodulators	24
1.4 Aim of the work	24
2 Materials and Methods	26
2.1 Materials.....	26
2.1.1 Devices and technical equipment.....	26
2.1.2 Consumables	26
2.1.3 Chemicals and reagents.....	26
2.1.4 Enzymes	28
2.1.5 Virus	28
2.1.6 Kits	28
2.1.7 Cell lines, tissues, and bacteria	28
2.1.8 Antibodies	29
2.1.9 Primers	29
2.1.10 Plasmids	29
2.1.11 Software	29
2.2 Methods.....	30
2.2.1 Serological study design and sample characteristics	30
2.2.2 Cell and tissue culture	31
2.2.3 SARS-CoV-2 isolation and propagation	31
2.2.4 SARS-CoV-2 infection.....	32
2.2.5 Plaque assay	32
2.2.6 Real-virus neutralization assay	32
2.2.7 Nucleic Acid extraction and qPCR	33
2.2.8 Real-time live-cell imaging of SARS-CoV-2 infected cells	34

2.2.9 Antibody response using surrogate virus neutralization assay.....	34
3 Results	35
3.1 Dynamics of humoral and cellular immune responses after homologous and heterologous SARS-CoV-2 vaccination with ChAdOx1 nCoV-19 and BNT162b2	35
3.1.1 Authors	35
3.1.2 Short Summary.....	35
3.1.3 Contributions.....	36
3.2 Improved SARS-CoV-2 Neutralization of Delta and Omicron BA.1 Variants of Concern after Fourth Vaccination in Hemodialysis Patients.....	37
3.2.1 Authors	37
3.2.2 Short Summary and Contributions.....	37
3.2.3 Contributions.....	38
3.3 Targeting genomic SARS-CoV-2 RNA with siRNAs allows efficient inhibition of viral replication and spread.....	39
3.3.1 Authors	39
3.3.2 Short Summary and Contributions.....	39
3.3.3 Contributions.....	40
4 Discussion.....	41
4.1 Serological examination of the SARS-CoV-2 vaccinated population	41
4.2 Inhibition of SARS-CoV-2 replication by siRNA machinery	42
5 Bibliography	45
List of publications.....	53
Appendix – Reprint Permissions	55
Acknowledgements.....	56

Abstract

The severe acute respiratory syndrome coronavirus 2 (SARS-CoV-2) pandemic struck the globe without a warning at the beginning of the year 2020 and lasted for more than three years, infecting more than 750 million people and causing approximately 7 million deaths worldwide to date. The pandemic also had severe consequences on world-wide trade, economy and travel. Availability of vaccines rapidly changed this situation but optimal vaccination schemes, the characteristics of the immune response induced and its durability were unknown. With the availability of a well-established biosafety level 3 (BSL3) laboratory, our institute followed-up a prospective cohort of health-care workers and a cohort of patients with severe kidney diseases to help understanding vaccine-induced immunity. In addition, we started investigating RNA interference as a novel antiviral approach against SARS-CoV-2. This cumulative thesis contains three articles that demonstrate our findings in two dimensions.

In the first aim of our study, we focused on human immunology research, which included the examination of the humoral and cellular immunity of convalescents recovered from and individuals vaccinated against Coronavirus Disease 2019 (COVID-19) in peripheral blood.

In the first article, we investigated the dynamics of immune responses following homologous and heterologous SARS-CoV-2 vaccination with ChAdOx1 nCoV-19 and BNT162b2. I studied the neutralizing antibody response against different SARS-CoV-2 variants. The study identified that a heterologous prime-boost vaccination schedule with ChAdOx1 nCoV-19 followed by BNT162b2 or vice versa led to superior humoral and cellular immune responses than homologous vaccination, which has important implications for optimizing COVID-19 vaccination strategies. Nonetheless, I found that that humoral immunity waned significantly after vaccination, regardless of the regimen, whereas all vaccination regimens induced stable, polyfunctional T-cell responses.

In the second article we examined the immune response of hemodialysis patients to SARS-CoV-2 vaccination - with the majority receiving mRNA vaccines only - focusing specifically on the efficacy of the vaccines against the Delta and Omicron BA.1 variants of concern. I could show that a fourth dose of the COVID-19 vaccine significantly boosted the level of neutralizing antibodies in hemodialysis patients, resulting in enhanced neutralization of both the Delta and Omicron BA.1 variants of concern, according to our data. The study indicates that a fourth dose of an mRNA vaccine may be an effective strategy for enhancing the immune response of susceptible populations, such

as hemodialysis patients, against emerging SARS-CoV-2 variants.

Our second objective was to develop a novel SARS-CoV-2 treatment based on small interfering (si)RNA. siRNAs are promising antivirals, but the optimal targets for siRNA-mediated inhibition of SARS-CoV-2 replication were not well understood. In a study using infectious SARS-CoV-2, we systematically investigated the individual replication steps of the virus following cell entry in order to ascertain the efficacy of prophylactic siRNA administration. My results indicate that siRNAs targeting only genomic RNA (gRNA) can effectively inhibit viral replication at an early stage and prevent virus-induced cell death. Furthermore, siRNAs targeting common regions located in both gRNA and subgenomic RNA (sgRNA) showed reduced RNAi silencing due to a competition with the highly abundant sgRNAs. This study demonstrated the potential of siRNAs for preventing the replication and spread of SARS-CoV-2 and shed light on the molecular mechanisms of the virus's replication strategy.

Zusammenfassung

Die Pandemie des schweren akuten respiratorischen Syndroms Coronavirus 2 (SARS-CoV-2) brach Anfang 2020 ohne Vorwarnung über den Globus herein, hielt mehr als drei Jahre lang an, infizierte mehr als 750 Millionen Menschen und verursachte bis heute etwa 7 Millionen Todesfälle weltweit. Die Pandemie hatte wesentliche Konsequenzen für die Weltwirtschaft, sowie für Handel und Reisetätigkeiten weltweit. Die Verfügbarkeit wirksamer Impfstoffe veränderte die Situation deutlich, aber die optimalen Impfschemata sowie Charakteristika und Beständigkeit der induzierten Immunantwort waren nicht bekannt.

Da unser Institut über ein gut etabliertes Labor der Biosicherheitsstufe 3 (BSL3) verfügt, konnten wir eine zwei wichtige Kohorten prospektiv untersuchen, eine Kohorte mit Krankenhaus-Mitarbeitern und eine mit Patienten mit terminalen Nierenerkrankungen, und dadurch zum Verständnis der impfinduzierten Immunität beitragen. Zudem habe ich das Potential von „small interfering RNAs“ (siRNAs) als antiviraler Therapieansatz gegen das SARS-CoV-2 untersucht. Diese kumulative Doktor-Arbeit enthält drei Artikel, die unsere Ergebnisse in diesen beiden Bereichen aufzeigen.

Der erste Teil meiner Arbeit konzentrierte sich auf die Forschung im Bereich der Human-Immunologie, und untersuchten die neutralisierende Antikörper-Antwort von Rekonvaleszenten, die von der Coronavirus-Krankheit 2019 (COVID-19) genesen waren, sowie von geimpften Personen, gegen SARS-CoV-2.

Im ersten Artikel wurde die Dynamik der Immunantwort nach homologer und heterologer SARS-CoV-2-Impfung mit ChAdOx1 nCoV-19 und BNT162b2 untersucht. Die Studie ergab, dass eine heterologe Prime-Boost-Impfung mit ChAdOx1 nCoV-19 gefolgt von BNT162b2 oder umgekehrt zu einer besseren humoralen und zellulären Immunantwort führte als eine homologe Impfung. Das hatte wichtige Auswirkungen auf die Optimierung von COVID-19-Impfstrategien. Dennoch ist es wichtig darauf hinzuweisen, dass die humorale Immunität nach der Impfung unabhängig vom Impfschema deutlich abnahm, während alle Impfschemata stabile, polyfunktionale T-Zell-Antworten induzierten.

Im zweiten Artikel untersuchten wir die Immunantwort von Hämodialyse-Patienten auf die SARS-CoV-2-Impfung – wobei die meisten der Patienten nur mRNA-Impfstoffe erhielten – und konzentrierten uns dabei speziell auf die Wirksamkeit der Impfstoffe gegen die bedenklichen Varianten Delta und Omicron BA.1. Laut meinen Daten steigerte die vierte Dosis eines mRNA-Impfstoffs den Gehalt an neutralisierenden Antikörpern bei Hämodialyse-Patienten erheblich, was zu einer verstärkten Neutralisierung sowohl der

Delta- als auch der Omicron-BA.1-Variante führte. Die Studie deutet darauf hin, dass eine vierte Dosis des Impfstoffs eine wirksame Strategie zur Verstärkung der Immunreaktion anfälliger Bevölkerungsgruppen, wie z. B. von Hämodialyse-Patienten, gegen neu auftretende SARS-CoV-2-Varianten ist.

Unser zweites Ziel war die Entwicklung neuer SARS-CoV-2-Behandlungen. Als antivirale Therapie für SARS-CoV-2 sind siRNAs vielversprechend, aber die optimalen Konditionen für die siRNA-vermittelte Hemmung der viralen Replikation waren nicht gut bekannt. In dieser Studie haben wir die einzelnen Replikationsschritte von SARS-CoV-2 nach dem Zelleintritt systematisch untersucht, um die Wirksamkeit einer prophylaktischen siRNA-Gabe zu ermitteln. Meine Ergebnisse deuten darauf hin, dass siRNAs, die nur auf genomische RNA (gRNA) abzielen, die virale Replikation in einem frühen Stadium wirksam hemmen und den virusinduzierten Zelltod verhindern können. Dahingegen zeigten siRNAs, die sowohl auf gRNA als auch auf subgenomische RNA (sgRNA) abzielen, ein vermindertes antivirales Potential aufgrund der Konkurrenz mit den im Überschuss vorhandenen sgRNAs. Diese Studie zeigt das Potenzial von kleinen interferierenden RNAs (siRNAs) als Strategie zur Verhinderung der Replikation und Ausbreitung von SARS-CoV-2 auf und wirft ein Licht auf die molekularen Mechanismen der Virusreplikation.

1 Introduction

1.1 Severe acute respiratory syndrome coronavirus 2

Severe acute respiratory syndrome coronavirus 2, widely known as SARS-CoV-2, was first found in December of 2019 and caused an unprecedented worldwide pandemic from asymptomatic infection to severe respiratory illness termed "Coronavirus Disease 2019 (COVID-19)". The outbreak has had far-reaching and long-lasting impacts on the global economy, social patterns, and even work formats, and it does not appear to be over after three years. This chapter will elucidate the biology of SARS-CoV-2. This includes the molecular biology and replication cycle of the virus, how the virus causes disease, and the evolution of various circulating variants.

1.1.1 Structure and the replication cycle of SARS-CoV-2

1.1.1.1 Structure of viral particles

SARS-CoV-2, an emerging species in the family of *Coronaviridae* known as one of the largest RNA viruses, is an enveloped single-stranded, positive-sense RNA virus with a genome size of around 30 kilobase pairs (kbs) [1, 2]. The infectious virions are 60 nm to 140 nm in diameter and were described under electron microscopy as round or oval profiles with a crown-like surface, after which the virus was named [3]. The viral structure can be divided into two main components: the genetic material and the viral envelope. The crown-like structure is composed of viral spike glycoprotein (S), which embeds in the host membrane-derived lipid bilayer together with membrane glycoprotein (M) and envelope protein (E) constituting the viral envelope. Inside the envelope located the genetic material, the viral RNA genome is enfolded by a long helical nucleocapsid built up with nucleocapsid protein (N) [4, 5].

1.1.1.2 Genome organization of SARS-CoV-2

The 30 kbs genome of SARS-CoV-2, which contains at least six viral open reading frames (ORFs), is stratified into several different regions [6]. From the very 5' end locates the 5' untranslated region (UTR) which contains sequences that are important for viral replication and translation. Followed by the ORF1a and 1b regions, which account for nearly two-thirds of the entire genome and encode two large polyproteins, polyprotein 1a (pp1a) and polyprotein 1ab (pp1ab). These polyproteins are cleaved by viral proteases and cellular proteases into 16 non-structural proteins (nsps) that participate in diverse aspects of the viral life cycle, including viral RNA synthesis, viral protein processing, and modulation of the host immune system [5, 7]. The nsps are desirable targets for drug development and therapeutic intervention because they are essential for viral replication

and are highly conserved among coronaviruses [7-9]. Several inhibitors targeting these nsps for the treatment of COVID-19 have been developed and are being used in clinical settings [8]. Understanding the structure and function of these nsps is crucial for developing effective COVID-19 treatments and vaccines [9].

After that, the remaining one-third of the genome encodes the viral structural proteins and accessory proteins. Structural proteins consisting of S, E, M, and N proteins are essential for the assembly and release of infectious viral particles, in addition to serving a variety of other functions associated with the viral life cycle [10]. The S protein is a trimeric glycoprotein composed of three identical protein subunits, each containing an S1 domain responsible for receptor recognition and binding and an S2 domain responsible for membrane fusion [11]. The S1 domain comprises the receptor bind domain (RBD), which interacts directly with the human angiotensin-converting enzyme 2 (ACE2) receptor. The S protein structure is highly flexible and dynamic, allowing it to endure conformational changes required for virus entry into host cells [12, 13]. Several COVID-19 vaccines and therapeutic antibodies seek to prevent the virus from entering and infecting host cells by targeting this essential protein. E and M proteins are involved in the assembly and release of new viral particles, as well as the regulation of host cell signaling pathways and induction of host cell apoptosis [14, 15]. The N protein plays a role in viral replication and assembly and is responsible for encapsidating the viral RNA genome. It may also modulate host cell signaling pathways and the immune response of the host [16]. The accessory proteins encoded by ORF3a, ORF6, ORF7a, ORF7b, ORF8, ORF9b, ORF9c, and ORF10 may regulate host immune responses, although their exact functions remain unclear [17].

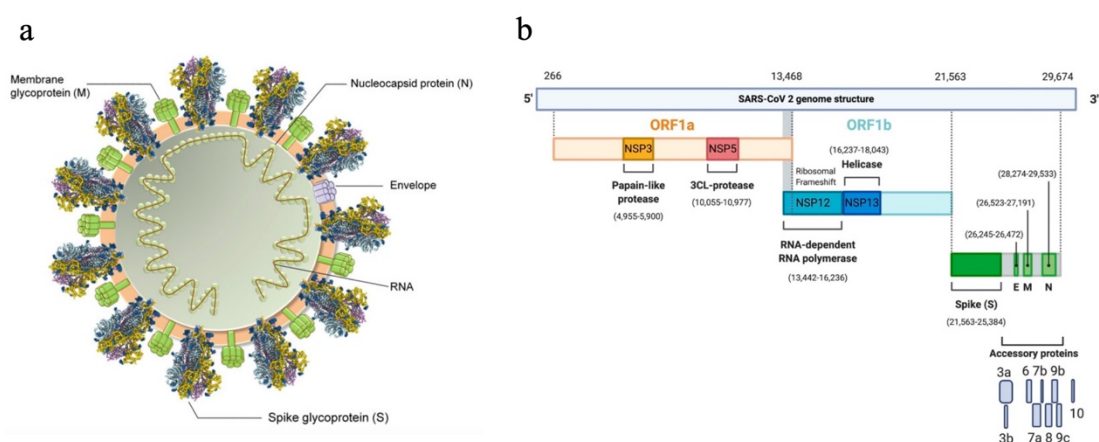


Figure 1: SARS-CoV-2 infectious particle structure and genome organization. (a) The SARS-CoV-2 spike glycoprotein (S), membrane glycoprotein (M), and envelope protein (E) are embedded in a lipid bilayer derived from the host membrane that encloses the helical nucleocapsid carrying viral genomic RNA. (Kumar et al., 2020) [5] (b) The first two-thirds of viral genome encodes ORF1a (yellow) and ORF1b (blue), which can be directly translated into 16 NSPs, such as Papain-like protease and 3CL-protease, RNA-dependent RNA polymerase, and viral RNA helicase. The last third of the genome encodes the structural proteins (green) S, E, M, and N, and accessory proteins (grey). (adapted

from Alzoughool et al., 2020) [7]

1.1.1.3 Viral life cycle

Multiple stages comprise the life cycle of SARS-CoV-2, including viral entry, genome replication, transcription and translation of viral proteins, assembly of new virions, and release of mature virions. Regarding viral entrance, SARS-CoV-2 enters host cells similarly to SARS-CoV via engaging S protein with the cellular ACE2 receptor [18, 19]. Notably, the S protein of SARS-CoV-2 has 10–20 times greater affinity than that of SARS-CoV [20], which explains the stronger infectivity and, in terms of epidemiology, the significantly increased basic reproduction number (R_0). After binding to the ACE2 receptor, S protein undergoes conformational changes which result in the fusion of viral and cellular membrane. In addition, serine protease TMPRSS2 also promotes the fusion by priming the S protein [21]. With the uncoating of nucleocapsid after internalization, the viral genomic RNA can be eventually released into the host cytoplasm.

Once the incoming positive strain genomic RNA is released, it can be directly used as a translation template to produce pp1a and pp1ab, which are further cleaved into 16 nonstructural proteins by virus-encoded and host proteases. Afterwards, nsps assemble with the infection-derived perinuclear double-membrane vesicles (DMVs) into the replication and transcription complex (RTC), which serves as a secure environment for viral genome replication and the synthesis of subgenomic RNAs (sgRNAs) [22]. Replicating SARS-CoV-2 machinery synthesizes the gRNA and nine canonical sgRNAs, all of which share the same 5' leader sequence, and the 3' end of the viral genome consists of the nucleocapsid (N) open reading frame and the 3' untranslated region, by a unique discontinuous transcription observed only in coronaviruses [23]. Towards this characteristic, novel therapeutics, such as RNAi machinery, could benefit from the design of siRNA targeting these common regions for the synchronous degradation of all SARS-CoV-2-derived RNAs [24]. sgRNAs function as templates for structural proteins expression including S, E, M, and N, as well as accessory proteins. The freshly generated positive-sense gRNA is selectively packaged with N proteins and buds into cisternae of the endoplasmic reticulum–Golgi intermediate compartment (ERGIC), where other structural proteins assemble the complete virion which is then released from the infected cell through exocytosis [4].

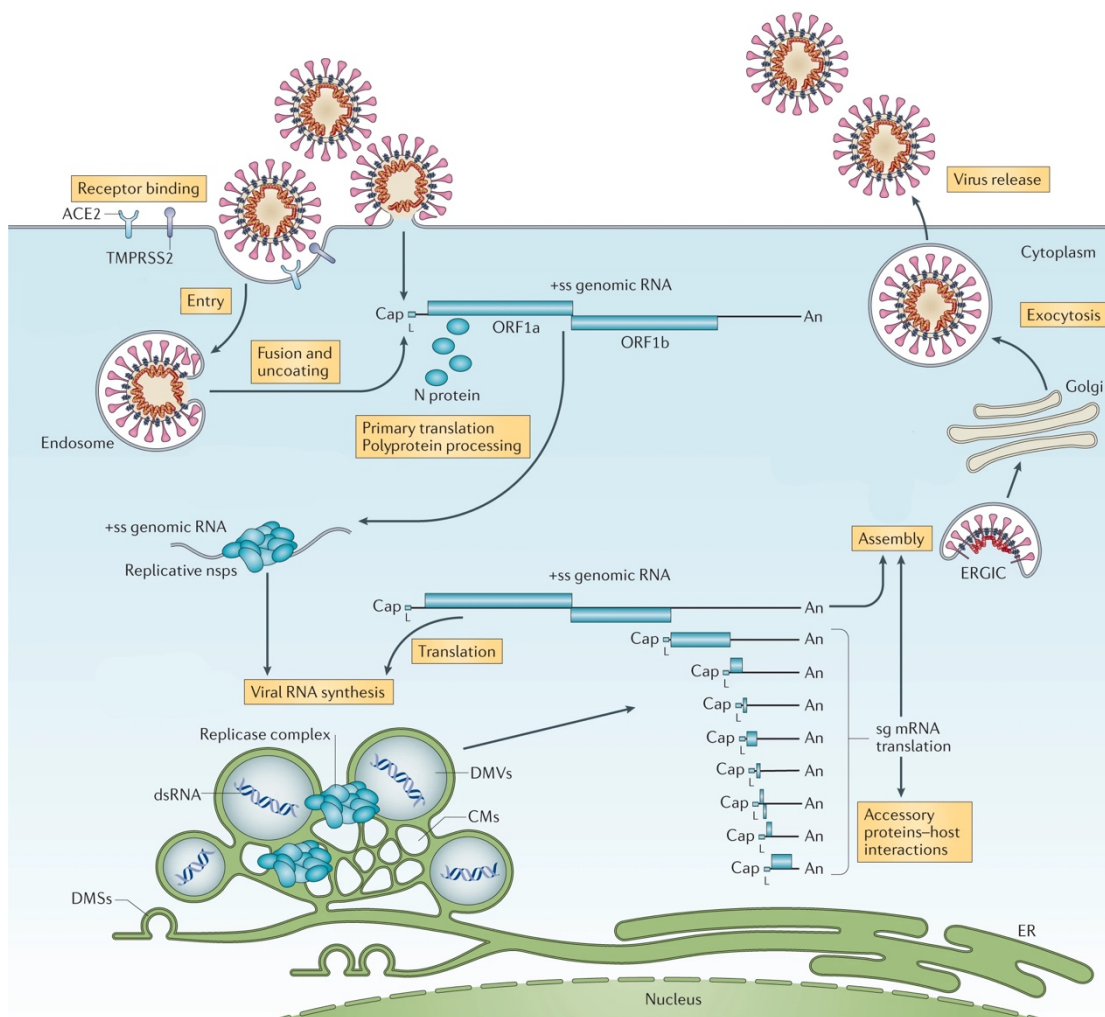


Figure 2: SARS-CoV-2 life cycle. The SARS-CoV-2 enters host cells by binding its spike protein to cellular receptors ACE2, which, together with the serine protease TMPRSS2, results in viral uptake and fusion at the cellular or endosomal membrane. Once inside the cell, the viral genomic RNA is released and immediately translated into two polyproteins, pp1a and pp1b, which are then processed into individual non-structural proteins (nsps) that form the viral replication and transcription complex. The expression of nsps results in the biogenesis of viral replication organelles, which consist of perinuclear double-membrane vesicles (DMVs), convoluted membranes (CMs), and small open double-membrane spherules (DMSs). These structures provide a protective microenvironment for viral genomic RNA replication and transcription of subgenomic messenger RNAs (sg mRNAs), which constitute the nested set of coronavirus mRNAs. Afterwards, translated structural proteins translocate into endoplasmic reticulum (ER) membranes and pass through the ER-to-Golgi intermediate compartment (ERGIC), where interaction with N-encapsulated, newly synthesized genomic RNA results in branching into the lumen of secretory vesicular compartments. Finally, the infected cell secretes the virions via exocytosis. (reprint with permission from V'kovski et al., 2021) [4]

1.1.2 SARS-CoV-2 pathogenesis and clinical features

1.1.2.1 Major infection route and symptoms

The fact that SARS-CoV-2 enters host cells with ACE2 receptors, in line with the contagious properties of the virus, makes the respiratory system, including pharynx, trachea, bronchial tube, and lung, the main tropism [25, 26]. Cells highly express ACE2 like ciliated epithelial cells in the nasopharynx and trachea or sustentacular cells in the

olfactory epithelium are likely to be targeted in the initial of the infection and can further spread to the lower respiratory tract to infect lung alveoli [27]. After entering host cells, SARS-CoV-2 undergoes a lytic life cycle which can directly cause cell damage via pyroptosis [28]. The infected cells are able to trigger a MDA5-mediated innate immune response by recognizing long viral dsRNA, resulting in the expression of type I and type III interferons [29]. In the meantime, the cell death leads to release of damage-associated molecular patterns (DAMPs) and pathogen-associated molecular patterns (PAMPs), which can further induce the activation of immune cells to release more proinflammatory cytokines and chemokines such as IL-1 β , IL-6, and type II interferon [30]. If the virus infection is not eliminated at this point, a transition from mild to severe symptoms could happen and develop into hyperinflammation, which greatly increases the chance of fatal acute respiratory distress syndrome (ARDS) and organ failure [31, 32].

The incubation period of the infection generally takes 2 to 14 days after exposure, while clinical features vary widely in severity and presentation [33]. The majority of the infected individuals have asymptomatic or mild symptoms. Typical COVID-19 patients manifest flu-like symptoms such as coughing, fever, fatigue, and sore throat [34]. Novel signs of infection, for instance, loss of taste or smell, were reported along with the virus evolution during the pandemic (National Institutes of Health, last updated March 2023). COVID-19 can occasionally lead to severe diseases in some cases, especially in susceptible groups including the elderly and those with underlying medical issues or immunosuppressive treatments.

1.1.2.2 SARS-CoV-2 multi-organ tropism and manifestation

In addition to the respiratory system, broad organ tropism of SARS-CoV-2, attributed to the wide distribution of ACE2 receptors, and multiorgan damage are also important features of severe COVID-19. SARS-CoV-2 RNA was detected in multiple organs beyond the respiratory tract, including kidneys, liver, heart, brain, and blood [35]. Multiorgan impairments, characterized by acute kidney injury, acute liver injury, cardiovascular dysfunction, and neurological disorders, are often distinct in patients with severe COVID-19 [36].

With a reported incidence of 11.4-61.1% of infected individuals, the gastrointestinal (GI) system may be the predominant manifestation of COVID-19 beyond the lungs [37, 38]. Most GI symptoms associated with COVID-19 are usually mild and resolve on their own. These symptoms can include loss of appetite, diarrhea, nausea, vomiting, and abdominal pain or discomfort. However, a small number of patients may experience more severe GI complications, such as acute pancreatitis, acute appendicitis, intestinal obstruction, bowel ischemia, bleeding into the abdominal cavity (hemoperitoneum), or abdominal

compartment syndrome [37, 39, 40]. These conditions can present as an acute abdomen and require immediate medical attention. In addition, SARS-CoV-2 has the potential to induce cardiovascular complications by affecting the heart and blood vessels. This includes the development of myocarditis, which is inflammation of the heart muscle, pericarditis, which is inflammation of the sac surrounding the heart, and the formation of blood clots that heighten the risk of heart attacks and strokes. Individuals with pre-existing cardiovascular conditions are at a higher vulnerability to these complications [41].

Focusing on the liver tropism of SARS-CoV-2, COVID-19 patients commonly manifest liver enzyme abnormalities such as elevated aspartate aminotransferase (AST) and alanine aminotransferase levels accompanied by modestly elevated total bilirubin level, with a strong association between AST elevation and increased mortality risk [42, 43]. The mechanisms of liver injury in COVID-19 are still not fully understood, but several studies suggest that direct viral infection, immune-mediated injury, drug-induced liver injury, and hypoxia may all contribute to liver damage in COVID-19 patients [44, 45]. Several investigations with in-vitro data and clinical observations showed evidence of direct viral infection and the production of new infectious virus in the liver and liver-associated cell lines [39]. Recent research investigating the connection between liver injury and immune response in COVID-19 patients revealed that liver injury was associated with increased levels of inflammatory cytokines, suggesting that immune-mediated injury may play a role in liver damage in COVID-19 [46].

1.1.2.3 Long COVID

Long COVID, also known as post-acute sequelae of SARS-CoV-2 infection (PASC), refers to a condition in which people continue to experience symptoms of COVID-19 for weeks or even months after the initial infection has cleared. The symptoms of long COVID can vary widely and may affect different parts of the body, including the respiratory system, cardiovascular system, and nervous system. Common symptoms of long COVID include fatigue, shortness of breath, chest pain, joint pain, muscle weakness, brain fog, difficulty concentrating, depression, anxiety, and insomnia. Other less common symptoms may include loss of taste or smell, headaches, dizziness, and skin rashes (Robert Koch Institute, last updated Apr 2023, [47]).

The exact cause of long COVID is not yet fully understood, it can affect anyone who has had COVID-19, regardless of the severity of the initial infection. Even people who had mild or asymptomatic cases of COVID-19 can develop long COVID. The risk of developing long COVID may be higher in people who are older, have pre-existing medical conditions, or who had a more severe initial infection. There is no cure for Long COVID, but certain treatments may help alleviate symptoms, including medications to

manage pain, physical therapy to enhance mobility and function, and cognitive-behavioral therapy for any psychological symptoms (Centers for Disease Control and Prevention, [47]).

1.1.3 Evolution of SARS-CoV-2

On account of its similarity to other coronaviruses discovered in bats, it is believed that SARS-CoV-2 originated in bats and then spread to an intermediate host, most likely a pangolin, before infecting humans [48, 49]. The specific route through which the virus infected humans remains unknown. In the class of RNA virus with high mutation rate, SARS-CoV-2 evolves along with the pandemic and has already been categorized into numbers of subgroups according to certain critical mutations mainly appeared in the S protein region [50, 51]. Knowing this, sequences from swabs around the world were monitored to track mutations that might alter the transmission, pathogenesis, or immune evasion properties of the virus, and a massive database called "GISAID" was created to provide open access to sequences collected from around the globe [52].

Shortly after characterizing the first Wu-Han strain in late 2019, a mutation D614G in the spike protein, which is believed to have increased the transmissibility of the virus, was identified. This new strain of SARS-CoV-2 initiated a new clade, caused widespread outbreaks at the beginning of 2020, and progressively supplanted the original virus [53]. Since then, numerous variants with higher transmissibility and immune escape listed as Variants of Concern (VOCs) have dominated the epidemics and pandemic one after the other. The most influential among all are Alpha (B.1.1.7), Beta (B.1.351), Gamma (P.1), Delta (B.1.617), and nowadays Omicron (B.1.1.529) in order of their emergence. The Alpha variant, whose multiple mutations in the spike protein made it an estimated 40-80% more transmissible than the original strain, was identified for the first time in the United Kingdom in September 2020 and dominated the pandemic until it was supplanted by the Delta variant [54]. Soon after, the Beta and Gamma variants emerged in South Africa and Brazil, respectively leading the epidemics in those nations. The Delta variant was first discovered in India at the end of 2020, but it wasn't until May 2021 that it surpassed the Alpha variant as the most circulating virus for the next six months. It was reported to be 50-60% more transmissible than the Alpha variant and associated with an increased risk of hospitalization and mortality compared to previous strains [55]. After the delta variant, the pandemic has been dominated since September 2021 by the notorious Omicron variant, which carries a vast number of mutations specific to the S protein and continues to derive new subtypes listed as VOCs and Variants of Interest (VOIs), including Omicron BA.5, BA.2.75, BQ.1, and XBB.1.5. Omicron has the greatest transmissibility among any antecede virus, but fortunately its severity and lethality are significantly reduced [56]. On the other hand, special attention must be paid to the

complicated mutation profile of the Omicron S protein, existing vaccines would be substantially less effective to some extent [57]. See Table 1 for additional information on the characteristics of the listed VoCs.

It is important to note that while the virus is evolving, this process is neither predictable nor linear. Some mutations may provide an advantage in one situation but not in another, and there is still a great deal that is unknown about how the virus is evolving and the potential consequences of these changes.

SARS-CoV-2 strain	Declaration as VOC	Majority extension	Transmissibility	Severity and lethality	Escape to immune response	Mutations found in the S protein gene
Original	Wuhan (China), 07/01/2020	Worldwide	$R_0 = 2.5$. Incubation period: 2–14 days, median 5.1 days. SAR: 0.7–75%.	81% mild 14% severe 5% critical 2.3% death.	PVE 95% for symptomatic infection.	
Alpha	United Kingdom, 29/12/2020	Europe, Oceania and North America	↑ Transmissibility (50% higher). SAR: 25.1%, 1.43–1.82 times higher.	↑ Severity and lethality . 1.55–1.73 times more lethality.	↑ Immune escape . PVE 89% for symptomatic infection, and 95% for hospitalization or death.	Del69-70, del144, N501Y, A570D, D614G, P681H, T716I, S982A, D1118H.
Beta	South Africa, 29/12/2020	Africa	↑ Transmissibility (50% higher, 2.5 times higher). SAR higher.	↑ Severity and lethality .	↑ Immune escape . PVE 84% for symptomatic infection, and 95% for hospitalization or death.	L18F, D80A, D215G, R246I, K417N, E484K, N501Y, D614G, A701V.
Gamma	Brazil, 29/12/2020	Latin America	↑ Transmissibility (1.7–2.4 times higher). $R_0 = 3.4$. SAR higher.	↑ Severity and lethality .	↑ Immune escape . PVE 84% for symptomatic infection, and 95% for hospitalization or death.	L18F, T20N, P26S, D138Y, R190S, K417T, E484K, N501Y, D614G, H655Y, T1027I, V1176F.
Delta	India, 11/05/2021	Worldwide	↑↑ Transmissibility (1.97 times higher). $R_0 = 7$. Intradomiciliary delta SAR (10.3–21%) 1.70 times higher than intradomiciliary alpha SAR. Shorter incubation period (median 4.5 days). Higher viral load, 2.5 times more in nasopharyngeal exudate and 15 times more in saliva.	↑↑ Severity and lethality . 2.20 times more hospitalization. 3.87 times more ICU admission. 2.37 times more lethality.	↑↑ Immune escape . PVE 87% for symptomatic infection, and 93% for hospitalization or death.	T19R, G142D, del156-157, R158G, K417N (delta plus), L452R, T478K, D614G, P681R.
Omicron	South Africa and Botswana, 26/11/2021	Worldwide	↑↑↑↑ Transmissibility (36.5% higher than delta). $R_0 = 10$. Intradomiciliary omicron SAR 15.8%–31% versus delta SAR 10.3–21%. Extradomiciliary omicron SAR 8.7% versus delta SAR 3.0%. 70-fold higher respiratory viral load at 24 hours in omicron than in original and delta strains. Shorter incubation period (median 3 days).	↓ Severity and lethality . 0.71 times less (29% less) hospitalization. 10-fold lower viral load in lung tissue at 24 hours in omicron than in original strain.	↑↑↑↑ Immune escape . PVE 10% for symptomatic infection, 49% if third dose. PVE 70% for hospitalization. 2.4–5.4 times higher risk of reinfection .	A67V, del69-70, T95I, G142D, del143-145, Y145D, del211, L212I, ins214EPE, G339D, S371L, S373P, S375F, K417N, N440K, G446S, S477N, T478K, E484A, Q493R, G496S, Q498R, N501Y, Y505H, T547K, D614G, H655Y, N679K, P681H, N764K, D796Y, N856K, Q954H, N969K, L981F.

Table 1: SARS-CoV-2 Variants of Concern and their dynamic characteristics. Basic reproduction number (R_0): average number of new cases generated (by contagion) from a single case. Secondary attack rate (SAR): number of new cases of a disease among the total number of exposed susceptible people within a specific group (i.e., household or close contacts), that is, the proportion of contacts of a primary case who become ill. Preventive vaccine effectiveness (PVE): in all cases after two doses with Comirnaty vaccine (based on messenger RNA technology). (adapted from M Lorente-González et al., 2022) [57]

1.2 Epidemiology of SARS-CoV-2

The epidemiology of SARS-CoV-2 is a complex and dynamic process that is shaped by multiple factors. As a novel virus, its unknown nature makes predicting its spread at the start of the pandemic challenging. Even when more knowledge becomes available, developing variants bring new challenges by not only changing clinical characteristics and severity but also increasing transmissibility. Numerous asymptomatic transmissions hinder the ability to identify and isolate individuals who were infected and control the virus's spread. Several public health measures, such as lockdowns, social distancing, and vaccination campaigns, can have a substantial effect on the epidemiology.

This chapter will provide a quick summary of the pandemic condition and highlight the interaction between the virus and human society.

1.2.1 The unfolding and development of the pandemic

The virus, which was first reported as causing pneumonia of unknown aetiology in Wuhan city, Hubei province, China in early December 2019, was given the provisional name "2019 novel coronavirus (2019-nCoV)" by the World Health Organization (WHO) and was later renamed "severe acute respiratory syndrome coronavirus 2" (SARS-CoV-2) by the International Committee on Taxonomy of Viruses. Meanwhile, the disease caused by SARS-CoV-2 was also referred to as "Coronavirus disease 2019 (COVID-19)". The virus is believed to have originated in a Wuhan wet market where both living and dead animals were sold for human consumption [58]. Current data indicates that SARS-CoV-2 may have originated in bats and then been transmitted to humans via an intermediary animal host, such as a pangolin or civet [48]. However, the exact origin of SARS-CoV-2 is still being investigated, and information remains limited.

Shortly after its emergence, the virus broke through the defenses of the lockdown measures applied in Wuhan and spread rapidly around the world, while the pandemic was declared in March 2020 by WHO. As the pandemic progressed, the virus spread to various parts of the globe, with Europe becoming a major epicenter in early 2020. Particularly hard-hit were Italy and Spain, with high death rates and overwhelmed healthcare systems. In mid-2020, the big epidemic broke out in the United States, where the number of confirmed cases and deaths skyrocketed, making the United States the epicenter of the pandemic at the moment. After that, practically every country was affected by the pandemic, and the situation only started to be improved until stringent limits and the development of vaccines were implemented in late-2020. Until today, accumulated over 759 million confirmed infected cases were reported, resulting in around 7 million deaths (WHO, Mar 2023).

Situation by WHO Region

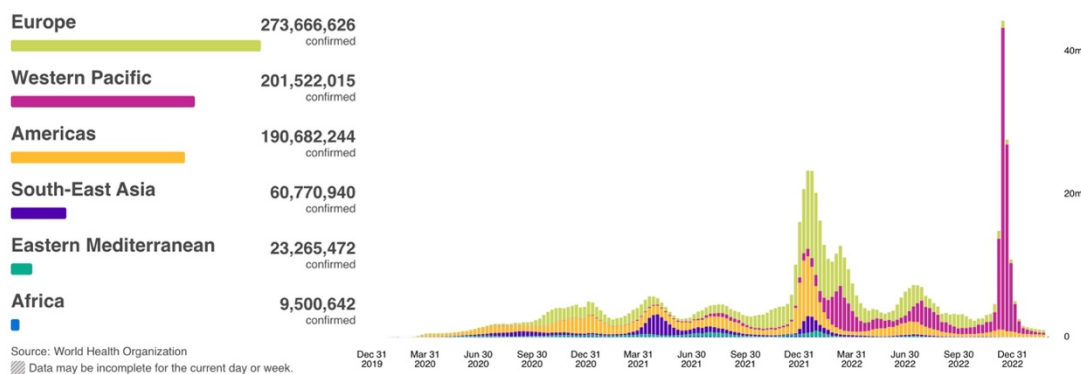


Figure 3: Cases of infection cumulatively reported and global region distribution from Dec 2019 to Mar 2023. The total number of confirmed cases is displayed on the left, organized by WHO area, and the timeline is shown on the right. (reprint with permission from WHO COVID-19 Dashboard, last updated Mar 2023)

1.2.2 SARS-CoV-2 transmission

SARS-CoV-2 mainly infects and replicates in the respiratory system, making its dominant close contact and airborne transmission via infectious respiratory fluids such as very fine respiratory droplets and aerosol particles. Respiratory particles released from infected individuals during breathing, speaking, coughing and sneezing could travel a maximum of up to 2 meters in a spectrum of sizes, moreover, the very fine droplets and aerosol particles could last suspension in the air for minutes to even hours [59].

The infection could be taken place in three principal ways regarding the contact. Inhalation of the fine droplets and aerosol particles is considered the main route while the infection often happened in enclosed spaces with hardly airflow or inappropriate ventilating systems where the particles could remain suspended for a long period. Furthermore, the exposure could happen without close contact with an infectious source since the concentration of these particles could preserve high at a far distance. The second route requires closer contact as long as the deposition of larger droplets (e.g. $> 5 \mu\text{m}$) onto exposed mucous membranes in the mouth, nose, and eye could occur (Centers for Disease Control and Prevention). The last pathway easily overlooked is touching the mucous membranes with hands adhered to by fluids. Several research have indicated that SARS-CoV-2 could survive on various surfaces for days or even a week. The survival time of SARS-CoV-2 on plastic, metal, and surgical mask were the longest from 3 to 7 days of all tested materials [60].

1.2.3 Diagnostics for SARS-CoV-2 infections

1.2.3.1 Swab test for diagnosing active infections

The detection of infection is important throughout the pandemic, especially when

numerous asymptomatic carriers are reported. A nasal or throat swab test investigating the presence of viral genetic material or proteins in the mucous is typically used in respiratory infections. Quantitative polymerase chain reaction (qPCR) test, which is capable of sensitively detecting specific viral nucleic acid, was brought into operation as a gold standard diagnostic all over the pandemic. The cycle threshold value (Ct value) from the readout of qPCR indicates the number of amplification cycles required to detect the target nucleic acid above a certain threshold. From this, a low Ct value indicates a high amount of viral genetic material in the sample, while a high Ct value indicates a lower amount [61]. The cut-off value for determining positivity is typically determined during assay development and validation, and is set based on the level of viral nucleic acid that is considered to be reliably detectable above background levels. In general, a Ct value of 35 is commonly used as the cut-off value for SARS-CoV-2 qPCR diagnostic tests [62].

Antigen tests are another type of diagnostic test that detect viral proteins in respiratory specimens. These tests are relatively rapid and inexpensive, with results ordinarily available within 15-30 minutes and at prices above 10 times lower, providing accessibility and convenience that allow the general public to perform the tests whenever and wherever possible. However, considering the subordinate sensitivity resulting in higher incidence of false results, antigen tests are commonly used for diagnosing COVID-19 in individuals with symptoms, as the viral load is normally higher [63]. To be noted, a negative antigen test result should be followed up with a PCR test, particularly in individuals with symptoms or who have had close contact with a confirmed COVID-19 case.

1.2.3.2 Serological antibody test for monitoring infected individuals

Apart from disclosing active infected carriers, a serological antibody test can reveal if a person has been previously infected with SARS-CoV-2, which helps track the spread of the virus and provide information on the possible ratio in a population that has developed immunity to the virus. In these tests, it is typical to evaluate IgG antibodies specific to SARS-CoV-2 S or N proteins in the sera of infected individuals using enzyme-linked immunosorbent assay (ELISA). Notably, with the increasing coverage of the S-protein-primed vaccinated population, anti-S IgG detection is now alternatively employed for vaccination protection and duration study, while antibodies recognizing viral N protein continue to function as an indicator of infection history.

1.3 Prophylaxis and therapeutics against SARS-CoV-2

The development of prophylaxis is believed to be the key to ending the pandemic and returning to normal life, and therapeutics are unquestionably another essential life-saving talisman. The development of effective antiviral preventatives and therapeutics has been

a top priority for scientists and medical professionals worldwide. This chapter provides an extensive overview of the current state of research on SARS-CoV-2 prophylaxis and therapy, including regulations, vaccines, antiviral medications, and other novel treatments.

1.3.1 Prophylaxis strategies for COVID-19

1.3.1.1 Restrictions for preventing virus spread

To prevent the spread of COVID-19, many countries and communities have imposed variety of regulations to limit person-to-person contact and transmission opportunities. Lockdown is one of the most severe restrictions, requiring people to remain at home with the exception of vital activities such as grocery shopping, medical treatment. This policy entails business and school closures, travel restrictions, and social distancing. Although the effectiveness of lockdowns has been debated among experts, several studies have demonstrated that countries who implemented earlier and more stringent lockdown measures had lower COVID-19 case and mortality rates than those that did not [64, 65]. However, lockdowns can have social and economic consequences, such as job losses, business closures, and a rise in mental health issues. On the other hand, the social distance derived from these policies has had a significant impact on our daily lives, resulting in a rapid expansion of e-commerce businesses and virtual platforms for remote work and learning.

Another influential regulation which was implemented globally is the facial mask mandate, which specifies where masks must be worn, including interior public locations, public transportation, and outdoor regions where social distancing is impossible. Several studies have proved the effectiveness of masks in preventing the spread of COVID-19, a study published in *The Lancet Digital Health* in June 2020 found that wearing face masks reduced the risk of infection by 85%. Various types of masks were prescribed, with cloth masks, surgical masks, and N95 respirators ranking worst to strongest in terms of protection. Among all, surgical masks are the most commonly used and are designed to protect both the wearer and others from respiratory droplets. They offer superior protection over cloth masks and can filter out between 65 and 80 percent of particles. In addition, N95 respirators, specialist masks that give a higher level of filtration of at least 95% of small particles, are typically reserved for frontline employees who are at a high risk of exposure, such as healthcare workers [66].

1.3.1.2 Prophylactic vaccinations development

Vaccines have functioned as effective preventative measures against infectious diseases since its discovery. By exposing the immune system to attenuated/inactivated pathogens or even a single structural component from pathogens, the immune system can be

educated to recognize and eliminate disease-causing pathogens. Depending on the categories of vaccines, protection can typically last for years due to T cell and B cell memory functions [67]. So far, vaccines have been one of the most significant medical developments in human history, saving innumerable lives and preventing the spread of fatal diseases.

With the development of the vaccine industry, inactivated and live attenuated vaccines were no longer the only choices, but various models of vaccines were discovered and implemented, including subunit vaccines, viral vector vaccines, and DNA and mRNA vaccines. Among all vaccines, mRNA vaccines have garnered the most attention during the COVID-19 pandemic due to their rapid development, as well as their high efficacy and safety. These vaccines contain virus-derived messenger RNA fragment that instructs cells to produce a nontoxic virus antigen, which the immune system then recognizes and responds to. Pfizer-BioNTech (BNT162b2) and Moderna's (mRNA-1273) COVID-19 vaccines are two well-known examples of mRNA vaccinations with a similar design of lipid nanoparticles encapsulating an mRNA-encoding SARS-CoV-2 spike. In clinical trials, the Pfizer-BioNTech and Moderna vaccines demonstrated 95% and 94.1% efficacy in preventing COVID-19 after two doses administered 21 and 28 days apart, respectively (Centers for Disease Control and Prevention). Additionally, both vaccines have demonstrated efficacy in preventing severe disease, hospitalization, and mortality [68, 69]. Many countries, including the United States, the United Kingdom, and the European Union, authorized their emergency use in December of 2020, making them the first commercially available vaccines during the pandemic. Benefiting from the high adaptability of mRNA vaccines, both pharmaceutical companies have modified and released new generation mRNA vaccines containing the updated S protein sequence from VOCs Omicron BA.4/5 in an effort to reduce the mutation-induced immune escape.

The viral vector vaccine is another widely used type of COVID-19 vaccine. These vaccines employ an innocuous virus, such as an adenovirus, to transport genetic material from the virus into cells, which then produce a protein that stimulates the immune system. For instance, the Oxford–AstraZeneca (ChAdOx1 nCoV-19) COVID-19 vaccine, one of the most implemented COVID-19 vaccines, uses a chimpanzee adenovirus vector to deliver the gene encoding the spike protein. In comparison to mRNA vaccines, the Oxford–AstraZeneca vaccine evidenced a lower efficacy of 76% after two doses administered 4-12 weeks apart, and it was also reported with more severe side effects (Centers for Disease Control and Prevention, [70]).

It's worth noting that the development of a vaccine can take years or even decades, beginning with the identification and isolation of the pathogen and continuing through

preclinical animal testing and three independent phases of clinical trials, before it can be submitted for regulatory approval to government agencies such as the U.S. Food and Drug Administration (FDA). Surprisingly, the development and use of COVID-19 vaccines were drastically accelerated to less than one year in response to the urgent need to curtail the spread of pandemic. With the prioritization and streamlining of the review and approval processes for COVID-19 vaccines by regulatory agencies, as well as the advanced vaccine technology platform and global collaboration, this unprecedented milestone could be achieved.

1.3.2 Therapeutics for SARS-CoV-2 infection

1.3.2.1 Antiviral drugs: chemical compounds and monoclonal antibodies

Since the onset of the COVID-19 pandemic, there has been a rapid increase in the number of therapeutics designed to treat SARS-CoV-2 infections. Repositioning already-approved broad-spectrum antiviral medications such as nucleoside analogues remdesivir, molnupiravir, and favipiravir, which have been applied to inhibit the replication of different viruses by targeting a conserved viral protein, RNA-dependent RNA polymerase in this case, is the simplest and quickest method. Remdesivir has been shown to reduce the duration to recovery in hospitalized COVID-19 patients, while molnupiravir reduces the risk of hospitalization or death in high-risk COVID-19 patients with mild to moderate disease [71]. Favipiravir has predominantly been utilized in Japan and Russia, where it has demonstrated promising efficacy in reducing the duration of viral clearance [72]. The screening of novel small molecule therapeutics against SARS-CoV-2 is still in progress, with viral protease inhibitors and nucleotide analogs being two of the most promising candidates in this field, and there are already a large number of potential drugs in pre-clinical and clinical trials.

Additionally, monoclonal antibody drugs are regarded as an effective COVID-19 treatment, were developed by combining traditional techniques for identifying and isolating antibodies with newer techniques such as synthetic antibody libraries and high-throughput screening. For instance, casirivimab/imdevimab and sotrovimab are monoclonal antibodies approved for emergency use in the United States by the FDA. Casirivimab/imdevimab is indicated for the treatment of mild to moderate COVID-19 in high-risk patients, whereas Sotrovimab is recommended for adults and pediatric patients (at least 12 years old and weighing at least 40 kg) at high risk for developing severe COVID-19 or hospitalization [73]. It has been shown that these monoclonal antibodies reduce the risk of hospitalization and mortality in patients at high risk with mild to moderate COVID-19. Beside monoclonal antibodies, some patients with severe COVID-19 have been treated with convalescent plasma from recovered COVID-19 patients.

Convalescent plasma contains antibodies that can aid in the fight against the virus, and it has been shown to reduce the risk of mortality in hospitalized COVID-19 patients who do not yet require mechanical ventilation [74].

1.3.2.2 Immunomodulators

To regulate the immune response to COVID-19, particularly the suppression of the detrimental cytokine storm, immunomodulators including tocilizumab and baricitinib have been introduced. Tocilizumab is a monoclonal antibody that targets the interleukin-6 receptor, which is implicated in the COVID-19 immune response. Tocilizumab has been utilized to treat COVID-19 severity in hospitalized patients with elevated interleukin-6 levels. Baricitinib is a Janus kinase inhibitor that has been demonstrated to reduce the risk of mortality or progression of disease in hospitalized COVID-19 patients who require supplemental oxygen or mechanical ventilation [75]. In the course of treating COVID-19, numerous more immunomodulatory agents such as Anakinra, Statins, and Interferon are also examined and applied [76].

Corticosteroids such as dexamethasone have been employed to reduce COVID-19-induced inflammation and injury [77]. It has been demonstrated that dexamethasone lowers the risk of mortality in hospitalized COVID-19 patients who require supplemental oxygen or mechanical ventilation. However, moderate cases of COVID-19 should not be treated with corticosteroids, as they may delay viral clearance [75].

Although the effectiveness of these therapeutics may vary based on the severity of the disease and other individual factors, they should only be used under the supervision of a healthcare professional. Ongoing research is conducted to identify novel therapeutics and improve existing COVID-19 treatments.

1.4 Aim of the work

At the beginning of the outbreak, our knowledge of the novel coronavirus was extremely limited, despite the fact that we were aware of its relatives, SARS-CoV and MERS from previous epidemics, but neither virus received much attention. Thus, our primary goal was to gain insight into the characteristics of SARS-CoV-2. With our biosafety level 3 facility and close collaboration with the university hospital, we were able to isolate and propagate live SARS-CoV-2 virus from clinical specimens and establish experimental assays for virus research. My goal was to establish a robust assay to determine the capacity of antibodies and antiviral candidates to neutralize infectious SARS-CoV-2. Based on the establishment of infection platforms as well as the application of my novel assays for detection and analysis, the purpose of our study has branched out in several directions; the thesis will focus on serological research, novel therapeutics, and additional

organ tropism.

Due to the critical need for human immunity data, we launched an initiative to monitor the blood immunity of convalescents and vaccinated individuals as part of our serological research. In this first study, we wanted to study the efficacy and duration of the humoral and cellular immunity elicited by either virus infection or vaccination [78]. As a follow up, we sought to compare the immune response induced by two distinct COVID-19 vaccines, ChAdOx1 nCoV-19 and BNT162b2, when administered in either a homologous or heterologous prime-boost regimen. In addition, we aimed at examining the effect of a fourth vaccine dose on the neutralization of the Delta and Omicron BA.1 variants of concern in immunocompromised hemodialysis patients.

Developing a novel treatment for SARS-CoV-2 infection is one of our major objectives. As a therapeutic strategy to inhibit the replication and spread of SARS-CoV-2, we designed and screened potential small interfering RNAs (siRNAs) targeting various regions of the SARS-CoV-2 genome. siRNA is an RNA molecule that can selectively target and degrade viral genes, providing a promising therapeutic strategy for viral infections. As a treatment, the use of siRNA that targets the viral genome has a number of advantages, including high specificity for the virus of interest, rapid action against viral replication, broad-spectrum activity against multiple strains of the same virus, a low risk of resistance, and the potential for long-lasting effects. My goal was to evaluate the effectiveness of siRNA candidates in targeting the viral RNA genome of SARS-CoV-2 and inhibiting its in vitro replication. This study was done in collaboration with Dr. Thomas Michler and Shubhankar Ambike.

2 Materials and Methods

2.1 Materials

2.1.1 Devices and technical equipment

Product	Supplier
Centrifuge 5920R	Eppendorf
ELISA-Reader infinite F200	Tecan
Freezing device	Nalgene / biocision Coolcell
Gel electrophoresis device	PegLab
Incucyte [®] S3 Live-Cell Analysis System	Essen BioScience
LightCycler [®] 480 II	Roche Diagnostics
Pipettes	Eppendorf

2.1.2 Consumables

Product	Supplier
Cell culture flasks, dishes, plates	TPP
Cover glass 24 x 50 mm	VWR international
Cryo vials, Greiner Bio One	Merck
Falcon tubes 15 ml / 50 ml	Greiner Bio One
Filter tips	Greiner Bio One
Filters 0.45 µm/0.2 µm	Sarstedt
PCR tubes	Thermo Scientific
Pipettes (disposable) 2, 5, 10, 25, 50 ml	Greiner Bio One
Reagent reservoirs, sterile	Corning
Surgical Disposable Scalpels	Braun
Syringes	Braun

2.1.3 Chemicals and reagents

Product	Supplier
Acetic acid	Roth
Agarose	PeqLab
Amphotericin B	Roth
Ampicillin	Roth

Antibiotics/Antimycotics, 100x	ThermoFisher scientific
Bovine serum albumin (BSA)	Roth
Dimethyl sulfoxide (DMSO)	Sigma-Aldrich
Dulbecco's Modified Eagles medium (DMEM)	Gibco
DMEM/F12	Gibco
DNA ladder 1kb / 100bp	Eurogentec
EDTA	Roth
Sodium hydroxide (NaOH)	Roth
Ethanol (EtOH)	Roth
Methanol (MetOH)	Roth
Fetal bovine serum (FBS)	ThermoFisher scientific
Fetal calf serum (FCS)	ThermoFisher scientific
Gentamicin	Gibco
Glycerol	Roth
Incucyte [®] Cytotox Red Reagent	Essen BioScience
Isopropanol	Roth
L-Glutamine, 200 mM	Gibco
LightCycler 480 SYBR green master mix	Roche
Lipofectamine 2000	Invitrogen
Lipofectamine 3000	Invitrogen
Lipofectamine RNAiMAX	ThermoFisher Scientific
Tris(hydroxymethyl)-aminomethan (TRIS)	Roth
2-Mercaptoethanol	Roth
Sodium chloride (NaCl)	Roth
Glycine	Roth
CellTiter-Blue [®] Cell Viability Assay	Promega
Trypsine	ThermoFisher scientific
Collagen R Solution 0,2%, (10x)	SERVA
Phosphate Buffered Saline pH 7,4 (PBS)	ThermoFisher scientific
Polyethylenimine 25 kDa	BASF
OptiMEM	ThermoFisher scientific
TRIzol [™] Reagent	Invitrogen
Tween 20	Roth
3,3',5,5'-Tetramethylbenzidin (TMB)	Invitrogen

2.1.4 Enzymes

Product	Supplier
BamHI Fast Digest	ThermoFisher scientific
EcoRI	ThermoFisher scientific
NotI Fast Digest	ThermoFisher scientific
T4 Ligase	ThermoFisher scientific
XhoI Fast Digest	ThermoFisher scientific

2.1.5 Virus

Virus strain	GISAID ID
SARS-CoV-2 EU1 (B.1)	EPI_ISL_582134
SARS-CoV-2 Delta (B.1.617.2)	EPI_ISL_2772700
SARS-CoV-2 Omicron BA.1 (B.1.1.529)	EPI_ISL_7808190
rSARS-CoV-2 GFP	-

2.1.6 Kits

Product	Supplier
CellTiter-Blue Cell Viability Assay kit	Promega
Dual-Luciferase [®] Reporter Assay System	Promega
iFlash-2019-nCoV Neutralization Antibody Test	Yhlo Biotechnology
NucleoSpin [®] RNA kit	Macherey-Nagel
Plasmid Plus Midi Kit	Qiagen
Phusion Hot Start Flex 2x Master Mix	New England Biolabs
SuperScript [™] III Reverse Transcriptase	ThermoFisher scientific
SuperScript [™] IV First-Strand Synthesis System	ThermoFisher scientific

2.1.7 Cell lines, tissues, and bacteria

Product	Description	Source
HEK293T	Human embryonic kidney cells	AG Protzer
Human precision-cut lung slices (hPCLSs)	Human lung tissue	Comprehensive Pneumology Center (CPC)

One Shot® Stbl3	Chemically competent E. coli	ThermoFisher scientific
VeroE6	African green monkey kidney cells	AG Protzer

2.1.8 Antibodies

Product	Supplier
Anti-dsRNA monoclonal antibody J2	Jena Bioscience
Goat anti-rabbit IgG2a, HRP conjugate	EMD Millipore
SARS-CoV-2 Nucleocapsid Antibody	Sino Biological

2.1.9 Primers

Name of Primer	Sequence
18S qPCR Fw	AAACGGCTACCACATCCA
18S qPCR Rev	CCTCCAATGGATCCTCGT
E-N Fw BamHI	GGTGGTGGATCCTGAGCCTGAAGAACATGTCC
E-N Rev EcoRI	GGTGGTGAATTCAGCTCTCCCTAGCATTGTTC
N CDS Fw XhoI	ATCATACTCGAGATGTCTGATAACGGACCCCA
N CDS Rev NotI	ATCATTGCGGCCGCGGCCTGAGTTGAGTCAGCAC
N qPCR fw	GACCCCAAATCAGCGAAAT
N qPCR Rev	TCTGGTACTGCCAGTTGAATCTG
Rdrp qPCR fw	CGTCTGCGGTATGTGGAAAG
Rdrp qPCR Rev	TAAGACGGGCTGCACTTACA

2.1.10 Plasmids

Name of Plasmid	Source
pcDNA1-SARS-CoV2 complete E-N genes	generated in manuscript
pcDNA1-SARS-CoV-2 partial RdRP	generated in manuscript
psiCHECKTM-2	Promega

2.1.11 Software

Software	Application	Supplier
GraphPad Prism 9.0 software	Half maximal inhibitory concentration calculation	Graphpad Software inc.
IncuCyte® S3 software	Live-cell analysis	Essen BioScience

LightCycler 480 SW 1.5.1	qPCR analysis	Roche
Serial cloner	DNA and protein analysis	SerialBasics

2.2 Methods

2.2.1 Serological study design and sample characteristics

The first article in which homologous and heterologous SARS-CoV-2 vaccinations were contrasted, we followed 472 homologously or heterologously vaccinated participants from three independent study centers in university hospitals rechts der Isar (München), Erlangen, and Colonge. Due to the accessibility, the vaccines included in the study were ChAdOx1 nCoV-19 (ChAd) from Oxford–AstraZeneca and BNT 162b2 (BNT) developed by Pfizer-BioNTech. And the participants were categorized into three cohorts according to their vaccination regimen: two homologous cohorts respectively administrated two doses of ChAd or BNT, and one heterologous cohort with ChAd for the first and followed by BNT as a second dose. We in total collected blood samples at four different time points from the day of first vaccination to months after second dose, sera and peripheral blood mononuclear cells (PBMCs) were isolated and analyzed in two different study centers.

In the second serological research on the cohort receiving hemodialysis, altogether 513 immunocompromised patients were enrolled. Among all, 142 patients relying on maintenance hemodialysis coupled with receiving the third booster (fourth) vaccination were selected to our serological study. These patients received four COVID-19 vaccinations between 19 December 2020 and 20 March 2022, eight and six of which received their first and second vaccination with AZD1222 (Vaxzevria®) by AstraZeneca. All other vaccinations were done with mRNA-based vaccines (BNT162b2 by BioNTech-Pfizer or mRNA-1273 by Moderna). Fifteen patients received two or more vaccinations with mRNA-1273 (Spikevax®, Moderna), and the remaining patients received BNT162b2 (Comirnaty®, BioNTech-Pfizer). The median duration between the first and the fourth vaccination was 338.0 (333.0 – 342.0) days, and between the third and the fourth vaccination 126.0 (105.0 – 126.0) days, respectively. The median duration between the third vaccination and the first blood sampling was 4.1 (3.4 – 4.1) months. Patients had a median age of 72.6 (61.5–80.6) years. 48 (33.8%) patients were female. The median dialysis vintage was 48.9 (21.3–83.7) months. At the time of the first, second, third, and fourth vaccination, 124 (87.3%), 125 (88.0%), 136 (95.8%), and 142 (100%) were on maintenance hemodialysis, respectively. The detailed information was described in previous publications [79, 80].

2.2.2 Cell and tissue culture

VeroE6 cells used in all three studies, and HEK293T cells used in the siRNA study, were maintained in Dulbecco's Minimum essential medium (DMEM, supplemented with 10% fetal bovine serum, 50 U/ml penicillin/streptomycin, 2 mM L-glutamine, 1% sodium pyruvate and 1% non-essential amino acids). Cells were kept at 37°C in humidified incubators at 5% CO² and mycoplasma contaminations were excluded in both cell lines by mycoplasma test.

The human lung tissue used in the siRNA study was obtained from three sources: the CPC-M bioArchive at the Comprehensive Pneumology Center in Munich, Germany, the University Hospital Großhadern of the Ludwig Maximilian University in Munich, Germany, and the Asklepios Biobank of Lung Diseases in Gauting, Germany [81]. All participants provided written informed consent and the study was approved by the local ethics committee of the Ludwig Maximilian University (Project 19-630). Precision-Cut Lung Slices (PCLSs) were prepared according to previously described methods [82]. Tumor-free peri-tumor tissue from the lungs was inflated with a 3% agarose solution and solidified at 4°C. Using a vibration microtome (Hyrax V50, Karl Zeiss AG, Oberkochen, Germany), the tissue blocks were cut into 500 µm thick slices. The PCLSs were then cultured in DMEM F-12 medium supplemented with 0.1% FBS. Prior to conducting experiments, circular PCLS punches with a diameter of 4 mm were created using a 4 mm biopsy puncher.

2.2.3 SARS-CoV-2 isolation and propagation

Swab samples were obtained from infected patients at the clinical facilities of the Technical University of Munich and University Hospital Ludwig Maximilian University. They were diluted in DMEM supplemented with 5% FCS, 40 g/ml Gentamicin, and 2 g/ml Amphotericin B. After that, the media containing the swab material was transferred to cell culture flasks that had already been seeded with VeroE6. These flasks were then incubated at 37°C in humid incubators for a maximum of one week. Microscopy was used to detect the cytopathic effect (CPE), and the progeny virus supernatant was harvested before the CPE became severe.

Following isolation, the virus-containing supernatant was grown for an additional three to five days in bigger scale with VeroE6 cells in the same growth media. Virus stock titers were then calculated using a plaque test, and identities were confirmed using next-generation sequencing. The sequences of the finalized virus stocks were then upload onto open-access GISAID data base and the virus accession IDs were obtained.

2.2.4 SARS-CoV-2 infection

VeroE6 cells were seeded in either 24-well or 96-well format one day before infection to gain approximately 90-95% confluency at time of infection. The SARS-CoV-2 stock was pre-diluted in growth media to achieve the desired multiple of infection (MOI) for the respective experiment. At time of infection, old growth media was removed, and the pre-diluted SARS-CoV-2 solution was added to cells. After 1h incubation at 37°C, a medium exchange was performed. Experiments were terminated at various time points, ranging from 1 to 72 hours post-infection, depending on the specific step of the viral replication cycle being investigated.

In the siRNA research, PCLS samples were prepared following the method mentioned earlier and cultured in DMEM F-12, which was supplemented with L-Glutamine, HEPES, 1×10^4 IU Penicillin, 1×10^4 IU streptomycin, and 0.1% fetal bovine serum. For each biological replicate, three PCLS were placed in a 48-well plate with 500 μ l of medium. Six hours prior to infection with SARS-CoV-2 EU1, the PCLS were transfected with 60 pmol of siRNA and PEI at an N/P ratio of 6. To initiate the infection, 3×10^5 plaque-forming units (PFU) of SARS-CoV-2 were added to each well, which contained PCLS with an estimated cell count of 3×10^5 cells, resulting in an approximate MOI of 1. Procedures for tissue and cell culture infection have already been disclosed by Ambike et al. (2021) [81].

2.2.5 Plaque assay

To titrate different variants, two comparable plaque assay protocols were conducted using different cell lines. For the previous variants, HepG2 cells were plated at a density of 5×10^5 cells per well in a 12-well plate. After 16-24 hours, the cells were infected with serial dilutions of the SARS-CoV-2 inoculum. Following a 1-hour incubation at 37°C, the virus inoculum was removed, and a 0.5% carboxymethyl cellulose solution (prepared in Minimum Essential Media) was added. The cells were then incubated for 48-72 hours, fixed with 10% formaldehyde, and stained with a 1% crystal violet solution. The number of plaques was counted, and viral titers were calculated by multiplying the dilution factors. Similarly, for titrating the newer variants such as Omicron variants, VeroE6 cells were seeded in a 96-well plate at a density of 1.5×10^4 cells per well. The final concentration of the carboxymethyl cellulose solution was increased to 1% to facilitate better stacking of plaques using VeroE6 cells.

2.2.6 Real-virus neutralization assay

One day prior to incubation, VeroE6 cells were seeded at a density of 1.5×10^4 cells per well in a 96-well format. Infection was initiated using SAR-CoV-2 at a multiplicity of

infection (MOI) of 0.03 plaque-forming units (PFU) per cell. To assess virus-neutralization activity, serum samples were serially diluted 1:2 with DMEM, starting from a 1:20 dilution up to a 2560 dilution. SARS-CoV-2 (480 PFU/15,000 cells/well) was added in a total volume of 50 μ L at 37°C. After a one-hour preincubation, the inoculum was transferred to the pre-seeded VeroE6 cells and incubated for another hour at 37°C. The inoculum was then replaced with supplemented DMEM. SARS-CoV-2 infection was terminated after 23 hours by adding 4% paraformaldehyde to fix the cells, and the infection rate was analyzed using an in-cell ELISA.

Following fixation, the cells were washed with PBS and permeabilized with 0.5% saponin (Sigma-Aldrich, Germany). To prevent non-specific antibody binding, a blocking buffer containing 0.1% saponin and 10% goat serum (Sigma-Aldrich) in PBS was added and incubated for one hour on the fixed cells. The primary antibody used was the SinoBiological anti-SARS-CoV-2-N T62 antibody (40143-T62). The antibody was diluted with 1% FCS-PBS to a 1:1500 ratio, and 50 μ l of the diluted antibody was added to each well and incubated at room temperature for 2 hours. After washing, the second antibody, goat anti-rabbit IgG2a-HRP antibody (EMD Millipore / order number 12-348), was added. The second antibody was diluted to a 1:4000 ratio with 1% FCS-PBS. 50 μ l of the diluted second antibody was added and incubated at room temperature for 1-2 hours. After the final washing step, 100 μ l of tetramethylbenzidine (TMB) was added and incubated for 20 minutes at room temperature. The reaction was stopped by adding 2M H₂SO₄. The quantification of the result was performed using optical detection with a Tecan Infinite 200 reader (TECAN, Switzerland) at a wavelength of 450 nm. The inhibition curve of each sample was analyzed using statistical analysis software GraphPad Prism (GraphPad Software, USA), and the 50% inhibitory concentration (IC₅₀) was determined using non-linear regression. This protocol was previously published by Cheng et al. (2022) [79] and Vogel et al. (2022) [80].

2.2.7 Nucleic Acid extraction and qPCR

RNA was extracted from cultured cells using the NucleoSpin RNA kit (Macherey-Nagel; Düren, Germany), and cDNA was synthesized using the SuperscriptTM III First-Strand Synthesis System (Thermo Fisher Scientific; Dreieich, Germany) following the manufacturer's instructions. Subsequent qPCR was performed to amplify SARS-CoV-2 transcripts using primers specific to either the N region, which covers all viral transcripts, or the RNA-dependent RNA polymerase (Rdrp) region, which serves as a measure of genomic RNA (gRNA). To quantify viral RNAs, a standard curve was created using plasmids containing integrated Rdrp or N sequences. The amount of subgenomic RNAs (sgRNAs) was calculated by subtracting the number of transcripts containing Rdrp (indicative of gRNA) from the N-containing transcripts, as the N primers also detect full-

length gRNA. 18S rRNA was used as a reference gene for relative quantification. All quantitative PCRs were performed on a LightCycler[®] 480 instrument (Roche Holding AG; Basel, Switzerland).

2.2.8 Real-time live-cell imaging of SARS-CoV-2 infected cells

VeroE6 cells were seeded in 96-well plates with growth media at least 6 hours prior to infection to achieve approximately 90-95% confluency at the time of infection. The cells were then infected with a recombinant SARS-CoV-2 virus, which expressed green fluorescent protein (GFP) from a sequence integrated at the ORF7 locus (rSARS-CoV-2-GFP). To achieve the desired multiplicity of infection (MOI), the rSARS-CoV-2-GFP virus infection solution was pre-diluted in 50 μ L of growth media. After adding 50 μ L of the infection solution to the cells, the media was exchanged after 1 hour. The multi-well plates were then placed into an IncuCyte[®] Live-Cell Analysis device to acquire phase contrast and fluorescence images of the entire well every 4 hours for three days. The infected cell population was quantified using the GFP channel and analyzed with the IncuCyte S3 software (Essen Bioscience; version 2019B Rev2) [81].

The quantification of dead cells can be also performed with this system using the Incucyte[®] Cytotox Red Dye (Sartorius AG, Göttingen, Germany; Cat. No. 4632). This dye is capable of monitoring the loss of cell membrane integrity. Since the cyanine nucleic acid dye is unable to pass through the plasma membranes of healthy cells, it can only bind to DNA if the cellular membrane integrity is compromised. The fluorescence signal, with a maximum at 631 nm, was measured using the red channel of the Incucyte S3 analyzing system at intervals of every 4 hours for a period of 3 days following the infection.

2.2.9 Antibody response using surrogate virus neutralization assay

To quantify the antibody response, we utilized the iFlash-1800 CLIA Analyzer (YHLO Shenzhen, China). The iFlash-2019-nCoV NAb assay, designed for the detection of neutralizing antibodies, was employed following the manufacturer's instructions. This assay operates on a competitive immunoassay principle. It is important to note that the iFlash-2019-nCoV NAb assay has been validated up to a maximum level of 800 AU/ml, in accordance with the WHO standard. Consequently, any results surpassing this threshold have been recorded as 800 AU/ml.

3 Results

3.1 Dynamics of humoral and cellular immune responses after homologous and heterologous SARS-CoV-2 vaccination with ChAdOx1 nCoV-19 and BNT162b2

Vogel, E., Kocher, K., Priller, A., Cheng, C.-C., et al. (2022) "Dynamics of humoral and cellular immune responses after homologous and heterologous SARS-CoV-2 vaccination with ChAdOx1 nCoV-19 and BNT162b2." *eBioMedicine* **85**: 104294.

3.1.1 Authors

Emanuel Vogel[†], Katharina Kocher[†], Alina Priller[†], Cho-Chin Cheng[†], Philipp Steininger, Bo-Hung Liao, Nina Körber, Annika Willmann, Pascal Irrgang, Jürgen Held, Carolin Moosmann, Viviane Schmidt, Stephanie Beileke, Monika Wytopil, Sarah Heringer, Tanja Bauer, Ronja Brockhoff, Samuel Jeske, Hrvoje Mijocevic, Catharina Christa, Jon Salmanton-García, Kathrin Tinnefeld, Christian Bogdan, Sarah Yazici, Percy Knolle, Oliver A. Cornely, Klaus Überla, Ulrike Protzer*, Kilian Schober*, and Matthias Tenbusch*

* Corresponding authors

† These authors contributed equally

3.1.2 Short Summary

Various vaccines from several leading pharmaceutical companies around the world were approved in the late 2020. Among all, two types of COVID vaccines shared the main market: mRNA vaccine developed by Pfizer-BioNTech and Moderna, and adenoviral vector-based vaccine from Oxford–AstraZeneca. The initial course of two doses was recommended with an interval of 3-4 weeks for mRNA vaccine and 4-12 weeks for adenoviral vaccine. Due to stronger side-effects in some individuals vaccinated with adenoviral vaccine, many countries further recommended a heterologous vaccination scheme administering mRNA vaccine for the second dose. At the time when the second dose was implemented, only very few studies reported the investigation of humoral immunity after heterogeneous vaccination. And the comparison of these two different regimens was not yet accomplished. Therefore, a corresponding joint project named "STIKO" study was compiled for the aim of investigating heterologous and homologous vaccination regimens early and late after vaccination.

Participants who received two doses of ChAdOx1 nCoV-19 or BNT162b2 or a heterologous combination of both vaccines were included in the study, and the results

indicated that both vaccines induced a robust immune response, with a significant increase in antibody and T-cell responses following the second dose. The heterologous combination of vaccines stimulated a more potent immune response than either vaccine alone, along with greater antibody avidity than homologous BNT-BNT vaccination. The ChAdOx1 nCoV-19 vaccine induced a stronger T-cell response than the BNT162b2 vaccine, but the BNT162b2 vaccine induced a stronger antibody response, according to our study. Surprisingly, the Omicron variant demonstrated a much stronger immune escape than the Delta variant across all three vaccination strategies, implying an urgent need for a vaccine with a modified design.

3.1.3 Contributions

Overview: experimental design, methodology, investigation, formal analysis, data curation, writing—original draft preparation

Highlights:

One of the most notable aspects of this work is the validation of humoral immunity utilizing a real SARS-CoV-2 virus in a neutralization assay. Cheng, C.-C. designed and carried out all BSL3 laboratory task, ranging from the isolation of variations to the growth and titration of viral stocks, as well as the entire serum-virus neutralization experiment.

In the formal analysis section, Cheng, C.-C. examined the raw data and employed Prism software to calculate inhibition curves in order to convert the data into statistical results.

3.2 Improved SARS-CoV-2 Neutralization of Delta and Omicron BA.1 Variants of Concern after Fourth Vaccination in Hemodialysis Patients

Cheng, C.-C., Platen, L., et al. (2022) "Improved SARS-CoV-2 Neutralization of Delta and Omicron BA.1 Variants of Concern after Fourth Vaccination in Hemodialysis Patients." *Vaccines* **10** (8): 1328.

3.2.1 Authors

Cho-Chin Cheng[†], Louise Platen[†], Catharina Christa, Myriam Tellenbach, Verena Kappler, Romina Bester, Bo-Hung Liao, Christopher Holzmann-Littig, Maia Werz, Emely Schönhals, Eva Platen, Peter Eggerer, Laëtitia Tréguer, Claudius Kuchle, Christoph Schmaderer, Uwe Heemann, Lutz Renders, Ulrike Protzer*, and Matthias Christoph Braunisch*

* Corresponding authors

[†] These authors contributed equally

3.2.2 Short Summary and Contributions

In the beginning of 2022, authorities were formulating regulations of third and even fourth vaccination for individuals in demand, including elders and patients with immune deficiency. However, more detailed studies whether continuous booster immunizations benefit these subpopulations were required. Inspecting the humoral immunity status of special immunocompromised cohorts after booster vaccination is essential for the adjustment of vaccination strategies. Therefore, a cooperation with Institute of Nephrology at Technischen Universität München for the study cohort named "COVIIMP" (German: COVID-19-Impfansprechen immunsupprimierter Patientinnen) was included in our serological study. This cohort study is a prospective observational study examining the efficacy of COVID-19 immunization and the clinical course of COVID-19 in patients immunocompromised due to kidney transplantation, rheumatologic disease, or dialysis who received SARS-CoV-2 immunization as recommended by the German health authorities.

Our results showed four doses of the COVID-19 vaccine significantly increased the level of neutralizing antibodies in hemodialysis patients, resulting in enhanced neutralization of both the Delta and Omicron BA.1 variants of concern. Our investigation also revealed that the level of neutralizing antibodies in hemodialysis patients following the fourth dose was comparable to that of healthy individuals after the standard two-dose regimen. In conclusion, a fourth dose of the COVID-19 vaccine may be an effective strategy for improving the immune response of susceptible populations, such as hemodialysis patients,

against emerging SARS-CoV-2 variants.

3.2.3 Contributions

Overview: conceptualization, investigation, data analysis, methodology, validation, writing—original draft preparation, writing—review and editing

Highlights:

Cheng, C.-C. performed all the neutralization tests for the serum samples from hemodialysis patients, followed by a comprehensive statistical analysis and stratification.

3.3 Targeting genomic SARS-CoV-2 RNA with siRNAs allows efficient inhibition of viral replication and spread

Ambike, S., Cheng, C.-C., et al. (2021) "Targeting genomic SARS-CoV-2 RNA with siRNAs allows efficient inhibition of viral replication and spread." *Nucleic Acids Research*, **50** (1): 333–349.

3.3.1 Authors

Shubhankar Ambike[†], Cho-Chin Cheng[†], Martin Feuerherd, Stoyan Velkov, Domizia Baldassi, Suliman Qadir Afridi, Diana Porras-Gonzalez, Xin Wei, Philipp Hagen, Nikolaus Kneidinger, Mircea Gabriel Stoleriu, Vincent Grass, Gerald Burgstaller, Andreas Pichlmair, Olivia M. Merkel, Chunkyu Ko, and Thomas Michler*

* Corresponding authors

[†] These authors contributed equally

3.3.2 Short Summary and Contributions

Small interfering RNAs (siRNAs) are a promising strategy for developing SARS-CoV-2 antiviral therapies. While previous studies have demonstrated that siRNAs can target SARS-CoV-2, no in-depth investigation has been conducted to determine which coronaviral replication steps can be targeted with siRNAs. This study sought to investigate whether siRNAs can effectively inhibit SARS-CoV-2 replication and spread by systematically analyzing the individual replication steps following cell entry.

Our study discovered that prophylactic administration of siRNAs can effectively target the virus genome during an early replication step, thereby preventing virus-induced cell death and its spread. Specifically, targeting only the genomic RNA (gRNA) resulted in greater antiviral activity than simultaneously targeting a region containing both gRNA and subgenomic RNA (sgRNA). Further analysis revealed that the reduced RNAi silencing of siRNAs targeting gRNA and sgRNAs is a result of sgRNA competition. This surprising finding suggests that inhibiting SARS-CoV-2 replication by targeting only gRNA may be more effective. In addition, we aimed to evaluate the negative sense RNA of SARS-CoV-2 as a siRNA target. Notably, our findings indicate that negative sense SARS-CoV-2 RNAs are resistant to RNA interference possibly due to the inaccessibility of RNAi machinery. To move the approach one step closer to clinical application, we transferred it to an ex-vivo platform incorporating chemically modified siRNA candidates in human lung tissues, where we observed a comparable inhibition as in cell-line results. Overall, our study indicates that targeting the viral genome with siRNAs may be a promising strategy for preventing the replication and dissemination of SARS-CoV-2. The

findings shed light on the molecular mechanisms of SARS-CoV-2 replication and suggest potential strategies for developing antiviral therapies against COVID-19.

3.3.3 Contributions

Overview: conceptualization, methodology, experimental design, investigation, data curation, validation, writing—original draft preparation, writing—review and editing

Highlights:

In this study, Cheng, C.-C. prepared the BSL3 materials including wildtype SARS-CoV-2 and recombinant GFP-SARS-CoV-2, hereafter established the cell culture based and human tissue ex-vivo infection models. For the experimental readout, Cheng, C.-C. further verified the SARS-CoV-2 specific RT-qPCR assay and live-imaging IncuCyte system for infectivity and pathogenicity evaluation.

4 Discussion

4.1 Serological examination of the SARS-CoV-2 vaccinated population

The SARS-CoV-2 pandemic struck the world expeditiously and fiercely, but fortunately, the development and implementation of vaccinations proceeded rapidly as well. However, various tests cannot be achieved within these clinical studies lasting less than one year. Therefore, we were dedicated to designing and conducting immunological studies of the efficacy and duration of vaccinations, different types of vaccines and vaccination regimens, as well as the investigation of specific immunocompromised cohorts following immunizations. In the ongoing fight against COVID-19, it is anticipated that these studies will have significant implications for public health policy and vaccine distribution strategies. In our first study, we evaluated the dynamics of antiviral immunity in convalescents with asymptomatic or mild SARS-CoV-2 infection throughout long-term follow-up and following immunization with BNT162b2 mRNA. While the majority of individuals with mild or asymptomatic COVID-19 developed long-lasting virus-specific cytokine-producing poly-functional T cell immunity, virus-specific and neutralizing antibody titers significantly dropped over 9 months after infection. As foreseen, the BNT162b2 vaccination induced potent humoral and cellular immunity in almost all recipients. Notably, the activated immune profile of convalescents is comparable to that of naive individuals who received two doses of the vaccine, indicating that the boost of the immune system of convalescents by a single dose of vaccine is effective [78]. Numerous articles reported equivalent findings, prompting authorities to determine that individuals infected with SARS-CoV-2 could be considered to have received a single dose of vaccination and their vaccination passports should reflect this. As a result, many vaccines can be saved for future use, resulting in a more equitable distribution of vaccines.

To follow up our investigation, extended serological tests were administered to the vaccinated group to determine the immunity's dynamics after the second dose. In the meantime, a substantial number of individuals who received their primary vaccination with a viral vector vaccine replaced their second shot with an mRNA vaccine since the more severe side effects and reduced efficacy of viral vector vaccines, as well as the increased availability of mRNA vaccines. Hence, we recruited distinct cohorts with diverse homologous and heterologous vaccination schemes due to the growing number of individuals with alternative vaccination strategies and doses. Eventually, we tracked 472 vaccinated participants from three independent study centers at university hospitals rechts der Isar (Munich), Erlangen, and Colonge. In this follow up study, we observed inferior humoral immunity upon two doses of ChAdOx1 nCoV-19 versus BNT162b2 as expected, whereas neither was superior to the heterologous ChAdOx1-BNT162b2

regimen, surprisingly. Regarding the difficulty of synchronizing blood sampling and analysis schedules, centers and cohorts varied in their sampling schedules and time points for serological tests. In light of the fact, minor differences occurred while analyzing the dynamics of humoral immunity, yet the conclusion that the neutralizing ability of plasma from all three regimens declined 98-158 days after second vaccination was not affected. Furthermore, regardless of vaccination regimen, vaccine-induced humoral immunity was less reactive against the Omicron variant than the Delta variant throughout all time periods. These findings suggest that continuous vaccination boosters may need to be considered, as well as the imperative need for new generation vaccines containing the S protein of Omicron variant.

As the booster vaccination began to be implemented, the Omicron variant was reported to have increased transmissibility but decreased severity and lethality, bringing up the topic of whether healthy individuals require additional booster vaccinations. Consequently, the policy was progressively shifting to vaccinate only high-risk groups such as the elderly, patients with chronic diseases, and immunocompromised patients; vaccination of healthy individuals was no longer mandatory. Meanwhile, another concern was raised: how do these high-risk populations respond to the second and third booster vaccinations? Therefore, a cooperation was initiated with Institute of Nephrology, and cohorts were recruited in four dialysis centers: Klinikum rechts der Isar, KfH Kidney Center Traunstein, Kidney Center Eifeldialyse, and KfH Kidney Center München-Harlaching. In total, 513 immunocompromised patients were enrolled in this COVIIMP study. Our serological analysis included 142 patients on maintenance hemodialysis who were receiving their third booster (fourth) vaccination with the majority of mRNA vaccines. Fortunately, we discovered that a fourth dose of vaccine substantially increased neutralization of the Delta and, to a lesser extent, the Omicron BA.1 variants of concern, with a 10-fold increase in neutralizing antibody titers and an improvement in the number of responders. Although we did observe a reduction in neutralizing antibody titers in patients treated with immunosuppressive medications, we were surprised to learn that B cell immunity was not diminished after hemodialysis, which is considered a prospective immune-reduction procedure. Nevertheless, long-term serological monitoring is necessary for these immunocompromised populations. Thus, a portion of this cohort was followed for an extended period of time after the fourth vaccination, and their immunity against the most recent VOCs and VOIs was examined after the fifth vaccination, with encouraging results. In the foreseeable future, these data will be reported and made available via open access.

4.2 Inhibition of SARS-CoV-2 replication by siRNA machinery

The discovery of small interfering RNA in the late 1990s has revolutionized the field of

molecular biology, as it provides a potent instrument for investigating gene function and has potential therapeutic applications. Nonetheless, its investigation as a potential therapeutic agent for diseases is an ongoing endeavor involving multiple academic and industrial groups. siRNA has several advantages over traditional drugs, involving its high specificity and rapid onset of action, as well as a lower risk of toxicity as a result of these characteristics and the fact that RNA is readily degraded [83]. Additionally, the design and production of siRNA can be extremely simple and straightforward when the target sequence is available. The most important question in mapping effective siRNAs for therapeutic purposes, take a virus infection as an example, lies in which genome region is most accessible and which viral replication step can be easier targeted. In consequence, we evaluated 20 siRNA candidates addressing multiple important regions of the SARS-CoV-2 genome and analyzed the individual replication steps following cell entry in a systematic manner. Unexpectedly, our data showed that siRNAs targeting ORF1a and 1b, which are present exclusively in gRNA, exhibited the most efficient knockdown effectiveness of viral replication among all, even though other siRNAs are capable of targeting common regions we can find in all sgRNAs and gRNA. We investigated one of our hypotheses, the out-competition by the exceedingly abundant sgRNAs, and it explains this phenomenon. Another theory is that ORF1a and 1b region has better accessibility to the RNAi machinery following viral entry and throughout the viral life cycle. This could be attributed to less protection from molecular binds or fewer secondary structures in ORF1a and 1b, but additional molecular mechanism studies are required to corroborate this theory. To sum up our research, we demonstrated conclusively that siRNAs can target an early replication step and inhibit replication before transcription begins, thereby preventing virus-induced cell death. Moreover, ORF1-targeting siRNAs appear to be the best candidate not only due to their highest efficacy, but also their significantly greater level of sequence-wise conservation among all circulating strains.

The scarcity of an appropriate delivery method and the poor stability of siRNAs are challenges in the development of siRNA-based therapeutics. Chemical modification is a well-known method for stabilizing RNA in order to increase their resistance to nuclease degradation; therefore, we applied it to our best ORF1-targeting siRNA and investigated them in an ex-vivo model utilizing human precision-cut lung slice (hPCLS). This test, instead of liposomal formulations, we delivered our siRNA using polyethylenimine (PEI), which has a well-defined toxicity profile allowing in vivo application and is capable of being nebulized, which is a crucial property for a lung-directed therapy. The results revealed viral replication was effectively inhibited, implying that the modified siRNA could be utilized in the future ex-vivo and in-vivo experiments. In the interim, we observed an unintended enhancement of SARS-CoV-2 infectivity by using PEI alone through an unknown mechanism; therefore, it is imperative to pinpoint an alternative

delivery medium and method. Thus, a collaboration with Prof. Olivia Merkel's team that employs the combination of siRNA and VIPER polyplexes aids in the resolution of the issue. Prior research demonstrated that the block copolymer VIPER is capable of forming polyplexes with optimal properties for pulmonary administration and enhanced stability in the challenging lung environment in comparison to PEI polyplexes. In this study, the siRNA/VIPER polyplexes were effectively delivered to lung epithelial cells and were well tolerated in vitro and in vivo. Furthermore, the inhibition activity against SARS-CoV-2 infection was successful in a special air-liquid interface cell culture and hPCLS model. In general, the study indicates that the combination of our candidate siRNA and VIPER polyplexes may have therapeutic potential as a COVID-19 treatment by inhibiting viral replication in the lung [84]. Nonetheless, additional research is required to determine the safety and efficacy of this method in humanized mouse models and in humans.

Additionally, we also sought to use the siRNA technology to construct a pan-reactive siRNA that can simultaneously target a variety of coronavirus strains, serving as a potential strategy for the next coronavirus epidemic or pandemic that is likely to occur. To accomplish this, we cooperated with Dr. Stoyan Velkov for his bioinformatic assistance and aligned as many coronavirus sequences from four genera in the *Coronaviridae* family as possible in order to identify an ideal conservation genome region for siRNA targeting. Despite the impossibility of identifying a conservation region for all coronaviruses, we screen sites that may have cross-reactivity with some significant coronaviruses, such as SARS-CoV, MERS, and SARS-CoV-2. Eventually, we selected approximately 300 siRNAs for investigating their inhibition ability and narrowed the list down to fewer than 15 highly effective siRNAs with specificity toward various coronavirus fields. This project has already been granted a patent, and we believe that in the future we will be able to combine the findings in the delivery development with our screened candidates for more clinical application, which will not only serve as a treatment for COVID-19, but also for any future coronavirus epidemics.

5 Bibliography

- [1] R.A. Khailany, M. Safdar, M. Ozaslan, Genomic characterization of a novel SARS-CoV-2, *Gene Rep* 19 (2020) 100682.
- [2] N. Zhu, D. Zhang, W. Wang, X. Li, B. Yang, J. Song, X. Zhao, B. Huang, W. Shi, R. Lu, P. Niu, F. Zhan, X. Ma, D. Wang, W. Xu, G. Wu, G.F. Gao, W. Tan, A Novel Coronavirus from Patients with Pneumonia in China, 2019, *N Engl J Med* 382(8) (2020) 727-733.
- [3] Y.M. Bar-On, A. Flamholz, R. Phillips, R. Milo, SARS-CoV-2 (COVID-19) by the numbers, *Elife* 9 (2020).
- [4] P. V'kovski, A. Kratzel, S. Steiner, H. Stalder, V. Thiel, Coronavirus biology and replication: implications for SARS-CoV-2, *Nature Reviews Microbiology* 19(3) (2021) 155-170.
- [5] N.R. Kumar S, Maurya VK, Saxena SK., Morphology, Genome Organization, Replication, and Pathogenesis of Severe Acute Respiratory Syndrome Coronavirus 2 (SARS-CoV-2). *Coronavirus Disease 2019 (COVID-19)* (2020) 23-31.
- [6] A.C. Brant, W. Tian, V. Majerciak, W. Yang, Z.-M. Zheng, SARS-CoV-2: from its discovery to genome structure, transcription, and replication, *Cell & Bioscience* 11(1) (2021) 136.
- [7] L. Alanagreh, F. Alzoughool, M. Atoum, The Human Coronavirus Disease COVID-19: Its Origin, Characteristics, and Insights into Potential Drugs and Its Mechanisms, *Pathogens* 9(5) (2020).
- [8] R. Raj, Analysis of non-structural proteins, NSPs of SARS-CoV-2 as targets for computational drug designing, *Biochem Biophys Rep* 25 (2021) 100847.
- [9] W. Yan, Y. Zheng, X. Zeng, B. He, W. Cheng, Structural biology of SARS-CoV-2: open the door for novel therapies, *Signal Transduction and Targeted Therapy* 7(1) (2022) 26.
- [10] S. Satarker, M. Nampoothiri, Structural Proteins in Severe Acute Respiratory Syndrome Coronavirus-2, *Arch Med Res* 51(6) (2020) 482-491.
- [11] Y. Huang, C. Yang, X.-f. Xu, W. Xu, S.-w. Liu, Structural and functional properties of SARS-CoV-2 spike protein: potential antiviral drug development for COVID-19, *Acta Pharmacologica Sinica* 41(9) (2020) 1141-1149.
- [12] R. Yan, Y. Zhang, Y. Li, L. Xia, Y. Guo, Q. Zhou, Structural basis for the recognition of SARS-CoV-2 by full-length human ACE2, *Science* 367(6485) (2020) 1444-1448.
- [13] Y. Cai, J. Zhang, T. Xiao, H. Peng, S.M. Sterling, R.M. Walsh, S. Rawson, S. Rits-Volloch, B. Chen, Distinct conformational states of SARS-CoV-2 spike protein, *Science* 369(6511) (2020) 1586-1592.
- [14] N.J. Hardenbrook, P. Zhang, A structural view of the SARS-CoV-2 virus and its assembly, *Current Opinion in Virology* 52 (2022) 123-134.

Bibliography

- [15] Y. Cao, R. Yang, I. Lee, W. Zhang, J. Sun, W. Wang, X. Meng, Characterization of the SARS-CoV-2 E Protein: Sequence, Structure, Viroporin, and Inhibitors, *Protein Sci* 30(6) (2021) 1114-1130.
- [16] Z. Bai, Y. Cao, W. Liu, J. Li, The SARS-CoV-2 Nucleocapsid Protein and Its Role in Viral Structure, Biological Functions, and a Potential Target for Drug or Vaccine Mitigation, *Viruses* 13(6) (2021).
- [17] M. Zandi, M. Shafaati, D. Kalantar-Neyestanaki, H. Pourghadamyari, M. Fani, S. Soltani, H. Kaleji, S. Abbasi, The role of SARS-CoV-2 accessory proteins in immune evasion, *Biomed Pharmacother* 156 (2022) 113889.
- [18] P. Zhou, X.-L. Yang, X.-G. Wang, B. Hu, L. Zhang, W. Zhang, H.-R. Si, Y. Zhu, B. Li, C.-L. Huang, H.-D. Chen, J. Chen, Y. Luo, H. Guo, R.-D. Jiang, M.-Q. Liu, Y. Chen, X.-R. Shen, X. Wang, X.-S. Zheng, K. Zhao, Q.-J. Chen, F. Deng, L.-L. Liu, B. Yan, F.-X. Zhan, Y.-Y. Wang, G.-F. Xiao, Z.-L. Shi, A pneumonia outbreak associated with a new coronavirus of probable bat origin, *Nature* 579(7798) (2020) 270-273.
- [19] M. Letko, A. Marzi, V. Munster, Functional assessment of cell entry and receptor usage for SARS-CoV-2 and other lineage B betacoronaviruses, *Nature Microbiology* 5(4) (2020) 562-569.
- [20] J. Shang, G. Ye, K. Shi, Y. Wan, C. Luo, H. Aihara, Q. Geng, A. Auerbach, F. Li, Structural basis of receptor recognition by SARS-CoV-2, *Nature* 581(7807) (2020) 221-224.
- [21] M. Hoffmann, H. Kleine-Weber, S. Schroeder, N. Krüger, T. Herrler, S. Erichsen, T.S. Schiergens, G. Herrler, N.H. Wu, A. Nitsche, M.A. Müller, C. Drosten, S. Pöhlmann, SARS-CoV-2 Cell Entry Depends on ACE2 and TMPRSS2 and Is Blocked by a Clinically Proven Protease Inhibitor, *Cell* 181(2) (2020) 271-280.e8.
- [22] P. Roingard, S. Eymieux, J. Burlaud-Gaillard, C. Hourieux, R. Patient, E. Blanchard, The double-membrane vesicle (DMV): a virus-induced organelle dedicated to the replication of SARS-CoV-2 and other positive-sense single-stranded RNA viruses, *Cell Mol Life Sci* 79(8) (2022) 425.
- [23] D. Kim, J.Y. Lee, J.S. Yang, J.W. Kim, V.N. Kim, H. Chang, The Architecture of SARS-CoV-2 Transcriptome, *Cell* 181(4) (2020) 914-921.e10.
- [24] Y. Shi, D.H. Yang, J. Xiong, J. Jia, B. Huang, Y.X. Jin, Inhibition of genes expression of SARS coronavirus by synthetic small interfering RNAs, *Cell Research* 15(3) (2005) 193-200.
- [25] I.P. Trougakos, K. Stamatelopoulos, E. Terpos, O.E. Tsitsilonis, E. Aivalioti, D. Paraskevis, E. Kastritis, G.N. Pavlakis, M.A. Dimopoulos, Insights to SARS-CoV-2 life cycle, pathophysiology, and rationalized treatments that target COVID-19 clinical complications, *Journal of Biomedical Science* 28(1) (2021) 9.
- [26] J. Liu, Y. Li, Q. Liu, Q. Yao, X. Wang, H. Zhang, R. Chen, L. Ren, J. Min, F. Deng, B. Yan, L. Liu, Z. Hu, M. Wang, Y. Zhou, SARS-CoV-2 cell tropism and multiorgan infection, *Cell Discovery* 7(1) (2021) 17.
- [27] A.G. Harrison, T. Lin, P. Wang, Mechanisms of SARS-CoV-2 Transmission and Pathogenesis, *Trends Immunol* 41(12) (2020) 1100-1115.
- [28] Q. Zheng, R. Lin, Y. Chen, Q. Lv, J. Zhang, J. Zhai, W. Xu, W. Wang, SARS-CoV-2 induces "cytokine storm"

- hyperinflammatory responses in RA patients through pyroptosis, *Front Immunol* 13 (2022) 1058884.
- [29] X. Yin, L. Riva, Y. Pu, L. Martin-Sancho, J. Kanamune, Y. Yamamoto, K. Sakai, S. Gotoh, L. Miorin, P.D. De Jesus, C.C. Yang, K.M. Herbert, S. Yoh, J.F. Hultquist, A. García-Sastre, S.K. Chanda, MDA5 Governs the Innate Immune Response to SARS-CoV-2 in Lung Epithelial Cells, *Cell Rep* 34(2) (2021) 108628.
- [30] M.M. Lamers, B.L. Haagmans, SARS-CoV-2 pathogenesis, *Nature Reviews Microbiology* 20(5) (2022) 270-284.
- [31] A. Aslan, C. Aslan, N.M. Zolbanin, R. Jafari, Acute respiratory distress syndrome in COVID-19: possible mechanisms and therapeutic management, *Pneumonia* 13(1) (2021) 14.
- [32] M.K. Bohn, A. Hall, L. Sepiashvili, B. Jung, S. Steele, K. Adeli, Pathophysiology of COVID-19: Mechanisms Underlying Disease Severity and Progression, *Physiology* 35(5) (2020) 288-301.
- [33] N.M. Linton, T. Kobayashi, Y. Yang, K. Hayashi, A.R. Akhmetzhanov, S.M. Jung, B. Yuan, R. Kinoshita, H. Nishiura, Incubation Period and Other Epidemiological Characteristics of 2019 Novel Coronavirus Infections with Right Truncation: A Statistical Analysis of Publicly Available Case Data, *J Clin Med* 9(2) (2020).
- [34] C. Huang, Y. Wang, X. Li, L. Ren, J. Zhao, Y. Hu, L. Zhang, G. Fan, J. Xu, X. Gu, Z. Cheng, T. Yu, J. Xia, Y. Wei, W. Wu, X. Xie, W. Yin, H. Li, M. Liu, Y. Xiao, H. Gao, L. Guo, J. Xie, G. Wang, R. Jiang, Z. Gao, Q. Jin, J. Wang, B. Cao, Clinical features of patients infected with 2019 novel coronavirus in Wuhan, China, *Lancet* 395(10223) (2020) 497-506.
- [35] V.G. Puelles, M. Lütgehetmann, M.T. Lindenmeyer, J.P. Sperhake, M.N. Wong, L. Allweiss, S. Chilla, A. Heinemann, N. Wanner, S. Liu, F. Braun, S. Lu, S. Pfefferle, A.S. Schröder, C. Edler, O. Gross, M. Glatzel, D. Wichmann, T. Wiech, S. Kluge, K. Püeschel, M. Aepfelbacher, T.B. Huber, Multiorgan and Renal Tropism of SARS-CoV-2, *N Engl J Med* 383(6) (2020) 590-592.
- [36] M. Lopes-Pacheco, P.L. Silva, F.F. Cruz, D. Battaglini, C. Robba, P. Pelosi, M.M. Morales, C. Caruso Neves, P.R.M. Rocco, Pathogenesis of Multiple Organ Injury in COVID-19 and Potential Therapeutic Strategies, *Front Physiol* 12 (2021) 593223.
- [37] J.C. Kariyawasam, U. Jayarajah, R. Riza, V. Abeysuriya, S.L. Seneviratne, Gastrointestinal manifestations in COVID-19, *Trans R Soc Trop Med Hyg* 115(12) (2021) 1362-1388.
- [38] F. Silva, B.B. Brito, M.L.C. Santos, H.S. Marques, R.T.D. Silva Júnior, L.S. Carvalho, E.S. Vieira, M.V. Oliveira, F.F. Melo, COVID-19 gastrointestinal manifestations: a systematic review, *Rev Soc Bras Med Trop* 53 (2020) e20200714.
- [39] M.H. Cha, M. Regueiro, D.S. Sandhu, Gastrointestinal and hepatic manifestations of COVID-19: A comprehensive review, *World J Gastroenterol* 26(19) (2020) 2323-2332.
- [40] V.C. Suresh Kumar, S. Mukherjee, P.S. Harne, A. Subedi, M.K. Ganapathy, V.S. Patthipati, B. Sapkota, Novelty in the gut: a systematic review and meta-analysis of the gastrointestinal manifestations of COVID-19, *BMJ Open*

Bibliography

Gastroenterol 7(1) (2020).

[41] Y.-Y. Zheng, Y.-T. Ma, J.-Y. Zhang, X. Xie, COVID-19 and the cardiovascular system, *Nature Reviews Cardiology* 17(5) (2020) 259-260.

[42] Z.Y. Ding, G.X. Li, L. Chen, C. Shu, J. Song, W. Wang, Y.W. Wang, Q. Chen, G.N. Jin, T.T. Liu, J.N. Liang, P. Zhu, W. Zhu, Y. Li, B.H. Zhang, H. Feng, W.G. Zhang, Z.Y. Yin, W.K. Yu, Y. Yang, H.Q. Zhang, Z.P. Tang, H. Wang, J.B. Hu, J.H. Liu, P. Yin, X.P. Chen, B. Zhang, Association of liver abnormalities with in-hospital mortality in patients with COVID-19, *J Hepatol* 74(6) (2021) 1295-1302.

[43] N. Wanner, G. Andrieux, P. Badia-i-Mompel, C. Edler, S. Pfefferle, M.T. Lindenmeyer, C. Schmidt-Lauber, J. Czogalla, M.N. Wong, Y. Okabayashi, F. Braun, M. Lütgehetmann, E. Meister, S. Lu, M.L.M. Noriega, T. Günther, A. Grundhoff, N. Fischer, H. Bräuninger, D. Lindner, D. Westermann, F. Haas, K. Roedl, S. Kluge, M.M. Addo, S. Huber, A.W. Lohse, J. Reiser, B. Ondruschka, J.P. Spermhake, J. Saez-Rodriguez, M. Boerries, S.S. Hayek, M. Aepfelbacher, P. Scaturro, V.G. Puelles, T.B. Huber, Molecular consequences of SARS-CoV-2 liver tropism, *Nature Metabolism* 4(3) (2022) 310-319.

[44] Y. Wang, S. Liu, H. Liu, W. Li, F. Lin, L. Jiang, X. Li, P. Xu, L. Zhang, L. Zhao, Y. Cao, J. Kang, J. Yang, L. Li, X. Liu, Y. Li, R. Nie, J. Mu, F. Lu, S. Zhao, J. Lu, J. Zhao, SARS-CoV-2 infection of the liver directly contributes to hepatic impairment in patients with COVID-19, *J Hepatol* 73(4) (2020) 807-816.

[45] X. Wang, J. Lei, Z. Li, L. Yan, Potential Effects of Coronaviruses on the Liver: An Update, *Front Med (Lausanne)* 8 (2021) 651658.

[46] N.M. Elemam, I.M. Talaat, A.A. Maghazachi, M. Saber-Ayad, Liver Injury Associated with COVID-19 Infection: Pathogenesis, Histopathology, Prognosis, and Treatment, *Journal of Clinical Medicine* 12(5) (2023) 2067.

[47] H.E. Davis, L. McCorkell, J.M. Vogel, E.J. Topol, Long COVID: major findings, mechanisms and recommendations, *Nature Reviews Microbiology* 21(3) (2023) 133-146.

[48] S. Lytras, W. Xia, J. Hughes, X. Jiang, D.L. Robertson, The animal origin of SARS-CoV-2, *Science* 373(6558) (2021) 968-970.

[49] D. Singh, S.V. Yi, On the origin and evolution of SARS-CoV-2, *Experimental & Molecular Medicine* 53(4) (2021) 537-547.

[50] X. Xu, P. Chen, J. Wang, J. Feng, H. Zhou, X. Li, W. Zhong, P. Hao, Evolution of the novel coronavirus from the ongoing Wuhan outbreak and modeling of its spike protein for risk of human transmission, *Sci China Life Sci* 63(3) (2020) 457-460.

[51] P.V. Markov, M. Ghafari, M. Beer, K. Lythgoe, P. Simmonds, N.I. Stilianakis, A. Katzourakis, The evolution of SARS-CoV-2, *Nature Reviews Microbiology* 21(6) (2023) 361-379.

[52] A. Telenti, E.B. Hodcroft, D.L. Robertson, The Evolution and Biology of SARS-CoV-2 Variants, *Cold Spring Harb*

Perspect Med 12(5) (2022).

[53] B. Korber, W.M. Fischer, S. Gnanakaran, H. Yoon, J. Theiler, W. Abfalterer, N. Hengartner, E.E. Giorgi, T. Bhattacharya, B. Foley, K.M. Hastie, M.D. Parker, D.G. Partridge, C.M. Evans, T.M. Freeman, T.I. de Silva, C. McDanal, L.G. Perez, H. Tang, A. Moon-Walker, S.P. Whelan, C.C. LaBranche, E.O. Saphire, D.C. Montefiori, Tracking Changes in SARS-CoV-2 Spike: Evidence that D614G Increases Infectivity of the COVID-19 Virus, *Cell* 182(4) (2020) 812-827.e19.

[54] N.G. Davies, S. Abbott, R.C. Barnard, C.I. Jarvis, A.J. Kucharski, J.D. Munday, C.A.B. Pearson, T.W. Russell, D.C. Tully, A.D. Washburne, T. Wenseleers, A. Gimma, W. Waites, K.L.M. Wong, K. van Zandvoort, J.D. Silverman, C.C.-W. Group¹‡, C.-G.U. Consortium[‡], K. Diaz-Ordaz, R. Keogh, R.M. Eggo, S. Funk, M. Jit, K.E. Atkins, W.J. Edmunds, Estimated transmissibility and impact of SARS-CoV-2 lineage B.1.1.7 in England, *Science* 372(6538) (2021) eabg3055.

[55] P. Mlcochova, S.A. Kemp, M.S. Dhar, G. Papa, B. Meng, I.A.T.M. Ferreira, R. Datir, D.A. Collier, A. Albecka, S. Singh, R. Pandey, J. Brown, J. Zhou, N. Goonawardane, S. Mishra, C. Whittaker, T. Mellan, R. Marwal, M. Datta, S. Sengupta, K. Ponnusamy, V.S. Radhakrishnan, A. Abdullahi, O. Charles, P. Chattopadhyay, P. Devi, D. Caputo, T. Peacock, C. Wattal, N. Goel, A. Satwik, R. Vaishya, M. Agarwal, H. Chauhan, T. Dikid, H. Gogia, H. Lall, K. Verma, M.S. Dhar, M.K. Singh, N. Soni, N. Meena, P. Madan, P. Singh, R. Sharma, R. Sharma, S. Kabra, S. Kumar, S. Kumari, U. Sharma, U. Chaudhary, S. Sivasubbu, V. Scaria, J.K. Oberoi, R. Raveendran, S. Datta, S. Das, A. Maitra, S. Chinnaswamy, N.K. Biswas, A. Parida, S.K. Raghav, P. Prasad, A. Sarin, S. Mayor, U. Ramakrishnan, D. Palakodeti, A.S.N. Seshasayee, K. Thangaraj, M.D. Bashyam, A. Dalal, M. Bhat, Y. Shouche, A. Pillai, P. Abraham, V.A. Potdar, S.S. Cherian, A.S. Desai, C. Pattabiraman, M.V. Manjunatha, R.S. Mani, G.A. Udupi, V. Nandicoori, K.B. Tallapaka, D.T. Sowpati, R. Kawabata, N. Morizako, K. Sadamasu, H. Asakura, M. Nagashima, K. Yoshimura, J. Ito, I. Kimura, K. Uriu, Y. Kosugi, M. Suganami, A. Oide, M. Yokoyama, M. Chiba, A. Saito, E.P. Butlertanaka, Y.L. Tanaka, T. Ikeda, C. Motozono, H. Nasser, R. Shimizu, Y. Yuan, K. Kitazato, H. Hasebe, S. Nakagawa, J. Wu, M. Takahashi, T. Fukuhara, K. Shimizu, K. Tsushima, H. Kubo, K. Shirakawa, Y. Kazuma, R. Nomura, Y. Horisawa, A. Takaori-Kondo, K. Tokunaga, S. Ozono, S. Baker, G. Dougan, C. Hess, N. Kingston, P.J. Lehner, P.A. Lyons, N.J. Matheson, W.H. Owehand, C. Saunders, C. Summers, J.E.D. Thaventhiran, M. Toshner, M.P. Weekes, P. Maxwell, A. Shaw, A. Bucke, J. Calder, L. Canna, J. Domingo, A. Elmer, S. Fuller, J. Harris, S. Hewitt, J. Kennet, S. Jose, J. Kourampa, A. Meadows, C. O'Brien, J. Price, C. Publico, R. Rastall, C. Ribeiro, J. Rowlands, V. Ruffolo, H. Tordesillas, B. Bullman, B.J. Dunmore, S. Fawke, S. Gräf, J. Hodgson, C. Huang, K. Hunter, E. Jones, E. Legchenko, C. Matara, J. Martin, F. Mescia, C. O'Donnell, L. Pointon, N. Pond, J. Shih, R. Sutcliffe, T. Tilly, C. Treacy, Z. Tong, J. Wood, M. Wylot, L. Bergamaschi, A. Betancourt, G. Bower, C. Cossetti, A. De Sa, M. Epping, S. Fawke, N. Gleadall, R. Grenfell, A. Hinch, O. Huhn, S. Jackson, I. Jarvis, B. Krishna, D. Lewis, J. Marsden, F. Nice, G. Okecha, O. Omarjee, M. Perera, M. Potts, N. Richo, V. Romashova, N.S. Yarkoni, R. Sharma, L. Stefanucci, J. Stephens, M. Strezlecki, L. Turner, E.M.D.D. De Bie, K. Bunclark, M. Josipovic, M. Mackay, S. Rossi, M. Selvan, S. Spencer, C. Yong, J. Allison, H. Butcher, D. Caputo, D. Clapham-Riley, E. Dewhurst, A. Furlong, B. Graves, J. Gray, T. Ivers, M. Kasanicki, E. Le Gresley, R. Linger, S. Meloy, F. Muldoon, N. Ovington, S. Papadia, I. Phelan, H. Stark, K.E. Stirrups, P. Townsend, N. Walker, J. Webster, I. Scholtes, S. Hein, R. King, A. Mavousian, J.H. Lee, J. Bassi, C. Silacci-Fegni, C. Saliba, D. Pinto, T. Irie, I. Yoshida, W.L.

Bibliography

- Hamilton, K. Sato, S. Bhatt, S. Flaxman, L.C. James, D. Corti, L. Piccoli, W.S. Barclay, P. Rakshit, A. Agrawal, R.K. Gupta, S.-C.-G.C. The Indian, C. The Genotype to Phenotype Japan, C.-N.B.C.-C. The, SARS-CoV-2 B.1.617.2 Delta variant replication and immune evasion, *Nature* 599(7883) (2021) 114-119.
- [56] Y. Fan, X. Li, L. Zhang, S. Wan, L. Zhang, F. Zhou, SARS-CoV-2 Omicron variant: recent progress and future perspectives, *Signal Transduction and Targeted Therapy* 7(1) (2022) 141.
- [57] S.-O.M. Lorente-González M, Landete P., Evolution and Clinical Trend of SARS-CoV-2 Variants., *Open Respiratory Archives* 4(2) (2022).
- [58] H.A. Rothan, S.N. Byrareddy, The epidemiology and pathogenesis of coronavirus disease (COVID-19) outbreak, *J Autoimmun* 109 (2020) 102433.
- [59] V. Stadnytskyi, C.E. Bax, A. Bax, P. Anfinrud, The airborne lifetime of small speech droplets and their potential importance in SARS-CoV-2 transmission, *Proceedings of the National Academy of Sciences* 117(22) (2020) 11875-11877.
- [60] A.W.H. Chin, J.T.S. Chu, M.R.A. Perera, K.P.Y. Hui, H.L. Yen, M.C.W. Chan, M. Peiris, L.L.M. Poon, Stability of SARS-CoV-2 in different environmental conditions, *Lancet Microbe* 1(1) (2020) e10.
- [61] I.M. Mackay, K.E. Arden, A. Nitsche, Real-time PCR in virology, *Nucleic Acids Res* 30(6) (2002) 1292-305.
- [62] D. Dutta, S. Naiyer, S. Mansuri, N. Soni, V. Singh, K.H. Bhat, N. Singh, G. Arora, M.S. Mansuri, COVID-19 Diagnosis: A Comprehensive Review of the RT-qPCR Method for Detection of SARS-CoV-2, *Diagnostics (Basel)* 12(6) (2022).
- [63] I. Wagenhäuser, K. Knies, V. Rauschenberger, M. Eisenmann, M. McDonogh, N. Petri, O. Andres, S. Flemming, M. Gawlik, M. Papsdorf, R. Taurines, H. Böhm, J. Forster, D. Weismann, B. Weißbrich, L. Dölken, J. Liese, O. Kurzai, U. Vogel, M. Krone, Clinical performance evaluation of SARS-CoV-2 rapid antigen testing in point of care usage in comparison to RT-qPCR, *eBioMedicine* 69 (2021).
- [64] S. Lai, N.W. Ruktanonchai, L. Zhou, O. Prosper, W. Luo, J.R. Floyd, A. Wesolowski, M. Santillana, C. Zhang, X. Du, H. Yu, A.J. Tatem, Effect of non-pharmaceutical interventions for containing the COVID-19 outbreak in China, *medRxiv* (2020).
- [65] J. Hellewell, S. Abbott, A. Gimma, N.I. Bosse, C.I. Jarvis, T.W. Russell, J.D. Munday, A.J. Kucharski, W.J. Edmunds, S. Funk, R.M. Eggo, Feasibility of controlling COVID-19 outbreaks by isolation of cases and contacts, *Lancet Glob Health* 8(4) (2020) e488-e496.
- [66] D.K. Chu, E.A. Akl, S. Duda, K. Solo, S. Yaacoub, H.J. Schünemann, Physical distancing, face masks, and eye protection to prevent person-to-person transmission of SARS-CoV-2 and COVID-19: a systematic review and meta-analysis, *Lancet* 395(10242) (2020) 1973-1987.
- [67] B. Pulendran, R. Ahmed, Immunological mechanisms of vaccination, *Nature Immunology* 12(6) (2011) 509-517.

- [68] F.P. Polack, S.J. Thomas, N. Kitchin, J. Absalon, A. Gurtman, S. Lockhart, J.L. Perez, G. Pérez Marc, E.D. Moreira, C. Zerbini, R. Bailey, K.A. Swanson, S. Roychoudhury, K. Koury, P. Li, W.V. Kalina, D. Cooper, R.W. Frenck, L.L. Hammitt, Ö. Türeci, H. Nell, A. Schaefer, S. Ünal, D.B. Tresnan, S. Mather, P.R. Dormitzer, U. Şahin, K.U. Jansen, W.C. Gruber, Safety and Efficacy of the BNT162b2 mRNA Covid-19 Vaccine, *New England Journal of Medicine* 383(27) (2020) 2603-2615.
- [69] L.R. Baden, H.M. El Sahly, B. Essink, K. Kotloff, S. Frey, R. Novak, D. Diemert, S.A. Spector, N. Rouphael, C.B. Creech, J. McGettigan, S. Khetan, N. Segall, J. Solis, A. Brosz, C. Fierro, H. Schwartz, K. Neuzil, L. Corey, P. Gilbert, H. Janes, D. Follmann, M. Marovich, J. Mascola, L. Polakowski, J. Ledgerwood, B.S. Graham, H. Bennett, R. Pajon, C. Knightly, B. Leav, W. Deng, H. Zhou, S. Han, M. Ivarsson, J. Miller, T. Zaks, Efficacy and Safety of the mRNA-1273 SARS-CoV-2 Vaccine, *New England Journal of Medicine* 384(5) (2020) 403-416.
- [70] M. Voysey, S.A.C. Clemens, S.A. Madhi, L.Y. Weckx, P.M. Folegatti, P.K. Aley, B. Angus, V.L. Baillie, S.L. Barnabas, Q.E. Bhorat, S. Bibi, C. Briner, P. Cicconi, A.M. Collins, R. Colin-Jones, C.L. Cutland, T.C. Darton, K. Dheda, C.J.A. Duncan, K.R.W. Emary, K.J. Ewer, L. Fairlie, S.N. Faust, S. Feng, D.M. Ferreira, A. Finn, A.L. Goodman, C.M. Green, C.A. Green, P.T. Heath, C. Hill, H. Hill, I. Hirsch, S.H.C. Hodgson, A. Izu, S. Jackson, D. Jenkin, C.C.D. Joe, S. Kerridge, A. Koen, G. Kwatra, R. Lazarus, A.M. Lawrie, A. Lelliott, V. Libri, P.J. Lillie, R. Mallory, A.V.A. Mendes, E.P. Milan, A.M. Minassian, A. McGregor, H. Morrison, Y.F. Mujadidi, A. Nana, P.J. O'Reilly, S.D. Padayachee, A. Pittella, E. Plested, K.M. Pollock, M.N. Ramasamy, S. Rhead, A.V. Schwarzbald, N. Singh, A. Smith, R. Song, M.D. Snape, E. Sprinz, R.K. Sutherland, R. Tarrant, E.C. Thomson, M.E. Török, M. Toshner, D.P.J. Turner, J. Vekemans, T.L. Villafana, M.E.E. Watson, C.J. Williams, A.D. Douglas, A.V.S. Hill, T. Lambe, S.C. Gilbert, A.J. Pollard, Safety and efficacy of the ChAdOx1 nCoV-19 vaccine (AZD1222) against SARS-CoV-2: an interim analysis of four randomised controlled trials in Brazil, South Africa, and the UK, *Lancet* 397(10269) (2021) 99-111.
- [71] M. Wang, R. Cao, L. Zhang, X. Yang, J. Liu, M. Xu, Z. Shi, Z. Hu, W. Zhong, G. Xiao, Remdesivir and chloroquine effectively inhibit the recently emerged novel coronavirus (2019-nCoV) in vitro, *Cell Research* 30(3) (2020) 269-271.
- [72] K. Govender, A. Chuturgoon, An Overview of Repurposed Drugs for Potential COVID-19 Treatment, *Antibiotics (Basel)* 11(12) (2022).
- [73] Y.-C. Hwang, R.-M. Lu, S.-C. Su, P.-Y. Chiang, S.-H. Ko, F.-Y. Ke, K.-H. Liang, T.-Y. Hsieh, H.-C. Wu, Monoclonal antibodies for COVID-19 therapy and SARS-CoV-2 detection, *Journal of Biomedical Science* 29(1) (2022) 1.
- [74] K. Duan, B. Liu, C. Li, H. Zhang, T. Yu, J. Qu, M. Zhou, L. Chen, S. Meng, Y. Hu, C. Peng, M. Yuan, J. Huang, Z. Wang, J. Yu, X. Gao, D. Wang, X. Yu, L. Li, J. Zhang, X. Wu, B. Li, Y. Xu, W. Chen, Y. Peng, Y. Hu, L. Lin, X. Liu, S. Huang, Z. Zhou, L. Zhang, Y. Wang, Z. Zhang, K. Deng, Z. Xia, Q. Gong, W. Zhang, X. Zheng, Y. Liu, H. Yang, D. Zhou, D. Yu, J. Hou, Z. Shi, S. Chen, Z. Chen, X. Zhang, X. Yang, Effectiveness of convalescent plasma therapy in severe COVID-19 patients, *Proceedings of the National Academy of Sciences* 117(17) (2020) 9490-9496.
- [75] F.L. van de Veerdonk, E. Giamarellos-Bourboulis, P. Pickkers, L. Derde, H. Leavis, R. van Crevel, J.J. Engel, W.J. Wiersinga, A.P.J. Vlaar, M. Shankar-Hari, T. van der Poll, M. Bonten, D.C. Angus, J.W.M. van der Meer, M.G. Netea,

Bibliography

A guide to immunotherapy for COVID-19, *Nature Medicine* 28(1) (2022) 39-50.

[76] F. Rommasi, M.J. Nasiri, M. Mirsaedi, Immunomodulatory agents for COVID-19 treatment: possible mechanism of action and immunopathology features, *Molecular and Cellular Biochemistry* 477(3) (2022) 711-726.

[77] G. El-Saber Batiha, A.I. Al-Gareeb, H.M. Saad, H.M. Al-kuraishy, COVID-19 and corticosteroids: a narrative review, *Inflammopharmacology* 30(4) (2022) 1189-1205.

[78] N. Koerber, A. Priller, S. Yazici, T. Bauer, C.-C. Cheng, H. Mijočević, H. Wintersteller, S. Jeske, E. Vogel, M. Feuerherd, K. Tinnefeld, C. Winter, J. Ruland, M. Gerhard, B. Haller, C. Christa, O. Zelger, H. Roggendorf, M. Halle, J. Erber, P. Lingor, O. Keppler, D. Zehn, U. Protzer, P.A. Knolle, Dynamics of spike-and nucleocapsid specific immunity during long-term follow-up and vaccination of SARS-CoV-2 convalescents, *Nature Communications* 13(1) (2022) 153.

[79] C.C. Cheng, L. Platen, C. Christa, M. Tellenbach, V. Kappler, R. Bester, B.H. Liao, C. Holzmann-Littig, M. Werz, E. Schönhals, E. Platen, P. Eggerer, L. Tréguer, C. Küchle, C. Schmaderer, U. Heemann, L. Renders, U. Protzer, M.C. Braunisch, Improved SARS-CoV-2 Neutralization of Delta and Omicron BA.1 Variants of Concern after Fourth Vaccination in Hemodialysis Patients, *Vaccines (Basel)* 10(8) (2022).

[80] E. Vogel, K. Kocher, A. Priller, C.-C. Cheng, P. Steininger, B.-H. Liao, N. Körber, A. Willmann, P. Irrgang, J. Held, C. Moosmann, V. Schmidt, S. Beileke, M. Wytopyl, S. Heringer, T. Bauer, R. Brockhoff, S. Jeske, H. Mijočević, C. Christa, J. Salmanton-García, K. Tinnefeld, C. Bogdan, S. Yazici, P. Knolle, O.A. Cornely, K. Überla, U. Protzer, K. Schober, M. Tenbusch, Dynamics of humoral and cellular immune responses after homologous and heterologous SARS-CoV-2 vaccination with ChAdOx1 nCoV-19 and BNT162b2, *eBioMedicine* 85 (2022).

[81] S. Ambike, C.-C. Cheng, M. Feuerherd, S. Velkov, D. Baldassi, S.Q. Afridi, D. Porras-Gonzalez, X. Wei, P. Hagen, N. Kneidinger, Mircea G. Stoleriu, V. Grass, G. Burgstaller, A. Pichlmair, Olivia M. Merkel, C. Ko, T. Michler, Targeting genomic SARS-CoV-2 RNA with siRNAs allows efficient inhibition of viral replication and spread, *Nucleic Acids Research* 50(1) (2021) 333-349.

[82] M. Gerckens, H.N. Alsafadi, D.E. Wagner, M. Lindner, G. Burgstaller, M. Königshoff, Generation of Human 3D Lung Tissue Cultures (3D-LTCs) for Disease Modeling, *J Vis Exp* (144) (2019).

[83] B. Hu, L. Zhong, Y. Weng, L. Peng, Y. Huang, Y. Zhao, X.-J. Liang, Therapeutic siRNA: state of the art, *Signal Transduction and Targeted Therapy* 5(1) (2020) 101.

[84] D. Baldassi, S. Ambike, M. Feuerherd, C.-C. Cheng, D.J. Peeler, D.P. Feldmann, D.L. Porras-Gonzalez, X. Wei, L.-A. Keller, N. Kneidinger, M.G. Stoleriu, A. Popp, G. Burgstaller, S.H. Pun, T. Michler, O.M. Merkel, Inhibition of SARS-CoV-2 replication in the lung with siRNA/VIPER polyplexes, *Journal of Controlled Release* 345 (2022) 661-674.

List of publications

- Ambike, S.*, **C. C. Cheng***, M. Feuerherd, S. Velkov, D. Baldassi, S.Q. Afridi, D. Porras-Gonzalez, X. Wei, P. Hagen, N. Kneidinger, M.G. Stoleriu, V. Grass, G. Burgstaller, A. Pichlmair, O. M. Merkel, C. Ko, and T. Michler. 2021. 'Targeting genomic SARS-CoV-2 RNA with siRNAs allows efficient inhibition of viral replication and spread', *Nucleic Acids Research*, 50: 333-49.
- Cheng, C. C. ***, L. Platen*, C. Christa, M. Tellenbach, V. Kappler, R. Bester, B. H. Liao, C. Holzmann-Littig, M. Werz, E. Schönhals, E. Platen, P. Eggerer, L. Tréguer, C. Kühle, C. Schmaderer, U. Heemann, L. Renders, U. Protzer, and M. C. Braunisch. 2022. 'Improved SARS-CoV-2 Neutralization of Delta and Omicron BA.1 Variants of Concern after Fourth Vaccination in Hemodialysis Patients', *Vaccines (Basel)*, 10.
- Vogel, E. *, K. Kocher*, A. Priller*, **C. C. Cheng***, P. Steininger, B.H. Liao, N. Körber, A. Willmann, P. Irrgang, J. Held, C. Moosmann, V. Schmidt, S. Beileke, M. Wytopil, S. Heringer, T. Bauer, R. Brockhoff, S. Jeske, H. Mijocevic, C. Christa, J. Salmanton-García, K. Tinnefeld, C. Bogdan, S. Yazici, P. Knolle, O.A. Cornely, K. Überla, U. Protzer, K. Schober, and M. Tenbusch. 2022. 'Dynamics of humoral and cellular immune responses after homologous and heterologous SARS-CoV-2 vaccination with ChAdOx1 nCoV-19 and BNT162b2', *eBioMedicine*, 85.
- Svilenov, H. L., J. Sacherl, A. Reiter, L. S. Wolff, **C. C. Cheng**, M. Stern, V. Grass, M. Feuerherd, F. P. Wachs, N. Simonavicius, S. Pippig, F. Wolschin, O. T. Keppler, J. Buchner, C. Brockmeyer, and U. Protzer. 2021. 'Picomolar inhibition of SARS-CoV-2 variants of concern by an engineered ACE2-IgG4-Fc fusion protein', *Antiviral Res*, 196: 105197.
- Koerber, N., A. Priller, S. Yazici, T. Bauer, **C. C. Cheng**, H. Mijočević, H. Wintersteller, S. Jeske, E. Vogel, M. Feuerherd, K. Tinnefeld, C. Winter, J. Ruland, M. Gerhard, B. Haller, C. Christa, O. Zelger, H. Roggendorf, M. Halle, J. Erber, P. Lingor, O. M. Keppler, D. Zehn, U. Protzer, and P. Knolle. 2022. 'Dynamics of spike-and nucleocapsid specific immunity during long-term follow-up and vaccination of SARS-CoV-2 convalescents', *Nature Communications*, 13: 153.
- Luedemann, M., D. Stadler, **C. C. Cheng**, U. Protzer, P. A. Knolle, and S. Donakonda. 2022. 'Montelukast is a dual-purpose inhibitor of SARS-CoV-2 infection and virus-induced IL-6 expression identified by structure-based drug repurposing', *Comput Struct Biotechnol J*, 20: 799-811.

Wrtil, Paul R., M. Stern, A. Priller, A. Willmann, G. Almanzar, E. Vogel, M. Feuerherd, **C. C. Cheng**, S. Yazici, C. Christa, S. Jeske, G. Lupoli, T. Vogt, M. Albanese, E. Mejías-Pérez, S. Bauernfried, N. Graf, H. Mijocevic, M. Vu, K. Tinnefeld, J. Wettengel, D. Hoffmann, M. Muenchhoff, C. Daechert, H. Mairhofer, S. Krebs, V. Fingerle, A. Graf, P. Steininger, H. Blum, V. Hornung, B. Liebl, K. Überla, M. Prelog, P. Knolle, O. T. Keppler, and U. Protzer. 2022. 'Three exposures to the spike protein of SARS-CoV-2 by either infection or vaccination elicit superior neutralizing immunity to all variants of concern', *Nature Medicine*, 28: 496-503.

Baldassi, D., S. Ambike, M. Feuerherd, **C. C. Cheng**, D. J. Peeler, D. P. Feldmann, D. L. Porras-Gonzalez, X. Wei, L.A. Keller, N. Kneidinger, M. G. Stoleriu, A. Popp, G. Burgstaller, S. H. Pun, T. Michler, and O. M. Merkel. 2022. 'Inhibition of SARS-CoV-2 replication in the lung with siRNA/VIPER polyplexes', *Journal of Controlled Release*, 345: 661-74.

* These authors contributed equally to this work.

Appendix – Reprint Permissions

For all these three articles published in Elsevier, MDPI, and Oxford University Press journals, copyright is retained by the authors. Articles are licensed under an open access Creative Commons CC BY 4.0 license, meaning that anyone may download and read the paper for free. In addition, the article may be reused and quoted provided that the original published version is cited. These conditions allow for maximum use and exposure of the work, while ensuring that the authors receive proper credit.

In exceptional circumstances articles may be licensed differently. If you have specific condition (such as one linked to funding) that does not allow this license, please mention this to the editorial office of the journal at submission. Exceptions will be granted at the discretion of the publisher.

Acknowledgements

I want to start by expressing thanks to my primary supervisor, Prof. Ulrike Protzer, for give me the opportunity to join the AG Protzer lab, a large research family with amazing colleagues. She was constantly encouraging and continuously providing supportive feedback for my work throughout the course of my PhD. And I want to highlight how grateful I am for the trust and encouragement she showed in me, especially in giving me the chance to participate in SARS-CoV-2 studies and have access to the BSL-3 facility.

A special thanks to Dr. Marc Ringelhan for guiding me in the beginning of my PhD as a mentor. Although my research direction and topic were entirely changed from the project which Marc and I worked together with, I still valued the time we spent working together and the helpful advice and knowledge Marc gave with me. My lab mentor number two is Dr. Chunkyu Ko. I feel extremely fortunate to have had the opportunity to work in the lab for so long with someone who is so organized, gentle, and warm. A special thanks for assisting me with the revision of my thesis as well.

I also want to thank the members of my thesis committee, Prof. Roland Rad and Dr. Ursula Ehmer. During all my thesis committee meetings, they were extremely friendly and supportive, which not only provided me with excellent scientific advice but also great spiritual support.

Moreover, I want to acknowledge my collaborators Louise Platen and Prof. Matthias Christoph Braunisch from the Institute of Nephrology, Katharina Koche, Prof. Matthias Tenbusch, Prof. Kilian Schober from University Hospital Erlangen, as well as Shubhankar, Emanuel, Alina, and Dr. Thomas Michler. Working with you is smooth and enjoyable, and the outcomes are also highly fruitful.

Next, I want to give sincere thanks to the best lab colleagues, especially to my beloved third floor lab friends. Bo-Hung is like my brother in the lab, and I am incredibly appreciative of his joining and supporting me in making my lab life brighter. I truly enjoy our unspoken understanding, which keeps our partnership successful and efficient at all times. Romina is like my mother in the lab. She is very kind and humorous, and always help me get through tough times in both my personal and professional lives. Merve, Kathi, and Omid are more than only reliable colleagues to me, they are close friends with whom we can discuss our ideas. I really enjoyed the time I spent with them, and the trip to India has always been a highlight of my life. A special thank you to Kathi for helping me with the correction of the Zusammenfassung.

Additionally, I would like to thank all of the current and former lab members, in particular

Shubhankar, Fenna, Philipp, Olli, Antje, Stoyan, Martin, Wen-Min, Theresa, Fuwang, Zhe, Lea, Lisa, Laura, Luis, Anna, and Eda. Without any of you, my PhD journey would not be complete. Thank you for giving me such a wonderful working atmosphere with so many thought-provoking chats, as well as all the funny and relaxing conversations during my time off from work.

I also want to express my heartfelt thanks to my Munich friends. Despite the difficulties of language and unfamiliarity, your unwavering help and accompany were crucial to me throughout my life in Munich. For all the great things we have done together—traveling, hiking, playing basketball, volleyball, and frisbee—you have always been my best companions.

Lastly, I would want to give my deepest appreciation to my family in Taiwan. Despite the fact that we are more than 9000 kilometers apart, your care and support helped me continue on this difficult path. Only with the support of each and every one of you did I overcome countless periods of loneliness and depression. Chi-Yun, my brother, has always been my mentor in life. He deserves all the praise since without his help, I wouldn't have been able to get this far.



Dynamics of humoral and cellular immune responses after homologous and heterologous SARS-CoV-2 vaccination with ChAdOx1 nCoV-19 and BNT162b2

Emanuel Vogel,^{a,1} Katharina Kocher,^{b,1} Alina Priller,^{c,1} Cho-Chin Cheng,^{a,1} Philipp Steininger,^d Bo-Hung Liao,^a Nina Körber,^a Annika Willmann,^a Pascal Irrgang,^d Jürgen Held,^b Carolin Moosmann,^b Viviane Schmidt,^b Stephanie Beileke,^d Monika Wytopil,^d Sarah Heringer,^e Tanja Bauer,^a Ronja Brockhoff,^e Samuel Jeske,^a Hrvoje Mijovic,^a Catharina Christa,^a Jon Salmanton-García,^e Kathrin Tinnefeld,^a Christian Bogdan,^b Sarah Yazici,^c Percy Knolle,^{c,f} Oliver A. Cornely,^{e,f,g,h} Klaus Überla,^d Ulrike Protzer,^{a,f,1*} Kilian Schober,^{b,1*} and Matthias Tenbusch^{d,1*}

^aInstitute of Virology, School of Medicine, Technical University of Munich / Helmholtz Zentrum München, Trogerstr. 30, 81675 München, Germany

^bMikrobiologisches Institut – Klinische Mikrobiologie, Immunologie und Hygiene, Universitätsklinikum Erlangen and Friedrich-Alexander-Universität (FAU) Erlangen-Nürnberg, Wasserturmstr. 3/5, 91054 Erlangen, Germany

^cInstitute of Molecular Immunology and Experimental Oncology, School of Medicine, University Hospital rechts der Isar, Technical University of Munich, Ismaninger Str. 22, 81675 München, Germany

^dInstitute of Clinical and Molecular Virology, University Hospital Erlangen, Friedrich-Alexander-Universität Erlangen-Nürnberg, Schlossgarten 4, 91054 Erlangen, Germany

^eUniversity of Cologne, Faculty of Medicine and University Hospital Cologne, Translational Research, Cologne Excellence Cluster on Cellular Stress Responses in Aging-Associated Diseases (CECAD), Herderstr. 52, 50931 Cologne, Germany

^fGerman Center for Infection Research (DZIF), partner sites Munich and Cologne

^gUniversity of Cologne, Faculty of Medicine and University Hospital Cologne, Department I of Internal Medicine, Center for Integrated Oncology Aachen Bonn Cologne Duesseldorf (CIO ABCD) and Excellence Center for Medical Mycology (ECMM), Kerpener Str. 62, 50937 Cologne, Germany

^hUniversity of Cologne, Faculty of Medicine and University Hospital Cologne, Clinical Trials Centre Cologne (ZKS Köln), Cologne, Germany

Summary

Background Vaccines are an important means to overcome the SARS-CoV-2 pandemic. They induce specific antibody and T-cell responses but it remains open how well vaccine-induced immunity is preserved over time following homologous and heterologous immunization regimens. Here, we compared the dynamics of humoral and cellular immune responses up to 180 days after homologous or heterologous vaccination with either ChAdOx1-nCoV-19 (ChAd) or BNT162b2 (BNT) or both.

Methods Various tests were used to determine the humoral and cellular immune response. To quantify the antibody levels, we used the surrogate neutralization (sVNT) assay from YHLO, which we augmented with pseudo- and real virus neutralization tests (pVNT and rVNT). Antibody avidity was measured by a modified ELISA. To determine cellular reactivity, we used an IFN- γ Elispot, IFN- γ /IL Flurospot, and intracellular cytokine staining.

Findings Antibody responses significantly waned after vaccination, irrespective of the regimen. The capacity to neutralize SARS-CoV-2 – including variants of concern such as Delta or Omicron – was superior after heterologous compared to homologous BNT vaccination, both of which resulted in longer-lasting humoral immunity than homologous ChAd immunization. All vaccination regimens induced stable, polyfunctional T-cell responses.

Interpretation These findings demonstrate that heterologous vaccination with ChAd and BNT is a potent alternative to induce humoral and cellular immune protection in comparison to the homologous vaccination regimens.

Funding The study was funded by the German Centre for Infection Research (DZIF), the European Union's "Horizon 2020 Research and Innovation Programme" under grant agreement No. 101037867 (VACCELERATE), the "Bayerisches Staatsministerium für Wissenschaft und Kunst" for the CoVaKo-2021 and the For-COVID projects

eBioMedicine 2022;85:104294

Published online 4 October 2022

<https://doi.org/10.1016/j.ebiom.2022.104294>

*Corresponding authors.

E-mail addresses: protzer@tum.de (U. Protzer), kilian.schober@uk-erlangen.de (K. Schober), matthias.tenbusch@fau.de (M. Tenbusch).

¹ These authors contributed equally.

and the Helmholtz Association via the collaborative research program “CoViPa”. Further support was obtained from the Federal Ministry of Education and Science (BMBF) through the “Netzwerk Universitätsmedizin”, project “B-Fast” and “Cov-Immune”. KS is supported by the German Federal Ministry of Education and Research (BMBF, 01KI2013) and the Else Kröner-Stiftung (2020_EKEA.127).

Copyright © 2022 The Authors. Published by Elsevier B.V. This is an open access article under the CC BY-NC-ND license (<http://creativecommons.org/licenses/by-nc-nd/4.0/>)

Keywords: Heterologous vaccination; COVID-19; vaccine; BNT162b2; ChAdOx1-nCoV-19; SARS-CoV-2; long-term; maintenance; T cell immunity; antibody avidity

Research in context

Evidence before this study

Due to some rare severe side effects after the administration of the adenoviral vaccine, ChAdOx1 nCoV-19, many countries recommended a heterologous vaccination scheme including mRNA vaccines like BNT162b2 for the second dose. We performed a PubMed search (with no restrictions on time span) using the search terms “SARS-CoV-2” and “heterologous vaccination” and obtained 247 results. Only a fraction of manuscripts included direct comparisons of patient cohorts that received either a heterologous or a homologous vaccination regimen. Of those, the vast majority investigated only short-term immunogenicity after vaccination. Thus, little is known about the preservation of immunity by heterologous compared to homologous vaccination.

Added value of this study

We add a very comprehensive and comparative study investigating heterologous and homologous vaccination regimens early and late after vaccination. Key features include the number of patients ($n = 472$), the number of vaccination cohorts ($n = 3$), the fact that samples were derived from three independent study centers and comparative analyses were performed at two independent study centers, as well as in-depth investigation of humoral and T cellular immunity.

Implications of all the available evidence

The recent data creates a line of evidence that heterologous vaccination, compared to homologous vaccination regimens, results in at least non-inferior maintenance of humoral and cellular immunity. The enhanced understanding of immunity induced by individual vaccination regimens is crucial for further recommendations regarding the necessity, timing and choice of additional vaccinations and public health policies.

Introduction

The widespread use of safe and effective vaccines is essential for overcoming the Severe Acute Respiratory Syndrome Coronavirus 2 (SARS-CoV-2) pandemic. As of today, billions of doses of Coronavirus Disease 19 (COVID-19) vaccines, based on adenoviral vectors or mRNA, have been administered worldwide. In very rare cases, the administration of the adenoviral vector-based ChAdOx1-nCoV-19 (ChAd) vaccine has been associated with the induction of a vaccine-induced thrombocytopenic thrombosis syndrome, particularly in young women.¹ Consequently, the vaccination authorities of several countries recommended that persons under the age of 60 years who had received a primary dose of ChAd should receive an mRNA-based Covid-19 vaccine for the second immunization.²

We and others have previously shown that the heterologous combination of ChAd and mRNA vaccination results in a non-inferior or even superior humoral and cellular immune response compared to homologous mRNA or ChAd vaccination regimens.^{3–12} While homologous ChAd vaccination elicited a strong T-cell response shortly after the second immunization, antibody responses were inferior to homologous or heterologous regimens with mRNA vaccines. Furthermore, in the case of homologous vaccination regimens, various studies have shown a decline in antibody and T-cell levels a few months after the second dose.¹³ For heterologous vaccination regimens, however, follow-up data on how long B- and T-cell immunity persists are limited.^{14,15} This particularly applies to the immune response against newly emerged SARS-CoV-2 variants of concern (VoC) such as the Delta or Omicron mutant.⁸ Currently, it therefore remains unclear how the heterologous combination of ChAd and mRNA vaccination compares to homologous mRNA or ChAd vaccination in terms of persistence of humoral and cellular immunity.

Here, we examined humoral and cellular immunity in up to 472 participants from three different study centers at different time points before, and up to 180 days after heterologous and homologous vaccination with mRNA with BNT162b2 (BNT) and ChAd. While T-cell responses showed only modest contraction, significant waning of humoral immunity was observed over time in all three vaccination regimens. Compared to homologous vaccination with ChAd or BNT, the heterologous regimen generally resulted in more constant antibody responses both in terms of quantity and quality.

Methods

Study design and participants

The study is a follow-up analysis of 472 homologously or heterologously vaccinated participants that were previously only assessed for the production of antibodies using sVNT.⁵ A priori, no power analysis was performed on the number of participants. This was due to the fact that at that time there were only a very small number of people who could have been included according to the criteria, as well as the voluntary basis of participation.

Study participants (all of European Caucasian ethnicity) were divided into three different cohorts according to their vaccination regimen. Subjects of the two homologous groups received two doses of BNT or ChAd, respectively. In contrast, subjects of the third group received the heterologous vaccination regimen consisting of ChAd vaccine for the first and BNT for the second dose. Participants' sera and peripheral blood mononuclear cells (PBMCs) were analyzed at two different study centers in Germany. Blood sampling schedules varied by study center and cohort. Not all tests were performed at every point in time. In general, four different points in time can be distinguished. Time point "before" is the initial time point at the day of the first vaccination. "Early after #1" refers to the moment of the second vaccination, "early after #2" corresponds in median 13 – 15 days after this vaccination and the "late after #2" time point analysis was carried out between 98 – 158 days in the median after the second vaccination, depending on the study center and vaccination regimen. The cohorts of homologous BNT and ChAd vaccinated people mainly include healthcare workers, whereas the heterologous vaccinated cohort did not comprise a specific professional group. Subjects were not pre-selected by the study team, but could voluntarily enroll for study participation. This was on condition that they had been vaccinated in accordance with the defined vaccination regimens. Accordingly, there was no selection bias by the study team. Subjects who reported SARS-CoV-2 infection at follow-up were excluded from the analysis. Likewise, those who were positive for N-specific antibodies after natural infection would have been excluded.

For longitudinal characterizations of the T-cell responses at the Munich study center (heterologous ChAd-BNT cohort), a separate cohort of vaccinees was included for the time points "early after #1", "early after #2", and "late after #2". For longitudinal characterizations of the T-cell responses at the Erlangen study center (homologous BNT cohort), a separate cohort of vaccinees was included for the time points "before", "early after #1", and "early after #2" for contextualization. A detailed description of the cohorts can be found in [Table 1](#).

Antibody response using surrogate virus neutralization assay

We used the iFlash-1800 CLIA Analyzer (YHLO Shenzhen, China) for the quantification of the antibody response. For the detection of neutralizing antibodies, we applied the iFlash-2019-nCoV NAb assay according to the manufacturer's instructions. The test principle is a competitive immunoassay. The iFlash-2019-nCoV NAb assay is only validated up to a level of 800 AU/ml according to the WHO standard. Therefore, all results exceeding this limit have been set to 800 AU/ml.

Antibody avidity

Binding strength of the SARS-CoV-2 IgG antibodies was determined by adaptation of the commercial IgG agile SARS-CoV-2 ELISA (Virion/Serion, Germany) using ammonium thiocyanate (NH₄SCN) (Roth, Germany) as previously described.^{16–18} Serum samples were measured using the IgG agile SARS-CoV-2 ELISA and diluted to 100 U/mL according to the standard curve provided by the manufacturer to exclude an influence of variable antibody concentrations. Thereafter, serum samples were incubated in the plates pre-coated with Wuhan SARS-CoV-2-spike-ectodomain S1, S2 and RBD recombinant antigens for 1h at 37°C in a humid chamber. After washing, antigen-antibody complexes were incubated in the presence of 1.0 M ammonium thiocyanate or PBS as control for 10 min at room temperature. After washing to remove antibodies bound with low avidity, the ELISA was completed according to the manufacturer's instructions. The relative avidity index was calculated as follows: IgG concentrations (NH₄SCN) / IgG concentrations (PBS) x 100, and is given in percent.

Real virus neutralization assay

Based on a previously established infection inhibition assay,¹⁶ VeroE6 cells (ATCC, US, RRID: CVCL_YQ49) were seeded in 10% fetal calf serum Dulbecco's Modified Eagles medium (Thermo Fisher Scientific, Germany) at 15,000 cells per well one day before incubation. Infection was started using SARS-CoV-2 at a multiplicity of infection (MOI) of 0.03 plaque-forming units (PFU) / cell. To detect virus-neutralization activity,

	Study Center Munich		Study Center Erlangen		
	BNT162b2 mRNA prime, BNT162b2 mRNA boost MUC <i>n</i> = 50	ChAdOx1 nCoV-19 prime, BNT162b2 mRNA boost CGN <i>n</i> = 50	BNT162b2 mRNA prime, BNT162b2 mRNA boost ERL <i>n</i> = 119	ChAdOx1 nCoV-19 prime, ChAdOx1 nCoV-19 boost ERL <i>n</i> = 52	ChAdOx1 nCoV-19 prime, BNT162b2 mRNA boost ERL <i>n</i> = 201
Volunteer source	Healthcare worker	General population at vaccination center	Healthcare worker	General population at vaccination center	General population at vaccination center
Age in years, median (IQR) [range]	40.5 (32-52.75) [22-75]	47 (33.25-55) [23-61]	44 (30-54) [17-85]	59 (46-64) [31-64]	42 (33-52) [19-60]
Sex, n (%) Female	31 (62%)	37 (74%)	81 (68.1%)	35 (67.3%)	127 (63.2%)
Sex, n (%) Male	19 (38%)	13 (26%)	38 (31.9%)	17 (32.7%)	74 (36.8%)
Time from prime to second dose in days, median (IQR) [range]	21 (20-22) [19-24]	63 (63-64) [60-84]	23 (21-25) [13-29]	63 (63-63) [63-63]	63 (63-63) [60-63]
Time from second dose to blood collection in days, median (IQR) [range]	Early: 13 (13-14) [11-16] Late: 98 (96-102) [91-158]	Early: 15 (14-15) [13-15] Late: 110 (105,5-111) [104-113]	Early: 14 (14-16) [10-36] Late: 158 (153-167) [140-180]	Early: 13 (13-15) [13-16] Late: 142 (141-144) [140-144]	Early: 14 (14-15) [12-17] Late: 142 (141-144) [140-146]
lost to follow-up, n	4	7	0	0	0

Table 1: Detailed representation of different study cohorts, separated by study center.

MUC, Munich; CGN, Cologne; ERL, Erlangen; IQR: interquartile range.

serum samples were serially diluted 1:2 with DMEM starting from 1:20 up to a 1:2560 or 1:5120 dilution, respectively. SARS-CoV-2 virus (GISAID EPI_ISL: 2772700 [Delta/ B.1.617.2], 7808190 [Omicron/ B.1.1.529 BA.1]) (480 PFU/15,000 cells/well) was added in a total volume of 50 μ L at 37°C. After one hour of pre-incubation, the inoculum was transferred to the pre-seeded VeroE6 cells for another one-hour incubation at 37°C before the inoculum was replaced by supplemented DMEM. SARS-CoV-2 infection was terminated after 23 hours by adding 4% paraformaldehyde to fix the cells, and infection rate was analyzed by an in-cell ELISA.

After fixation, cells were washed with PBS and permeabilized with 0.5% saponin (Sigma-Aldrich, Germany). Blocking buffer, consisting of 0.1% saponin-10% goat serum (Sigma-Aldrich) in PBS, was added and incubated for one hour on fixed cells to avoid unspecific binding of antibodies. As a primary antibody, the SinoBiological anti-SARS-CoV-2-N T62 antibody (40143-T62, RRID:AB2892769) was used. The antibody was diluted with 1% FCS-PBS to 1:1500 ratio and 50 μ L were added in each well and incubated at room temperature for 2 hours. After washing, the second antibody was added. Goat anti-rabbit IgG2a-HRP antibody (EMD Millipore / order number 12-348, RRID: AB_390191) with 1% FCS-PBS was diluted to 1:4000 ratio. 50 μ L were added and incubated at room temperature for 1-2 hours. After the final washing step 100 μ L tetramethylbenzidine (TMB) were incubated for 20 min at room temperature. As final step 2M H₂SO₄ were added to stop the reaction. The result was quantified using optical detection with a Tecan Infinite 200 reader (TECAN, Switzerland) at 450 nm wavelength. The inhibition curve of each sample was analyzed by statistical analysis software Graph Pad Prism (GraphPad Software, USA), and 50% inhibitory concentration (IC₅₀) was determined using non-linear regression.

FACS-based analysis of anti-S binding antibodies

A modified version of our previously published serological assay was used, in which HEK 293T (RRID: CVCL_4U22) cells either stably expressing the spike protein from the original Wuhan strain or transiently expressing the spike protein of B.1.167.2 or B.1.1.529, respectively, were used as target cells.¹⁹ To quantify antigen-specific antibodies, 5×10^5 HEK 293T cells were incubated with serum samples diluted in 100 μ L FACS-PBS (PBS with 0.5% BSA and 1 mM sodium azide) for 20 minutes at 4°C to bind to spike protein on the surface. After washing with 200 μ L buffer, bound S-specific antibodies were detected with anti-human IgG-AF647 (4°C, 30 min incubation; clone HP6017, Biolegend, Cat #409320, RRID:AB_2563330). After further washing, samples were measured on an AttuneNext (ThermoFisher) and analyzed using FlowJo software

(Tree Star Inc.). A standard plasma sample with a defined concentration of 1,01 mg/ml anti-SARS-CoV-2S IgG was used as reference control. The median fluorescence intensity (MFI) correlates with the level of bound antibodies.¹⁹

Pseudotype neutralization assay

Neutralization of the early D614G (WT) and the B.1.617.2 variants was assessed with the help of spike-pseudotyped simian immunodeficiency virus particles as described before.²⁰ To produce pseudotyped reporter particles, HEK293T cells were transfected with the SIV-based self-inactivating vector encoding luciferase (pGAE-LucW, RRID:Addgene_21375), the SIV-based packaging plasmid (pADSIV3), and the respective spike variant-encoding plasmid as described previously.²¹

For the assessment of pseudotype neutralization, HEK293T-ACE2 cells were seeded at 2×10^4 cells/well in a 96well flat bottom plate. 24 h later, 60 μ L of serial dilutions of the serum samples were incubated with 60 μ L lentiviral particles for 1 h at 37°C. HEK293T cells were washed with PBS and the particle-sample mix was added to the cells. 48 h later, medium was discarded, and the cells washed twice with 200 μ L PBS. Following 50 μ L PBS and 25 μ L ONE-Glo™ (Promega Corp, Madison, USA) was added and after 3 minutes the luciferase signal was assessed on a microplate luminometer (VICTOR X5, PerkinElmer) and analyzed using PerkinElmer 2030 Manager software. The reciprocal serum ID₅₀ was determined with Prism GraphPad 9 (San Diego, California, USA) by application of the Sigmoidal 4PL function. For sera that did not reach neutralization by at least 50% at the highest serum dilution, the ID₅₀ was set to the highest reciprocal serum dilution, namely 20.

Isolation and cultivation of peripheral blood mononuclear cell (PBMC)

PBMCs were isolated from citrate peripheral blood of vaccinated individuals by density gradient centrifugation using Biocoll® separating solution, density 1.077 g/ml (Bio&Sell) and frozen in heat-inactivated FCS + 10% DMSO (Sigma-Aldrich) for liquid nitrogen storage. Thawed PBMCs were cultured in complete RPMI medium (RPMI 1640 medium (Thermo Fisher) supplemented with 10% heat-inactivated FCS, 50 μ M -Mercaptoethanol, 0.05 mg/ml gentamicin, 1.192 g/l HEPES, 0.2 g/l L-glutamine, and 100 U/ml penicillin-streptomycin) at 37°C and 5% CO₂.

IFN- γ Enzyme-linked immunospot (ELISPOT)

Cryopreserved PBMCs were thawed and rested overnight at 1×10^6 cells/ml in complete RPMI medium. ELISPOT plates (Millipore) were coated with anti-human IFN- γ monoclonal antibody (clone 1-DIK, Mabtech) at 0.5 μ g/well overnight at 4°C. Plates were

washed with sterile PBS and subsequently blocked with complete RPMI medium for 1–2 h at 37°C. 400,000 PBMCs/well were seeded and stimulated with 11aa overlapping 15-mer PepMix™ SARS-CoV-2 spike glycoprotein peptide pool (1 µg/ml), provided in two peptide sub-pools S1 and S2 (JPT), for 20 h at 37°C. For the unstimulated condition, PBMCs were cultured in complete RPMI medium and respective dilution of solvent DMSO. As a positive control, PBMCs were stimulated with 25 ng/ml phorbol myristate acetate (PMA) (Sigma-Aldrich) and 1 µg/ml ionomycin (Sigma-Aldrich). Following this incubation, all steps were performed at room temperature. Plates were washed with PBS containing 0.05% Tween-20 (Sigma-Aldrich) and incubated with biotinylated anti-human IFN-γ monoclonal antibody (clone 7-B6-1, Mabtech, RRID:AB_907272) at 0.2 µg/well for 2 h. Following a second wash step with PBS containing 0.05% Tween-20, plates were incubated with an avidin-biotinylated peroxidase complex (VECTASTAIN® Elite ABC-HRP Kit, Vector Laboratories) for 1–2 h. After final washing steps with first PBS containing 0.05% Tween-20 and then PBS, plates were developed by the addition of AEC substrate solution (Sigma-Aldrich) for 15 minutes. Subsequently, plates were washed with water, dried for 24 h in the dark, and analyzed on an ImmunoSpot® Analyzer (Cellular Technologies Limited). A positive peptide-specific response was quantified by subtraction of mean spots of the unstimulated control and depicted as spot forming units (SFU)/10⁶ PBMCs.

IFN-γ/IL-2 Fluorospot assay

Cryopreserved PBMCs were thawed and rested overnight at 2×10^6 cells/ml in complete RPMI medium. Human IFN-γ/IL-2 Fluorospot assays (CTL Europe, Germany) were performed according to the manufacturer's instructions. One day before the Fluorospot assays were performed, the plates were activated by adding 70% ethanol for less than one minute. Followed by a washing step and addition of IFN-γ/IL-2 capture antibodies overnight. After decanting the plate, 200,000 PBMCs/well were seeded and stimulated with 11aa overlapping 15-mer PepMix™ SARS-CoV-2 spike glycoprotein peptide pool (1 µg/ml), provided in two peptide sub-pools S1 and S2 (JPT), for 20 h at 37°C. As antigen-specific positive control, we used a CEF pool of in total 32 15mer peptides derived from Cytomegalovirus (5 peptides), Epstein-Barr virus (15 peptides), and Influenza virus (Flu) (12 peptides) proteins (National Institute for Biological Standards and Control (NIBSC), UK). For the unstimulated condition, PBMCs were cultured in complete RPMI medium. After the stimulation period, the plates were washed and 80 µL of anti-human IFN-γ (FITC, RRID:AB_2733588)/anti-human IL-2 (Hapten2), detection antibody solution was added for 2h at room temperature. For the visualization of

secreted cytokines, plates were washed and a tertiary solution including anti-FITC Alexa Fluor® 488 (visualizes IFN-γ) and anti-Hapten2 CTL-Red™ (visualizes IL-2) was added for one hour. The staining procedure was stopped by washing the plate. After drying the plates for 24h on paper towels on bench top, Fluorospot plates were scanned and analyzed using an automated reader system (ImmunoSpot Ultimate UV Image analyzer/ImmunoSpot 7.0.17.0 Professional DC Software, CTL Europe GmbH, Germany). Positive reactivity to experimental stimulatory agents was given when the spot count in antigen-stimulated cells was greater than twice the spot count in unstimulated (background) wells.

Intracellular cytokine staining (ICCS)

Cryopreserved PBMCs were thawed and rested overnight at 1×10^6 cells/ml in complete RPMI medium. 10⁶ PBMCs were stimulated with spike glycoprotein peptide pool as described above for 20 h at 37°C in the presence of 1 µl/ml GolgiPlug™ (BD Biosciences). For the unstimulated condition, PBMCs were cultured in complete RPMI medium and respective dilution of solvent DMSO. As a positive control, PBMCs were stimulated with 25 ng/ml PMA and 1 µg/ml ionomycin. Following this incubation, all steps were performed at 4°C. PBMCs were washed twice with FACS buffer (PBS containing 0.5% BSA) and stained with ethidium-monoazide-bromide (EMA) (Thermo Fisher) for 15 minutes for live/dead discrimination. After two washing steps with FACS buffer, PBMCs were stained for surface markers CD8-eFluor450 (clone OKT8, Thermo Fisher, dilution 1:200, RRID:AB_2535439) and CD4-PE (clone RPA-T4, Thermo Fisher, 1:400, RRID:AB_1257144) for 20 minutes. Excess antibody was removed by two washing steps with FACS buffer followed by fixation/permeabilization using Cytofix/Cytoperm (BD Biosciences). PBMCs were washed twice with 1x Perm Wash buffer (BD Biosciences) and subsequently stained intracellularly for IL-2-APC (clone 5344.11, BD Biosciences, 1:20, RRID:AB_400574) and IFN-γ-FITC (clone 25723.11, BD Biosciences, 1:10, RRID:AB_400425) for 30 minutes. Following washing steps with first 1x Perm Wash buffer and then FACS-buffer, PBMCs were filtered through a nylon mesh and acquired on a LSRFortessa™ flow cytometer (BD Biosciences). A positive peptide-specific response was quantified by subtracting the mean frequency of IL-2 and IFN-γ double-positive T cells of the unstimulated control.

Ethics

Ethics approval was granted by the local ethics committees in Erlangen (Az. 340-21B) and Munich (Az. 26/21 and Az. 330/21 S). All subjects were informed about the

study and confirmed their participation by means of an informed consent form.

Statistics

The following statistical tests were used:

Mann-Whitney test: Applied to all comparisons comparing a time point consisting of only two groups whose data sets were not paired and for which we could not assume a normal distribution due to sample size.

Kruskal-Wallis test followed by Dunn's multiple comparison test: Applied to all comparisons comparing a time point consisting of more than two groups whose data sets were not paired and for which we could not assume a normal distribution due to the sample size.

Wilcoxon test: Applied to all comparisons that compared two time points of a cohort and that had different sample sizes at time points one and two. The reason for this is the loss to follow-up.

Friedman test with multiple comparisons: Applied to all comparisons that compared two time points in a cohort that had identical sample sizes at time one and two.

Due to the a priori determination of the vaccination regimens, randomization and blinding were not possible. Sample size determination was limited by the number of available subjects, as well as the available testing capacity.

Data are presented with frequencies and percentages for categorical variables and with median, interquartile range (IQR) and range for continuous variables. Categorical data were compared using chi-squared test or Fisher's exact test as appropriate. Median comparison was performed with Mann-Whitney U test (2 categories) or Kruskal-Wallis H (3 categories) as appropriate. A linear regression model analysis was built in order to determine which variables had impact in the late IC50. In case any of these variables had a p value <0.1 in the univariable model it was included in the multivariable one. The multivariable model was performed with the backwards Wald methods. A p value ≤ 0.05 was considered statistically significant.

Statistics as well as figures were created with PRISM GraphPad 9.3.1 as well as IBM SPSS Statistics for Windows, Version 27.0. Armonk, NY, United States.

Role of Funders

The funders did not interfere with the study design, data collection, data analysis, interpretation, or writing of report.

Results

Heterologous COVID-19 vaccination induced strong antibody responses which are superior or comparable to homologous mRNA vaccination regimens

We compared humoral and cellular immune responses in 472 healthy individuals in median 13 – 15 days ("early after #2") and 98 – 158 days ("late after #2") after heterologous or homologous vaccination with ChAd and BNT (Table 1). Previously, we had reported limited data on antibody responses early after second vaccination.⁵ Analyses were performed at the study centers in Munich (Munich and Cologne samples) and Erlangen (Erlangen samples) (Table 1). There are differences in sample collection time points and other study participant characteristics and only for the Erlangen study center exist data from all three vaccination regimens (Suppl. Table 1). Furthermore, a proportion analysis comparing the cohorts receiving different vaccination regimens revealed higher age and body mass index (BMI) for the ChAd-ChAd group (Suppl. Table 2). This might be due to the specific recommendation in Germany at that time to not use the ChAd vaccine in people under the age of 60. In light of the above-mentioned differences, the results were stratified for the two study sites.

We first assessed the quantities of antibody levels by sVNT (Figure 1). This assay correlates well with a real virus neutralization assay not only for the EU-strain SARS-CoV-2 D614G virus, as previously described,⁵ but also for the Delta VoC (Suppl. Figure 1). Regardless of the vaccination schedule, we observed significant ($p < 0.0001$ for all comparisons [Wilcoxon test]) waning of antibody levels in almost all individuals at the late time point.

At the study center in Munich (Figure 1a), antibody neutralization capacity at the follow-up time point was significantly ($p < 0.0001$ [Wilcoxon test]) reduced compared to the time point early after second vaccination, but the remaining antibody levels were similar after ChAd-BNT (median = 234.65 AU/ml; $n = 43$) and BNT-BNT (median = 328.17 AU/ml; $n = 46$) vaccination. At an independent study center in Erlangen, these results were confirmed (Figure 1b). Furthermore, additional analyses of samples from a homologous ChAd-ChAd vaccination scheme cohort showed that neutralizing antibody levels late after homologous ChAd-ChAd vaccination (median of 9.32 AU/ml; $n = 52$) were still significantly ($p < 0.0001$ [Kruskal-Wallis test]) lower compared to homologous BNT-BNT (median = 31.74 AU/ml; $n = 119$) or heterologous ChAd-BNT (median = 41.72 AU/ml; $n = 201$) vaccination (Figure 1b). Thus, the heterologous ChAd-BNT vaccination regimen results in neutralizing antibody levels against SARS-CoV-2 WT virus which are as high as after homologous BNT-BNT and higher than after homologous ChAd-ChAd immunization. Using a linear

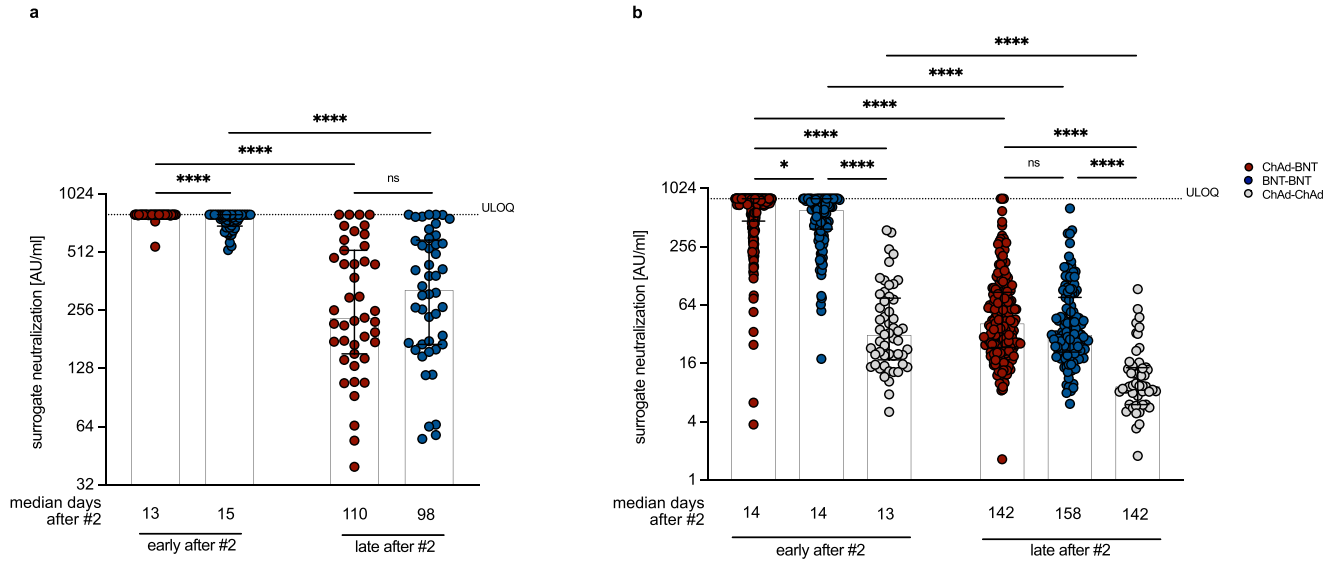


Figure 1. Neutralizing antibody levels after heterologous ChAd-BNT vaccination are non-inferior compared to homologous vaccination regimens. Surrogate virus neutralization levels measured at the Munich (a) and Erlangen (b) study site after heterologous ChAd-BNT or homologous BNT-BNT or ChAd-ChAd vaccination. The sVNT is only validated up to a maximum of 800 AU/ml, therefore all values measured as greater than 800 AU/ml were set to 800 AU/ml. (a) „Early after #2” refers to a median of 15 days (for BNT-BNT) or 13 days (for ChAd-BNT) after the second vaccination. „Late after #2” refers to sampling at median 98 days (for BNT-BNT) or 110 days (for ChAd-BNT) after the second vaccination. $n = 50$ and 43 (ChAd-BNT; “early after #2” and „late”, respectively) and $n = 50$ and 46 (BNT-BNT; “early after #2” and „late after #2”, respectively). (b) „Early after #2” refers to sampling at median 14 days (for BNT-BNT and ChAd-BNT) and 13 days (for ChAd-ChAd) after the second vaccination. „Late after #2” refers to a median of 158 days (for BNT-BNT) or 142 days (for ChAd-BNT and ChAd-ChAd) after the second vaccination. $n = 201$ (ChAd-BNT), 119 (BNT-BNT) and 52 (ChAd-ChAd). ULOQ = upper limit of quantification (800 AU/ml). For inter-group statistics concerning one time point Mann-Whitney (a) or Kruskal-Wallis followed by Dunn’s multiple comparisons test was used (b). Bars represent group medians, whiskers interquartile range. Over-time comparison within one group was done by Wilcoxon test. * $p < 0.05$, ** $p < 0.01$, *** $p < 0.001$, **** $p < 0.0001$, and n.s. indicates not significant. A detailed description of the data can be found in Supplemental Table for [Figure 1a](#) and b.

regression analysis, we confirmed that neither body mass index, comorbidities, time intervals between the vaccinations, nor blood sampling significantly affected the neutralization levels at the late time points, whereas age ($p = 0.022$) and the vaccination regimen ($p < 0.001$) were significantly associated using a univariable model (Table 2). However, in the multivariable model age was not statistically significantly associated anymore ($p = 0.206$), leaving vaccination regimen as the only parameter in the model that is statistically significantly associated with the late IC₅₀ values ($p < 0.001$). With this outcome, the model is not multivariable anymore, but it underlines the interpretation that the vaccination regimens strongly influence the IC₅₀ values at late time points after 2nd vaccination.

Serum neutralization capacity of variants of concern is superior after heterologous vaccination

To investigate potential differences in serological responses between the different cohorts in more detail, we next applied rVNT for the most relevant SARS-CoV-2 VoC. At the Munich study center, neutralization of VoC B.1.617.2 (Delta) and B.1.1.529 (Omicron) was investigated using sera collected 13 – 15 days and 98 – 110 days in median after heterologous ChAd-BNT or homologous BNT-BNT vaccination (Figure 2a). Early after the second vaccine dose, heterologous ChAd-BNT vaccination resulted in significantly ($p = 0.0003$ [Mann-Whitney test]) better serum neutralization capacity of Delta, and to a lesser extent ($p = 0.0122$ [Mann-Whitney test]) also Omicron, than homologous BNT-BNT vaccination (ChAd-BNT median IC₅₀ = 929.15; $n = 50$; BNT-BNT median IC₅₀ = 432.85; $n = 50$). Serum neutralization capacity for Omicron compared to Delta was reduced 25.8-fold and 21.6-fold for ChAd-BNT (median IC₅₀ = 36) and BNT-BNT (median IC₅₀ = 20), respectively, in an analysis of sub-cohorts consisting of 15 participants each. 98 – 110 days in median after the

second vaccination, serum neutralization capacity for Delta still significantly ($p < 0.0001$ [Mann-Whitney test]) differed between ChAd-BNT (median IC₅₀ = 398.20, $n = 43$) and BNT-BNT vaccination (median IC₅₀ = 72.93, $n = 46$). However, there was barely any neutralization capacity left against Omicron in either cohort (Figure 2a).

To confirm these results, serum samples from the Erlangen study center collected at 142 – 158 days in median after second vaccination („late after #2“) were analyzed in the rVNT assay for the ability to neutralize the Delta variant. These analyses again additionally included a cohort of homologous ChAd-ChAd vaccinated participants. Late after ChAd-ChAd immunization, barely any neutralization capacity against Delta was detectable (median IC₅₀ = 20; $n = 21$), which was significantly different from the ChAd-BNT and BNT-BNT cohorts ($p = 0.0072$ and $p = 0.0002$ [Kruskal-Wallis test]). In contrast to the results obtained at the Munich study center, there was no significant ($p = 0.8119$ [Kruskal-Wallis test]) difference in neutralization capacity against Delta between the ChAd-BNT (median IC₅₀ = 107.8; $n = 30$) and BNT-BNT (median IC₅₀ = 172; $n = 30$) group (Figure 2b). These findings were further confirmed using pVNT, although overall the neutralization titers were slightly lower than in the rVNT (Suppl. Figure 2). Whether the discrepancy between the two centers are due to the later sampling time point of the Erlangen cohort, the lower numbers of participants, or variations in the conditions for the neutralization assay, cannot be clarified. However, the differences between vaccination regimens at one site are not affected by this, since analyses for a single given time point were conducted in the same experiment. The reduced capacity to recognize the spike (S) proteins of VoC in comparison to the S protein of the original Wuhan strain observed in the pVNT assay (Suppl. Figure 2) was confirmed by a flow cytometric analysis using HEK293 cells expressing the corresponding S

	UNIVARIABLE MODEL				MULTIVARIABLE MODEL			
	p value	B	95% CI for B		p value	B	95% CI for B	
			Lower Bound	Upper Bound			Lower Bound	Upper Bound
Vaccination regimen	<.001	-30,630	-45,973	-15,287	<.001	-30,630	-45,973	-15,287
Age	0,022	-1,045	-1,936	-0,154	0,206	-0,590	-1,507	0,327
Sex	0,210	15,112	-8,556	38,780				
BMI	0,745	0,445	-2,247	3,137				
Comorbidities	0,340	-14,632	-44,742	15,479				
Time from prime to second dose	0,586	0,169	-0,441	0,778				
Time to blood collection, early after 2nd	0,366	-1,884	-5,972	2,205				
Time to blood collection, late after 2nd	0,664	-0,261	-1,443	0,921				

Table 2: Linear regression analysis for study center Erlangen.

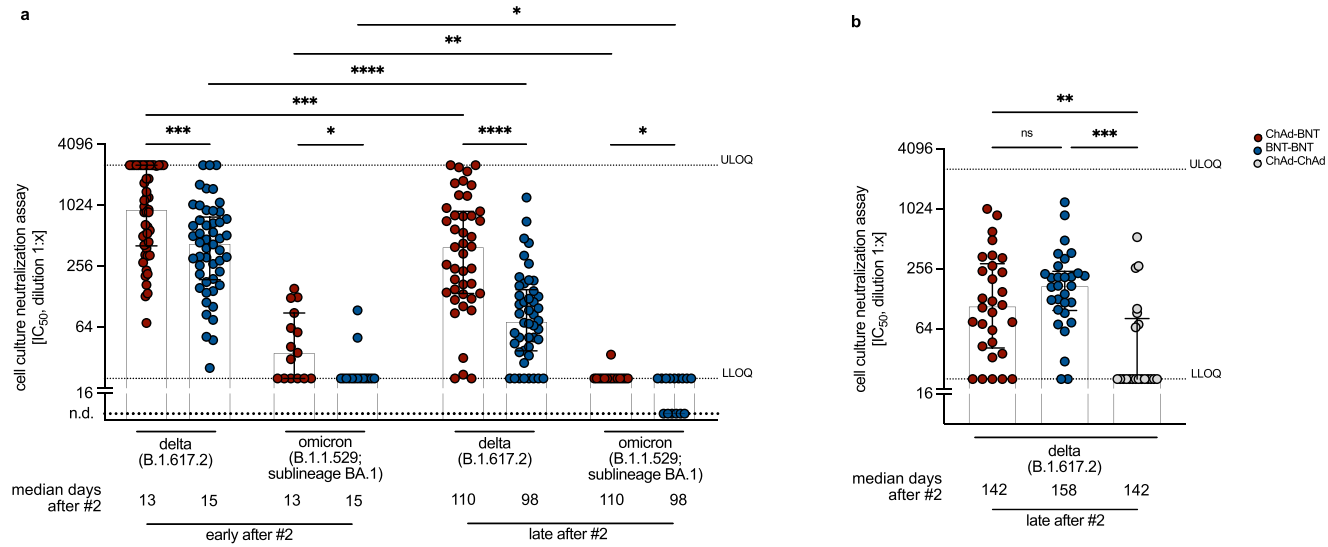


Figure 2. Individuals of the heterologous cohort neutralize variants of concerns more efficiently than individuals from homologous cohorts. Real virus neutralization levels measured against Delta [B.1.617.2] and Omicron [B.1.1.529 BA.1] at the Munich (a) or Erlangen (b) study site after heterologous ChAd-BNT or homologous BNT-BNT or ChAd-ChAd vaccination. (a) „Early after #2” refers to on average (median) 13-15 days after second BNT vaccination. „Late after #2” refers to on average (median) 98-110 days after second vaccination. $n = 50$ and 43 (ChAd-BNT; “early after #2” and „late after #2”, respectively) and $n = 50$ and 46 (BNT-BNT; “early after #2” and „late after #2”, respectively). Each group was measured against Delta and Omicron at each time point. (b) „late after #2” refers to on average (median) 158 days after second BNT (for BNT-BNT) and 142 days after second BNT or ChAd (for ChAd-BNT and ChAd-ChAd) vaccination. $n = 30$ (ChAd-BNT), $n = 30$ (BNT-BNT) and $n = 21$ (ChAd-ChAd). Here, only neutralization of Delta was tested. Bars represent group medians, whiskers interquartile range. ULOQ = upper limit of quantification (2560). LLOQ = lower limit of quantification (20). n.d. = not detected. (a) For inter-group statistics Kruskal-Wallis followed by Dunn’s multiple comparisons test was used (b). Over-time comparison within one group was done by Wilcoxon test ((a) (b)). * $p < 0.05$, ** $p < 0.01$, *** $p < 0.001$, **** $p < 0.0001$, and n.s. indicates not significant. A detailed description of the data can be found in Supplemental Table for Figure 2a and b.

proteins in their natural conformation on the cell surface (Suppl. Figure 3). Overall, these results demonstrate that humoral immunity against VoC was reduced irrespective of the vaccination regimen, but that differences in antibody neutralization capacity between the immunization cohorts remained unchanged.

Heterologous vaccination results in increased antibody avidity

The neutralization capacity of antibodies depends not only on their quantity, but also on their quality.¹⁶ We therefore next applied a modified quantitative anti-S₁ ELISA to determine antibody avidity against the S₁ domain of the SARS-CoV-2 WT spike antigen. To this end, we used samples of the sub-cohorts from the Omicron rVNT analysis (Figure 3). 13-15 days after second vaccination we observed a higher avidity of antibodies in the heterologous ChAd-BNT (median = 57.96 %) compared to the homologous BNT-BNT (median = 30.86 %) cohort. This difference remained constant at follow-up (Figure 3). Over time, there was a tentative increase in antibody avidity for both groups (BNT-BNT median = 49.49 %; ChAd-BNT median = 65.69 %) which was, however, not statistically significant ($p = 0.0537$ and $p = 0.4118$ [Friedman test]). (Figure 3). These results indicate that higher antibody avidity after heterologous ChAd-BNT compared to homologous BNT-BNT

vaccination contributes to non-inferior neutralization capacity (Figure 1).

Homologous and heterologous vaccination induce stable polyfunctional SARS-CoV-2 spike-reactive T-cell responses

Given the critical role of T lymphocytes in protection against SARS-CoV-2 infection, we next also characterized the T-cell response elicited by heterologous or homologous vaccination regimens. We acquired peripheral blood mononuclear cells (PBMCs) from vaccinated individuals at the two study centers and characterized CD4 and CD8 T-cell responses by IFN- γ enzyme-linked immunospot (ELISPOT), IFN- γ /IL-2 Fluorospot as well as intracellular cytokine staining followed by flow cytometry analysis (ICCS). To this end, PBMCs were stimulated overnight with two 15mer peptide pools covering the S₁ and S₂ domains of the full-length SARS-CoV-2 spike glycoprotein, respectively.

To evaluate the dynamics of spike-specific T cells, the frequency of antigen-reactive, IFN- γ -producing T cells was first longitudinally characterized within the ChAd-BNT in Munich (Figure 4a) and the BNT-BNT cohort in Erlangen (Figure 4b) early after first and second vaccination, as well as at the late follow-up time point. Limited T-cell responses to spike peptide stimulation were observed in some individuals already before vaccination (Figure 4b), which might result from cross-reactive

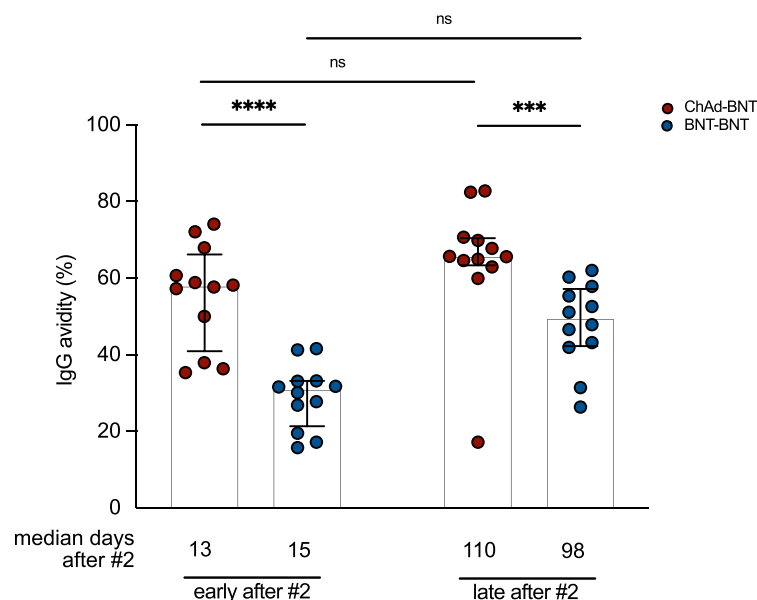


Figure 3. Higher antibody avidity upon heterologous ChAd-BNT compared to homologous BNT-BNT vaccination. Antibody avidity of a subcohort ($n = 12$) from study center Munich after heterologous ChAd-BNT and homologous BNT-BNT vaccination. „Early after #2“ refers to on average (median) 13-15 days after secondary BNT vaccination. „Late after #2“ refers to on average (median) 98 and 110 days after second vaccination. Bars represent group medians, whiskers interquartile range. For inter-group statistics concerning one time point Mann-Whitney test was used. Over-time comparison within one group was done by Friedman test. A detailed description of the data can be found in Supplemental Table for Figure 3.

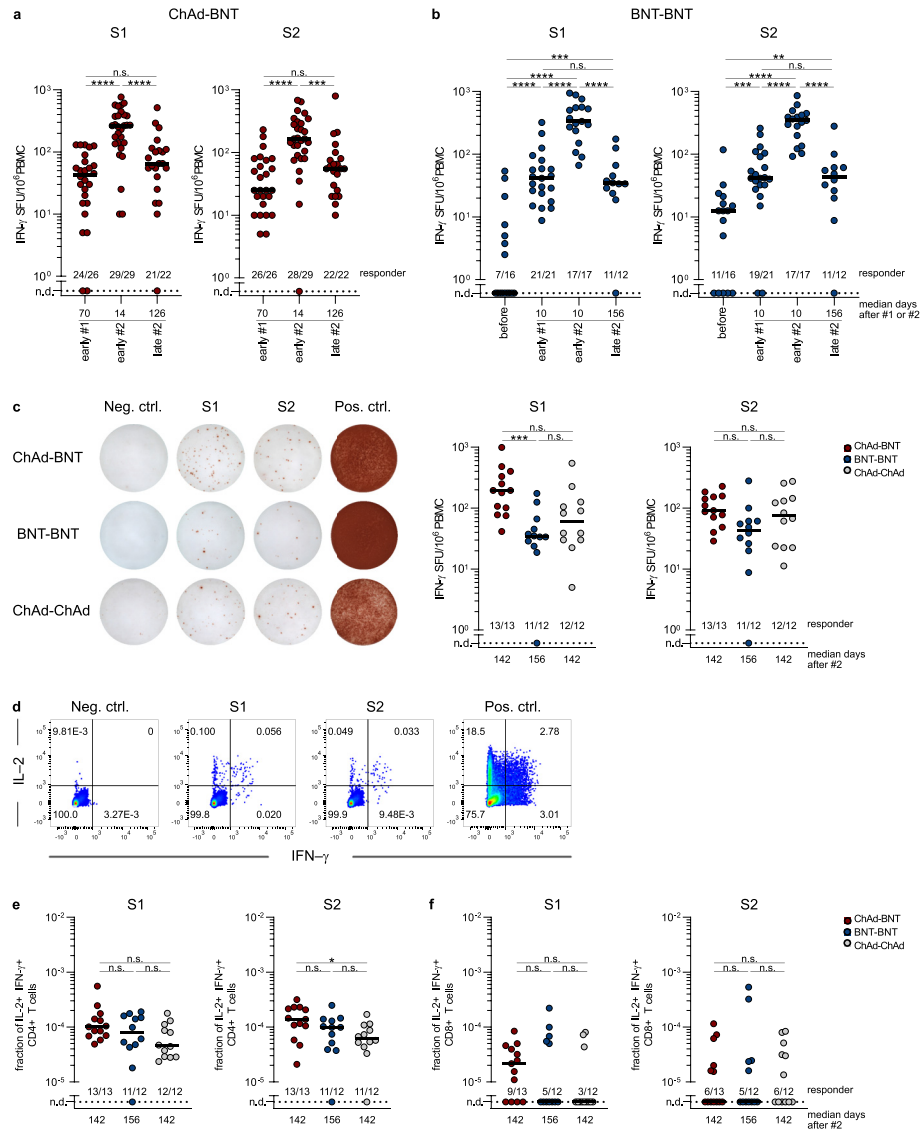


Figure 4. Long-term maintenance of SARS-CoV-2 spike-reactive T cells after homologous and heterologous vaccination. (a)–(b) Longitudinal characterization of spike-specific T cells, quantified by IFN- γ spot forming units (SFU) after stimulation with SARS-CoV-2 spike peptide pools S1 and S2. (a) Vaccinees of Munich study center quantified by IFN- γ Fluorospot. “early after #1”: 55 to 137 days after initial ChAd vaccination, $n = 26$. “early after #2”: 12 to 36 days after second BNT vaccination, $n = 29$. “late after #2”: 91 to 153 days after second BNT vaccination, $n = 22$. (b) Vaccinees of Erlangen study center quantified by IFN- γ ELISPOT. “before”: pre-vaccination, $n = 16$. “early after #1”: 9–12 days after first BNT vaccination, $n = 21$. “early after #2”: 9–11 days after second BNT vaccination, $n = 17$. “late after #2”: 148–210 days after second BNT vaccination, $n = 12$. The time points “before”, “early after #1”, and “early after #2” refer to a separate cohort of vaccinees that was included for contextualization. (c) Cohort comparison of spike-specific T cells after stimulation with SARS-CoV-2 spike peptide pools S1 and S2, in dilution of solvent (Neg. ctrl.), or with PMA/ionomycin (Pos. ctrl.). Vaccinees of Erlangen study center 141–210 days after second vaccination (late after #2). Representative data (left) and quantification of IFN- γ SFU for all donors of indicated vaccination cohorts (right) are displayed. (d)–(f) Flow cytometric analyses of polyfunctional spike-specific T cells after stimulation with SARS-CoV-2 spike peptide pools S1 and S2, in dilution of solvent (Neg. ctrl.), or with PMA/ionomycin (Pos. ctrl.). Vaccinees of Erlangen study center 141–210 days after second vaccination (late after #2). (d) Representative flow cytometry data. Shown gates are pre-gated for CD4⁺ living lymphocytes. Quantification of IL-2 and IFN- γ double-positive CD4 (e) and CD8 (f) T cells for all donors of indicated vaccination cohorts. Dots represent individual vaccinees. Numbers indicate vaccinees with a positive response defined by a detectable T-cell response above background. Non-responsive vaccinees are represented as not detected (n.d.). For inter-group statistics concerning one time point Kruskal-Wallis test was performed followed by Dunn’s multiple comparisons test ((c), (e), (f)). Over-time comparison within one group was done by Mann-Whitney test ((a), (b)). * $p < 0.05$, ** $p < 0.01$, *** $p < 0.001$, **** $p < 0.0001$, and n.s. indicates not significant.

clonotypes derived from exposure to common cold coronaviruses.^{22,23} Induction of spike-specific T cells was observed 55–137 days after one vaccination with ChAd (Munich study site, [Figure 4a](#)) or 9–12 days after one vaccination with BNT ($p < 0.0001$ [Mann-Whitney test]) (Erlangen study site, [Figure 4b](#)) in almost all individuals (“early after #1”). T-cell responses peaked 12–36 days ($p < 0.0001$ [Mann-Whitney test]) (Munich study site, [Figure 4a](#)) or 9–11 days ($p < 0.0001$ [Mann-Whitney test]) (Erlangen study site, [Figure 4b](#)) after second immunization with BNT (“early after #2”), 148–210 days (Erlangen study site) and 91–153 days (Munich study site) after second immunization with BNT (“late after #2”), comparable responses of spike-reactive T cells were observed for both homologous vaccination regimens as well as the heterologous vaccine cohort.

Having demonstrated that spike-reactive T cells were detectable at least 4 months after the second vaccination, we next examined the effect of different vaccination regimens on the quality of the T-cell response in more detail. We therefore quantified IFN- γ secreting, spike-specific T cells 141–210 days after vaccination with the different vaccine regimens in study participants at the Erlangen study center ([Figure 4c](#)). IFN- γ ELISPOT detected reactive T cells in almost all individuals of ChAd-BNT, BNT-BNT and ChAd-ChAd vaccination cohorts. After heterologous ChAd-BNT vaccination, S1-reactive T cells were detected at higher frequencies compared to the homologous BNT-BNT vaccination ($p = 0.0010$ [Kruskal-Wallis test]) cohort while there was no difference for S2-specific T cells and the other vaccination schemes (ChAd-BNT vs. BNT-BNT: $p = 0.0529$, ChAd-ChAd vs. BNT-BNT: $p = 0.4797$, ChAd-BNT vs. ChAd-ChAd: $p > 0.9999$ [Kruskal-Wallis test]). Thus, heterologous vaccination was at least as efficient as homologous vaccination in inducing spike-reactive T-cell responses that are stable over time ([Figure 4c](#)).

T-cell polyfunctionality is a hallmark of high-quality immunity and predictive of protective immune responses.²⁴ To examine whether heterologous and homologous vaccination regimens induce and maintain polyfunctional T lymphocytes equally well, T cells were characterized for simultaneous production of the effector cytokines IL-2 and IFN- γ ([Figure 4d](#); Suppl. Figure 4). Quantification of these double-positive T cells revealed a dominant, polyfunctional CD4 T-cell response that persisted in the majority of individuals irrespective of the vaccination regimen used (S1: ChAd-BNT vs. BNT-BNT: $p = 0.9115$, ChAd-ChAd vs. BNT-BNT: $p = 0.7499$, ChAd-BNT vs. ChAd-ChAd: $p = 0.0831$; S2: ChAd-BNT vs. BNT-BNT: $p = 0.3462$, ChAd-ChAd vs. BNT-BNT: $p > 0.9999$, ChAd-BNT vs. ChAd-ChAd: $p = 0.0429$ [Kruskal-Wallis test]) ([Figure 4e](#)). For CD8 T cells, we observed a greater inter-individual variability ([Figure 4f](#)) with 40–60% of cells not reacting to peptide stimulation at all. This

effect was most probably due to variable recognition of CD8 epitopes within the 15mer peptides that were used for antigenic stimulation.

Overall, the frequency of polyfunctional T cells quantified by ICS correlated with the frequency of spike-reactive T cells determined by IFN- γ ELISPOT, further validating the findings (S1: $r = 0.7$, $p < 0.0001$; S2: $r = 0.5$, $p = 0.0047$ [Spearman correlation]) (Suppl. Figure 5). Fluorospot assays further confirmed the induction of IL-2 and IFN- γ secreting polyfunctional T cells after primary immunization with ChAd and secondary immunization with BNT, as well as the persistence of a polyfunctional CD4-dominated T-cell response at the level of primary vaccination throughout the entire observation period (Suppl. Figure 6). In summary, all vaccination regimens induce stable and polyfunctional T-cell responses.

Discussion

We here analyzed the humoral and cellular immune response of 472 participants from three different study sites, 13–15 days and 98–158 days in median after homologous and heterologous ChAd and BNT vaccination. Overall, heterologous vaccination with ChAd followed by BNT induced equal or even superior humoral and cellular immune responses compared to homologous BNT-BNT or ChAd-ChAd vaccination.

We and others had previously reported enhanced neutralization capacity early after heterologous ChAd-BNT vaccination compared to homologous BNT-BNT-vaccination, both of which in turn induced clearly higher neutralizing antibody titers than a homologous ChAd vaccination regimen.^{3–12} Apart from significant waning of neutralization capacity towards WT virus at late time points for all regimens, we here observed that differences in humoral immunity towards WT virus between ChAd-BNT and BNT-BNT vaccination vanished, while homologous ChAd-ChAd still showed reduced neutralization titers compared to the other two vaccination schemes. One caveat in this regard is that we did not analyze time points longer than 5 months. In light of the unusually long germinal center reaction especially after mRNA vaccination,^{25–29} it is conceivable that at even later time points further differences between the vaccination regimens may emerge.

In line with previous reports,^{16,30–40} S-specific antibodies induced by the current vaccines encoding the S protein from the original Wuhan strain have significantly reduced neutralizing activity against the SARS-CoV-2 VoC Delta, and even less activity against Omicron. Of note, we here detect such loss of neutralization for all vaccination schedules. In terms of differences between the immunization regimens, ChAd-BNT and BNT-BNT groups showed higher neutralizing antibody response against VoCs than the ChAd-ChAd group, as observed for WT virus.

The relative binding capacity to the different spike variants might be also indicative for the degree of immune evasion by the different VoCs. Since neutralizing antibody levels directly correlate with the level of protection against infection,⁴¹ vaccine efficacy (VE) against infection with VoCs also decreased dramatically over time.^{42–44} Nevertheless, 98 – 158 days in median after the second vaccination, VE were reported to be comparable for BNT-BNT and ChAd-BNT, but lower for ChAd-ChAd schedules.^{45,46}

Antibody quality might be even more important than the mere quantity for potent vaccine responses, as demonstrated by the high avidity of anti-spike antibodies after a third exposition.¹⁶ In our study, antibody avidity increased slightly from the early to the late time point for both the ChAd-BNT and the BNT-BNT cohort, which might indicate ongoing B-cell maturation. It has been reported that this process could last up to 6 months in recipients of homologous mRNA vaccines or convalescent patients, while comparable data on heterologous vaccinations are missing.^{25–29} A higher avidity of antibodies induced by heterologous ChAd-BNT vaccination offers an explanation why they show a superior neutralization capacity against VoC at both study centers. One potential reason for differential affinity maturation of memory B cells is the difference in the interval between the first and second vaccine dose, which was in the median 63 days for the ChAd-BNT vaccinees and 21–23 days for homologous BNT-BNT vaccinated individuals. Furthermore, the duration of antigen presentation in the germinal centers might be different after viral vector immunization or mRNA vaccination. The presence of vaccine-derived mRNA and spike protein has been shown in lymph node biopsies from mRNA vaccinated individuals up to 8 weeks.²⁹ Of note, we cannot rule out that the larger time difference between the individual immunizations for the ChAd-BNT vaccinees could also influence the quantity of the antibody response, as reported recently for homologous vaccination regimens.⁴⁷ Further investigations to elucidate the differences for the current vaccines are highly relevant for the implementation of future vaccine regimens using gene-based vaccines.

Although the VE against symptomatic infections wanes over time due to the reduced neutralizing capacity of vaccine-induced antibodies, and despite the fact that Omicron by now dominates SARS-CoV-2 case numbers worldwide, protection from severe disease progression currently still prevails. Apart from boosters of humoral immunity through a third vaccination, a central reason for this is a more long-lasting^{48–52} and conserved^{53–58} T-cell response. In this context, we also addressed the question to which extent SARS-CoV-2 spike protein-specific T cells will persist in response to different vaccination regimens. Maintenance of spike-reactive T cells was observed for the vast majority of individuals after homologous and heterologous

immunization at the late time point. Longitudinal characterization of the frequency in individual vaccinees indicated longer lasting quantities of these spike-specific T cells at a level obtained after the first immunization. This observation was made at both independent study centers. Depending on the readout, the heterologous vaccination regimen was consistently non-inferior and sometimes statistically significantly superior to the homologous BNT immunization. It has already been shown that a priming dose of ChAd induces a stronger T-cell response compared to a primary immunization with BNT, which was however no longer the case after a secondary BNT immunization.⁵⁹ Nevertheless, this could still indicate that the overall superiority of humoral and cellular immunogenicity through the heterologous vaccination regimen results from a more potent primary immune response. For example, strong CD4 T-cell responses induced by primary ChAd vaccination may also explain why serological antibody responses after heterologous ChAd-BNT vaccination are more prominent than after homologous BNT-BNT vaccination.⁵⁹

Polyfunctionality as a predictor of an effective T-cell immune response was demonstrated for persisting T cells after all vaccination regimens.²⁴ Especially polyfunctional CD4 T cells were well maintained 141–210 days after the second vaccination. For CD8 T cells this was less clear, most probably owing to variable recognition of (shorter) CD8 epitopes within the 15mer peptides that were used for antigenic stimulation. Overall, our data show that heterologous vaccination is at least as capable as homologous vaccination regimens in inducing longer lasting maintenance of polyfunctional spike-specific T cells, which are likely to convey protective immunity.

In summary, these data document at least non-inferior humoral and cellular immunogenicity after heterologous ChAd-BNT vaccination compared to the respective homologous regimens. While waning of humoral immunity and reduced neutralization capacity against VoC was detected for all vaccination regimens, T-cell responses were more consistently conserved. An enhanced understanding of humoral and cellular immunity induced by individual vaccination regimens is crucial for further recommendations regarding the necessity, timing, and choice of additional vaccinations and public health policies.

Contributors

Conceptualization U.P., O.A.C., K.Ü., M.T., P.S.
 Methodology P.I., P.S., S.B., J.H.; M.W.
 Formal Analysis P.I., M.T., E.V., A.P., N.K., C.C.C., A.W., B.H.L., T.B., J.S.
 Investigation P.I., M.T., E.V., A.P., N.K., C.C.C., A.W., B.H.L., S.H., T.B., R.B., S.J., C.M., V.S., C.C., S.S., K.T., S.Y., P.S.

Resources K.Ü., M.T., U.P., P.K.

Data Curation S.B., P.S., E.V., M.T., N.K., C.C.C., A.W., B.H.L., T.B., H.M., M.W.

Writing M.T., K.S., E.V., K.K., A.P., U.P., C.B.

Visualization A.P., E.V., K.K., M.T.

Supervision K.Ü., U.P., M.T., K.S., N.K., T.B., P.K., P.S.

Project Administration O.A.C., K.Ü., U.P., M.T., C.B.

Funding Acquisition O.A.C., K.Ü., U.P.

All authors read and approved the final version of the manuscript.

M.T., K.S. and U.P. have directly accessed and verified the underlying data.

Data sharing statement

The datasets generated during and/or analysed during the current study are available from the corresponding authors on reasonable request.

Declaration of interests

J.H. reports grants and speaker honoraria from Pfizer, outside the study. JSG received speaker honoraria from Gilead Nordica and Pfizer Ireland, outside the study. P. K. reports to serve as scientific adviser to Avexis and Freeline and a grant from Roche outside from this study. U.P. reports grants from ALiOS and VirBio, and personal fees from AbbVie, Arbutus, Gilead, GSK, Johnson & Johnson, Roche, Sobi, and Vaccitech, outside the study. U.P. is co-founder and shareholder of SCG Cell Therapy O.A.C. reports grants or contracts from Amplyx, Basilea, BMBF, Cidara, DZIF, EU-DG RTD (101037867), F2G, Gilead, Matinas, MedPace, MSD, Mundipharma, Octapharma, Pfizer, Scynexis; Consulting fees from Amplyx, Biocon, Biosys, Cidara, Da Volterra, Gilead, Matinas, MedPace, Menarini, Molecular Partners, MSG-ERC, Noxxon, Octapharma, PSI, Scynexis, Seres; Honoraria for lectures from Abbott, Al-Jazeera Pharmaceuticals, Astellas, Grupo Biotoscana/United Medical/Knight, Hikma, Medscape, MedUpdate, Merck/MSD, Mylan, Pfizer; Payment for expert testimony from Cidara; Participation on a Data Safety Monitoring Board or Advisory Board from Actelion, Allegra, Cidara, Entasis, IQVIA, Janssen, MedPace, Paratek, PSI, Shionogi; A patent at the German Patent and Trade Mark Office (DE 10 2021 113 007.7); Other interests from DGHO, DGI, ECMM, ISHAM, MSG-ERC, Wiley, outside the submitted work.

All other authors declare no competing interests.

Acknowledgments

We thank Manuela Stefanie Glocker, Thomas Wochmig, Romina Bester, Philip Hagen, Kirsten Fraedrich, Norbert Donhauser, Manuela Laumer for excellent technical assistance.

Supplementary materials

Supplementary material associated with this article can be found in the online version at doi:10.1016/j.ebiom.2022.104294.

References

- Greinacher A, Thiele T, Warkentin TE, Weisser K, Kyrle PA, Eichinger S. Thrombotic thrombocytopenia after ChAdOx1 nCoV-19 vaccination. *N Engl J Med*. 2021;384(22):2092–2101.
- Vygen-Bonnet S, Koch J, Bogdan C, et al. *Beschluss der STIKO zur 5. Aktualisierung der COVID-19-Impfempfehlung und die dazugehörige wissenschaftliche Begründung*. Robert Koch-Institut; 2021.
- Hillus D, Schwarz T, Tober-Lau P, et al. Safety, reactogenicity, and immunogenicity of homologous and heterologous prime-boost immunisation with ChAdOx1 nCoV-19 and BNT162b2: a prospective cohort study. *Lancet Respir Med*. 2021;9(11):1255–1265.
- Barros-Martins J, Hammerschmidt SI, Cossmann A, et al. Immune responses against SARS-CoV-2 variants after heterologous and homologous ChAdOx1 nCoV-19/BNT162b2 vaccination. *Nat Med*. 2021;27(9):1525–1529.
- Tenbusch M, Schumacher S, Vogel E, et al. Heterologous prime-boost vaccination with ChAdOx1 nCoV-19 and BNT162b2. *Lancet Infect Dis*. 2021;21(9):1212–1213.
- Khoo NKH, Lim JME, Gill US, et al. Differential immunogenicity of homologous versus heterologous boost in Ad26.COV2.S vaccine recipients. *Med*. 2022;3(2). 104-118.e4.
- Gro R, Zanoni M, Seidel A, et al. Heterologous ChAdOx1 nCoV-19 and BNT162b2 prime-boost vaccination elicits potent neutralizing antibody responses and T cell reactivity against prevalent SARS-CoV-2 variants. *EBioMedicine*. 2022;75:103761.
- Behrens GMN, Cossmann A, Stankov MV, et al. SARS-CoV-2 delta variant neutralisation after heterologous ChAdOx1-5/BNT162b2 vaccination. *Lancet*. 2021;398(10305):1041–1042.
- Kaku CI, Champney ER, Normark J, et al. Broad anti-SARS-CoV-2 antibody immunity induced by heterologous ChAdOx1/mRNA-1273 vaccination. *Science*. 2022;375(6584):1041–1047.
- Schmidt T, Klemis V, Schub D, et al. Immunogenicity and reactogenicity of heterologous ChAdOx1 nCoV-19/mRNA vaccination. *Nat Med*. 2021;27(9):1530–1535.
- Normark J, Vikström L, Gwon Y-D, et al. Heterologous ChAdOx1 nCoV-19 and mRNA-1273 vaccination. *N Engl J Med*. 2021;385(11):1049–1051.
- Liu X, Shaw RH, Stuart ASV, et al. Safety and immunogenicity of heterologous versus homologous prime-boost schedules with an adenoviral vectored and mRNA COVID-19 vaccine (Com-COV): a single-blind, randomised, non-inferiority trial. *Lancet*. 2021;398(10303):856–869.
- Altmann DM, Boyton RJ. Waning immunity to SARS-CoV-2: implications for vaccine booster strategies. *Lancet Respirat Med*. 2021;9(12):1356–1358.
- Marking U, Havervall S, Greilert-Norin N, et al. Duration of SARS-CoV-2 immune responses up to six months following homologous or heterologous primary immunization with ChAdOx1 nCoV-19 and BNT162b2 mRNA Vaccines. *Vaccines*. 2022;10(3):359.
- Ho T-C, Chen Y-MA, Chan H-P, et al. The effects of heterologous immunization with prime-boost COVID-19 vaccination against SARS-CoV-2. *Vaccines*. 2021;9(10):1163.
- Wrátil PR, Stern M, Priller A, et al. Three exposures to the spike protein of SARS-CoV-2 by either infection or vaccination elicit superior neutralizing immunity to all variants of concern. *Nat Med*. 2022;28:496–503.
- Almanzar G, Ottensmeier B, Liese J, Prelog M. Assessment of IgG avidity against pertussis toxin and filamentous hemagglutinin via an adapted enzyme-linked immunosorbent assay (ELISA) using ammonium thiocyanate. *J Immunol Methods*. 2013;387(1-2):36–42.
- Kneitz R-H, Schubert J, Tollmann F, Zens W, Hedman K, Weissbrich B. A new method for determination of varicella-zoster virus immunoglobulin G avidity in serum and cerebrospinal fluid. *BMC Infect Dis*. 2004;4:33.
- Lapuente D, Maier C, Irrgang P, et al. Rapid response flow cytometric assay for the detection of antibody responses to SARS-CoV-2. *Eur J Clin Microbiol Infect Dis*. 2021;40(4):751–759.
- Dispinseri S, Marzinotto I, Brigatti C, et al. Seasonal betacoronavirus antibodies' expansion Post-BNT161b2 vaccination associates

- with reduced SARS-CoV-2 VoC neutralization. *J Clin Immunol*. 2022;42:448–458.
- 21 Lapuente D, Fuchs J, Willar J, et al. Protective mucosal immunity against SARS-CoV-2 after heterologous systemic prime-mucosal boost immunization. *Nat Commun*. 2021;12(1):6871.
 - 22 Braun J, Loyal L, Frentsch M, et al. SARS-CoV-2-reactive T cells in healthy donors and patients with COVID-19. *Nature*. 2020;587(7833):270–274.
 - 23 Grifoni A, Weiskopf D, Ramirez SI, et al. Targets of T cell responses to SARS-CoV-2 Coronavirus in humans with COVID-19 disease and unexposed individuals. *Cell*. 2020;181(7):1489–1501.e15.
 - 24 Seder RA, Darrah PA, Roederer M. T-cell quality in memory and protection: implications for vaccine design. *Nat Rev Immunol*. 2008;8(4):247–258.
 - 25 Sokal A, Chappert P, Barba-Spaeth G, et al. Maturation and persistence of the anti-SARS-CoV-2 memory B cell response. *Cell*. 2021;184(5):1201–1213.e14.
 - 26 Kim W, Zhou JQ, Horvath SC, et al. Germinal centre-driven maturation of B cell response to mRNA vaccination. *Nature*. 2022:1–8.
 - 27 Mudd PA, Minervina AA, Pogorelyy MV, et al. SARS-CoV-2 mRNA vaccination elicits a robust and persistent T follicular helper cell response in humans. *Cell*. 2022;185(4):603–613.e15.
 - 28 Turner JS, O'Halloran JA, Kalaidina E, et al. SARS-CoV-2 mRNA vaccines induce persistent human germinal centre responses. *Nature*. 2021;596(7870):109–113.
 - 29 Röltgen K, Nielsen SC, Silva O, et al. Immune imprinting, breadth of variant recognition, and germinal center response in human SARS-CoV-2 infection and vaccination. *Cell*. 2022;185(6):1025–1040.e14.
 - 30 Muecksch F, Wang Z, Cho A, et al. Increased potency and breadth of SARS-CoV-2 neutralizing antibodies after a third mRNA vaccine dose. *bioRxiv* 2022.
 - 31 Sheward DJ, Kim C, Ehling RA, et al. Neutralisation sensitivity of the SARS-CoV-2 omicron (B.1.1.529) variant: a cross-sectional study. *Lancet Infect Dis*. 2022;22(6):813–820.
 - 32 Hoffmann M, Krüger N, Schulz S, et al. The Omicron variant is highly resistant against antibody-mediated neutralization: Implications for control of the COVID-19 pandemic. *Cell*. 2022;185(3):447–456.e11.
 - 33 Planas D, Saunders N, Maes P, et al. Considerable escape of SARS-CoV-2 Omicron to antibody neutralization. *Nature*. 2022;602(7898):671–675.
 - 34 Dejnirattisai W, Shaw RH, Supasa P, et al. Reduced neutralisation of SARS-CoV-2 omicron B.1.1.529 variant by post-immunisation serum. *Lancet*. 2022;399(10321):234–236.
 - 35 Muik A, Lui BG, Wallisch A-K, et al. Neutralization of SARS-CoV-2 Omicron by BNT162b2 mRNA vaccine-elicited human sera. *Science*. 2022;375(6581):678–680.
 - 36 Pajon R, Doria-Rose NA, Shen X, et al. SARS-CoV-2 Omicron variant neutralization after mRNA-1273 booster vaccination. *N Engl J Med*. 2022;386(11):1088–1091.
 - 37 Dejnirattisai W, Huo J, Zhou D, et al. SARS-CoV-2 Omicron-B.1.1.529 leads to widespread escape from neutralizing antibody responses. *Cell*. 2022;185(3):467–484.e15.
 - 38 Gruell H, Vanshylla K, Tober-Lau P, et al. mRNA booster immunization elicits potent neutralizing serum activity against the SARS-CoV-2 Omicron variant. *Nat Med*. 2022:1–4.
 - 39 Cheng SMS, Mok CKP, Leung YWY, et al. Neutralizing antibodies against the SARS-CoV-2 Omicron variant BA.1 following homologous and heterologous CoronaVac or BNT162b2 vaccination. *Nat Med*. 2022:1–4.
 - 40 Pérez-Then E, Lucas C, Monteiro VS, et al. Neutralizing antibodies against the SARS-CoV-2 Delta and Omicron variants following heterologous CoronaVac plus BNT162b2 booster vaccination. *Nat Med*. 2022;28:481–485.
 - 41 Khoury DS, Cromer D, Reynaldi A, et al. Neutralizing antibody levels are highly predictive of immune protection from symptomatic SARS-CoV-2 infection. *Nat Med*. 2021;27(7):1205–1211.
 - 42 Hansen CH, Schelde AB, Moustsen-Helm IR, et al. Vaccine effectiveness against SARS-CoV-2 infection with the Omicron or Delta variants following a two-dose or booster BNT162b2 or mRNA-1273 vaccination series: a Danish cohort study. *medRxiv* 2021.2021.12.20.21267966.
 - 43 Andrews N, Stowe J, Kirsebom F, et al. Covid-19 vaccine effectiveness against the Omicron (B.1.1.529) variant. *N Engl J Med*. 2022;386:1532–1546.
 - 44 Martínez-Baz I, Trobajo-Sanmartín C, Miqueleiz A, et al. Product-specific COVID-19 vaccine effectiveness against secondary infection in close contacts, Navarre, Spain, April to August 2021. *Euro Surveill*. 2021;26(39):pii=2100894.
 - 45 Nordström P, Ballin M, Nordström A. Risk of infection, hospitalisation, and death up to 9 months after a second dose of COVID-19 vaccine: a retrospective, total population cohort study in Sweden. *Lancet*. 2022;399(10327):814–823.
 - 46 Nordström P, Ballin M, Nordström A. Effectiveness of heterologous ChAdOx1 nCoV-19 and mRNA prime-boost vaccination against symptomatic Covid-19 infection in Sweden: a nationwide cohort study. *Lancet Reg Health Eur*. 2021;11:100249.
 - 47 Wei J, Pouwels KB, Stoesser N, et al. Antibody responses and correlates of protection in the general population after two doses of the ChAdOx1 or BNT162b2 vaccines. *Nat Med*. 2022;28(5):1072–1082.
 - 48 Woldemeskel BA, Garliss CC, Blankson JN. mRNA vaccine-elicited SARS-CoV-2-specific T cells persist at 6 months and recognize the delta variant. *Clin Infect Dis*. 2022;75(1):e898–e901.
 - 49 Oberhardt V, Luxenburger H, Kemming J, et al. Rapid and stable mobilization of CD8+ T cells by SARS-CoV-2 mRNA vaccine. *Nature*. 2021;597(7875):268–273.
 - 50 Mateus J, Dan JM, Zhang Z, et al. Low-dose mRNA-1273 COVID-19 vaccine generates durable memory enhanced by cross-reactive T cells. *Science*. 2021;374(6566):eabj9853.
 - 51 Moss P. The T cell immune response against SARS-CoV-2. *Nat Immunol*. 2022;23(2):186–193.
 - 52 Guerrero G, Picozza M, D'Orso S, et al. BNT162b2 vaccination induces durable SARS-CoV-2-specific T cells with a stem cell memory phenotype. *Sci Immunol*. 2021;6(66):eabl5344.
 - 53 Gao Y, Cai C, Grifoni A, et al. Ancestral SARS-CoV-2-specific T cells cross-recognize the Omicron variant. *Nat Med*. 2022:1–5.
 - 54 Keeton R, Tincho MB, Ngomti A, et al. T cell responses to SARS-CoV-2 spike cross-recognize Omicron. *Nature*. 2022;603(7901):488–492.
 - 55 Naranbhai V, Nathan A, Kaseke C, et al. T cell reactivity to the SARS-CoV-2 Omicron variant is preserved in most but not all individuals. *Cell*. 2022.
 - 56 GeurtsvanKessel CH, Geers D, Schmitz KS, et al. Divergent SARS CoV-2 Omicron-reactive T- and B cell responses in COVID-19 vaccine recipients. *Sci Immunol*. 2022:eab02202.
 - 57 Liu J, Chandrashekar A, Sellers D, et al. Vaccines elicit highly conserved cellular immunity to SARS-CoV-2 Omicron. *Nature*. 2022;603:493–496.
 - 58 Tarke A, Coelho CH, Zhang Z, et al. SARS-CoV-2 vaccination induces immunological T cell memory able to cross-recognize variants from Alpha to Omicron. *Cell*. 2022;185(5):847–859.e11.
 - 59 Pozzetto B, Legros V, Djebali S, et al. Immunogenicity and efficacy of heterologous ChAdOx1-BNT162b2 vaccination. *Nature*. 2021;600(7890):701–706.

Article

Improved SARS-CoV-2 Neutralization of Delta and Omicron BA.1 Variants of Concern after Fourth Vaccination in Hemodialysis Patients

Cho-Chin Cheng^{1,†}, Louise Platen^{2,†}, Catharina Christa¹, Myriam Tellenbach², Verena Kappler², Romina Bester¹, Bo-Hung Liao¹, Christopher Holzmann-Littig^{2,3}, Maia Werz², Emely Schönhals², Eva Platen⁴, Peter Eggerer⁵, Laëtitia Tréguer⁶, Claudius Küchle², Christoph Schmaderer², Uwe Heemann², Lutz Renders^{2,7}, Ulrike Protzer^{1,7,8,*} and Matthias Christoph Braunisch^{2,*}

- ¹ Institute of Virology, School of Medicine, Technical University of Munich, 81675 Munich, Germany
² Department of Nephrology, School of Medicine, Technical University of Munich, Klinikum Rechts der Isar, 81675 Munich, Germany
³ TUM Medical Education Center, School of Medicine, Technical University of Munich, 81675 Munich, Germany
⁴ Kidney Center Eifel Dialyse, 53894 Mechernich, Germany
⁵ KfH Kidney Center Harlaching, Munich-Harlaching, 81545 Munich, Germany
⁶ KfH Kidney Center, 83278 Traunstein, Germany
⁷ German Center for Infection Research (DZIF), Partner Site, 81675 Munich, Germany
⁸ Institute of Virology, Helmholtz Munich, 85764 Munich, Germany
* Correspondence: protzer@tum.de (U.P.); matthias.braunisch@mri.tum.de (M.C.B.); Tel.: +0049-(0)-89-4140-6863 (U.P.); +0049-(0)-89-4140-2231 (M.C.B.); Fax: +0049-(0)-89-4140-6823 (U.P.); +0049-(0)-89-4140-7734 (M.C.B.)
† These authors contributed equally to this work.
‡ These authors contributed equally to this work.



Citation: Cheng, C.-C.; Platen, L.; Christa, C.; Tellenbach, M.; Kappler, V.; Bester, R.; Liao, B.-H.; Holzmann-Littig, C.; Werz, M.; Schönhals, E.; et al. Improved SARS-CoV-2 Neutralization of Delta and Omicron BA.1 Variants of Concern after Fourth Vaccination in Hemodialysis Patients. *Vaccines* **2022**, *10*, 1328. <https://doi.org/10.3390/vaccines10081328>

Academic Editor: Stephen N. Crooke

Received: 20 July 2022

Accepted: 13 August 2022

Published: 16 August 2022

Publisher's Note: MDPI stays neutral with regard to jurisdictional claims in published maps and institutional affiliations.



Copyright: © 2022 by the authors. Licensee MDPI, Basel, Switzerland. This article is an open access article distributed under the terms and conditions of the Creative Commons Attribution (CC BY) license (<https://creativecommons.org/licenses/by/4.0/>).

Abstract: Hemodialysis patients are exposed to a markedly increased risk when infected with SARS-CoV-2. To date, it is unclear if hemodialysis patients benefit from four vaccinations. A total of 142 hemodialysis patients received four COVID-19 vaccinations until March 2022. RDB binding antibody titers were determined in a competitive surrogate neutralization assay. Vero-E6 cells were infected with SARS-CoV-2 variants of concern (VoC), Delta (B.1.617.2), or Omicron (B.1.1.529, sub-lineage BA.1) to determine serum infection neutralization capacity. Four weeks after the fourth vaccination, serum infection neutralization capacity significantly increased from a 50% inhibitory concentration (IC₅₀, serum dilution factor 1:x) of 247.0 (46.3–1560.8) to 2560.0 (1174.0–2560.0) for the Delta VoC, and from 37.5 (20.0–198.8) to 668.5 (182.2–2560.0) for the Omicron VoC (each $p < 0.001$) compared to four months after the third vaccination. A significant increase in the neutralization capacity was even observed for patients with high antibody titers after three vaccinations ($p < 0.001$). Ten patients with SARS-CoV-2 breakthrough infection after the first blood sampling had by trend lower prior neutralization capacity for Omicron ($p = 0.051$). Our findings suggest that hemodialysis patients benefit from a fourth vaccination in particular in the light of the highly infectious SARS-CoV-2 Omicron-variants. A routinely applied four-time vaccination seems to broaden immunity against variants and would be recommended in hemodialysis patients.

Keywords: hemodialysis; SARS-CoV-2; COVID-19 vaccination; in-vitro viral neutralization

1. Introduction

In hemodialysis patients, a SARS-CoV-2 infection is associated with a markedly increased morbidity and mortality compared to the general population, with a mortality rate of more than 20% in hospitalized patients [1–3]. In the last two years, we have learned that double vaccination might not be enough to achieve adequate long-term immune protection in all hemodialysis patients, and triple vaccination offers significantly better

protection against COVID-19 in this patient group [1,4]. Even if an infection cannot always be prevented, the course of the COVID-19 disease, in general, is milder depending on the number of vaccinations in hemodialysis patients [5]. However, even in hemodialysis patients with an inadequate immune response after multiple vaccinations, morbidity remains significantly increased [6].

A third vaccination is associated with an increased virus neutralization capacity in the general population [7,8]. Therefore, to date, the third vaccination has become part of the standard vaccination regimen, and meanwhile, a fourth vaccination is recommended in risk groups like hemodialysis patients [9]. The usefulness of a third and now a fourth vaccination is based on data from the general population and was obtained during the SARS-CoV-2 Delta wave. However, infections with the Omicron variant of concern (VoC) dramatically increased in 2022 [10]. Therefore, the question remains whether the currently recommended vaccination regimen in hemodialysis patients also offers effective protection towards VoC Omicron.

The aim of this study was to investigate whether hemodialysis patients benefit from a fourth vaccination and if the immune response after the fourth vaccination has a comparable efficacy towards the VoCs Delta and Omicron BA.1.

Here, we present the results of the live-virus infection neutralization of SARS-CoV-2 Delta and Omicron BA.1 VoCs and antibody-mediated immunity shortly before compared to four weeks after the fourth COVID-19 vaccination in a cohort of 142 hemodialysis patients.

2. Materials and Methods

2.1. Study Design

The COVIIMP study (German: “COVID-19-Impfansprechen immunsupprimierter Patient*innen”) is a prospective observational study examining the COVID-19 immunization success and the clinical course of COVID-19 in patients immunocompromised due to kidney transplantation, a rheumatologic disease, or dialysis who received immunization against SARS-CoV-2 as recommended by the German health authorities.

All participants provided written informed consent. The study, conforming to the ethical guidelines of the Helsinki Declaration, was approved by the Medical Ethics Committee of the Klinikum rechts der Isar of the Technical University of Munich (approval number 163/21 S-SR, 19 March 2021) and registered at the Paul Ehrlich Institute (NIS592).

2.2. Study Population

Of 513 enrolled patients, 142 patients requiring maintenance hemodialysis were selected. These patients received four COVID-19 vaccinations between 19 December 2020 and 20 March 2022 and underwent blood analysis before and after the fourth vaccination (Figure 1A). This subpopulation was recruited in four dialysis centers (Klinikum rechts der Isar, KfH Kidney Center Traunstein, Kidney Center Eifeldialyse, KfH Kidney Center München-Harlaching). Demographic data, medical history, history of transplantation, and comorbidities as assessed by the Charlson Comorbidity Index (CCI) were collected. Immunosuppressive medication during the vaccination period was documented.

2.3. Hepatitis B Vaccination

Hepatitis B vaccination status was based on medical reports and, if available, serological laboratory data on anti-HBs antibodies. Patients were considered non-responders if an anti-HB titer below 10 IU/l despite three hepatitis B vaccinations was documented or their treating physicians classified them as a hepatitis B non-responder, according to local standards.

2.4. SARS-CoV-2 Infection

We identified participants as SARS-CoV-2 convalescent if they had a prior positive SARS-CoV-2 PCR or at least one positive serological SARS-CoV-2 nucleocapsid-specific IgG measurement [4,11].

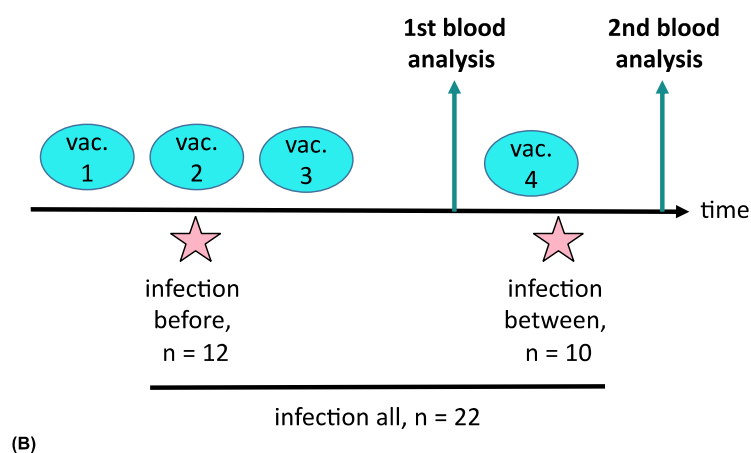
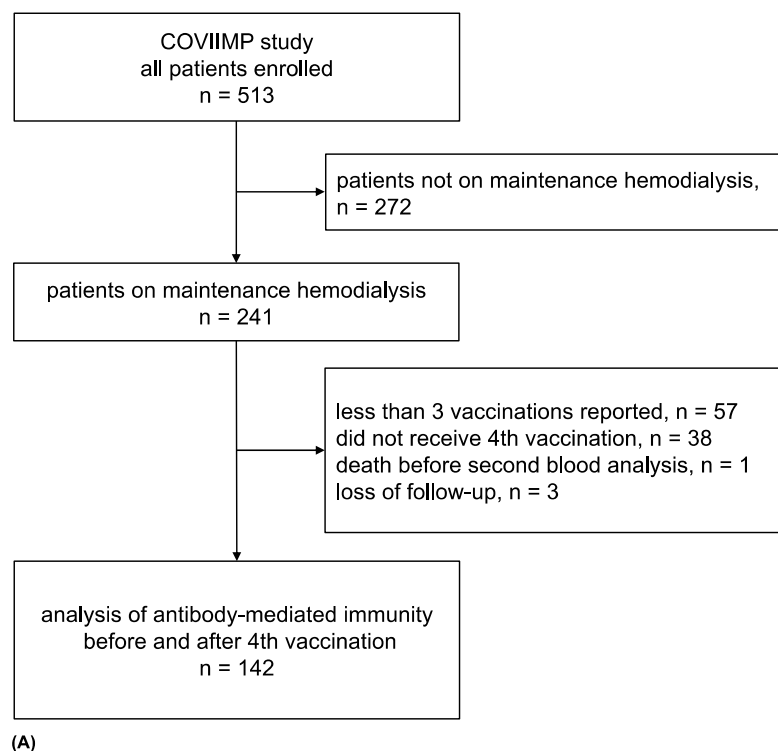


Figure 1. Flow chart of the COVIIMP study (A). Study design and observed SARS-CoV-2 infection cases (B). Abbreviations: vac., vaccination.

2.5. Sample Collection

Blood was collected for analysis in a median two (2.0–3.25) days before (analysis 1) and 26 (26.0–26.0) days after (analysis 2) the fourth vaccination.

2.6. SARS-CoV-2 IgG Assay

Antibodies in patients' sera were detected using commercial surrogate paramagnetic particle chemiluminescence immunoassays (CLIA, Yhlo Biotechnology, Shenzhen, China) performed on the iFlash 1800 platform. Nucleocapsid-specific IgG antibodies (anti-N IgG) were determined using the 2019-nCoV IgG kit. The surrogate neutralization assay (NAb) was performed with the iFlash 2019-nCoV NAb kit based on the competition of serum antibodies with recombinant angiotensin-converting enzyme 2 for binding the SARS-CoV-2 Wuhan strain receptor binding domain (RBD) and has been adapted for quantification to manufacturer's instructions [11,12]. The cut-off level for seropositivity

was set at 10 neutralizing units per milliliter (AU/ml) according to the manufacturer's instructions. Surrogate neutralization activity expressed as AU/ml can be adapted to WHO standard ($\text{AU/mL} \times 2.4 = \text{BAU/mL}$ [binding units/mL]). The maximum measurable value for NAb was 800 AU/mL, lower level of detection was 4 AU/mL. If values exceeded the upper limit of quantification, a value of 801 AU/mL was used for statistical analysis. NAb high-response was defined as levels ≥ 700 AU/mL before the fourth vaccination. N-specific IgGs ≥ 10 AU/mL were qualitatively determined as reactive. In one patient analysis of NABs after the fourth vaccination was missing.

2.7. SARS-CoV-2 Infection-Neutralization Assay

Serum infection-neutralization capacity was analyzed as previously described [8]. Briefly, SARS-CoV-2 isolates were isolated from nasopharyngeal swabs of COVID-19 infected individuals. To obtain a high titer of virus stock, Vero-E6 cells were infected with VoC Delta (B.1.617.2, GISAID EPI ISL: 2772700) or Omicron (B.1.1.529, sub-lineage BA.1, GISAID EPI ISL: 7808190) and incubated in Dulbecco's modified Eagle's medium. After 2–3 days following inoculation, the cell culture medium was collected, centrifuged, and the virus-containing supernatant was stored at -80 °C. Prior to the neutralization experiments, viral titers were verified by plaque assay, and strain identity was confirmed by next-generation sequencing. All measurements were performed using serum samples stored at -80 °C and defrosted and stored at 4 °C on the day before the analysis. Samples from all patients were analyzed in parallel. For quantification of the neutralization capacity, two-fold serial dilutions of the sera from 1:20 to 1:2560 were incubated with a predefined multiplicity of infection (MOI) of 0.03 (450 PFU/15,000 cells/well) of either of the VoCs for 1 h at 37 °C. The MOI was determined from an in-cell ELISA pre-test by which we observed viral signal saturation 24 h after infection. After the 1-h inoculation, the inoculum was transferred onto pre-seeded Vero E6 cells for another one-hour incubation at 37 °C. The infection was terminated after one day and followed by an in-cell ELISA to detect SARS-CoV-2 N-protein. Cells were fixed with 4% paraformaldehyde and permeabilized by 0.5% saponin buffer. After blocking with 10% goat serum, cells were stained using anti-SARS-CoV-2-N primary (40143-T62, Sino Biological, Beijing, China) and a goat anti-rabbit IgG2a-HRP secondary antibody (EMD Millipore/#12-348, Shanghai, China), and eventually transformed into a colorimetric signal by adding substrate tetramethylbenzidine (TMB). To determine serum IC₅₀ values, a nonlinear regression curve was applied, and the dilution factor at which 50% inhibition was observed and calculated using PRISM software (GraphPad, Shanghai, China). Patients were classified as low or non-responders if the IC₅₀ value of the infection neutralization was $\leq 1:20$.

2.8. Statistical Analysis

Categorical variables are presented as frequencies and percentages. Continuous variables are expressed as mean \pm standard deviation (SD) or median and interquartile range (IQR), as appropriate. Group differences were tested with the χ^2 test or Fisher test. The independent samples *t*-test or Mann-Whitney-U test was used for continuous variables, as appropriate. Paired samples were examined with the Wilcoxon test and the McNemar test, as appropriate. Spearman correlation was used for correlation analysis.

Univariate and multivariate linear regression models were applied to identify possible predictors of the infection-neutralizing capacity of VoC Delta or Omicron BA.1 (IC₅₀) out of the following candidate variables: age, dialysis vintage, presence of immunosuppression, comorbidities, and hepatitis B vaccination non-response. Possible predictors were preselected prior to the statistical analysis. Logistic regression was used to examine the neutralization capacity towards an infection with SARS-CoV-2.

All tests were conducted two-sided, and $p < 0.05$ was considered significant. Statistical analysis was performed using R version 4.0.2 (R Foundation for Statistical Computing, Vienna, Austria).

3. Results

Overall, 142 patients on maintenance hemodialysis were included (Figure 1A). Patients had a median age of 72.6 (61.5–80.6) years. 48 (33.8%) patients were female. The median dialysis vintage was 48.9 (21.3–83.7) months. At the time of the first, second, third, and fourth vaccination, 124 (87.3%), 125 (88.0%), 136 (95.8%), and 142 (100%) were on maintenance hemodialysis, respectively. Further details of patient characteristics can be found in Table 1 for all patients and stratified by infection neutralization response against VoC Omicron BA.1.

Table 1. Patient characteristics.

	Total <i>n</i> = 142	Omicron BA.1 Neutralization after Fourth Vaccination		<i>p</i>
		Low/Non-Responder <i>n</i> = 12	Responder <i>n</i> = 130	
Age (years)	72.6 (61.5–80.6)	77.1 (67.0–79.7)	72.2 (60.5–80.6)	0.47
Female	48 (33.8%)	7 (58.3%)	41 (31.5%)	0.11
Dialysis vintage (months)	48.9 (21.3–83.7)	38.7 (13.4–63.6)	49.3 (21.9–84.0)	0.34
Vaccines				1.0
mRNA and vector	8 (5.6%)	0 (0.0%)	8 (6.2%)	
only mRNA	134 (94.4%)	12 (100.0%)	122 (93.8%)	
COVID-19 infection before second blood examination	22 (15.5%)	2 (16.7%)	20 (15.4%)	1.0
Time lap between infection and second blood examination (days)	215.7 ± 223.3	157.5 ± 222.7	224.6 ± 231.1	0.71
Charlson Comorbidity Index	5.0 (4.0–7.0)	5.5 (4.0–6.2)	5.0 (4.0–7.0)	0.95
History of kidney transplantation	16 (11.3%)	1 (8.1%)	15 (11.5%)	1.00
Immunosuppressive medication	16 (11.3%)	4 (33.3%)	12 (9.2%)	0.031
Hepatitis B vaccination non-response	51 (36.4%)	5 (41.7%)	46 (35.4%)	0.94
Renal diagnosis				
Glomerulopathy	22 (16.1%)			
Diabetic nephropathy	24 (17.5%)			
Hypertensive nephropathy	17 (12.4%)			
Congenital or cystic renal disease	13 (9.5%)			
Tubulointerstitial disease	2 (1.5%)			
Reflux nephropathy	3 (2.2%)			
Other	18 (13.1%)			
Nephropathy of unknown origin	43 (30.3%)			

Results are presented as mean (±SD) and median (interquartile range) for normally and non-normally distributed data, respectively; categorical data as total number (percentage). *p* values present the results of group-wise comparisons of patients neutralizing Omicron BA.1 after the fourth vaccination.

3.1. COVID-19 and Vaccinations

All patients received four vaccinations, eight and six of which received their first and second vaccination with AZD1222 (Vaxzevria[®], AstraZeneca Canada Inc., Mississauga, ON, Canada) by AstraZeneca. All other vaccinations were done with mRNA-based vaccines (BNT162b2 by BioNTech-Pfizer, New York, NY, USA or mRNA-1273 by Moderna, Cambridge, MA, USA). Fifteen patients received two or more vaccinations with mRNA-1273 (Spikevax[®], Moderna), and the remaining patients received BNT162b2 (Comirnaty[®], BioNTech-Pfizer). The median duration between the first and the fourth vaccination was 338.0 (333.0–342.0) days, and between the third and the fourth vaccination 126.0 (105.0–126.0) days, respectively. The median duration between the third vaccination and the first blood sampling was 4.1 (3.4–4.1) months.

A SARS-CoV-2 breakthrough infection indicated by SARS-CoV-2 nucleocapsid-specific IgG antibody positivity or a positive SARS-CoV-2 PCR occurred in 22 (15.5%) individuals before the second blood sampling after the fourth vaccination (Figure 1B). In these patients, the average time between the SARS-CoV-2 infection and the second blood collection was 215.7 ± 223.3 days. Of these, seven patients had no known history of SARS-CoV-2 infection but were classified as convalescent due to positive anti-nucleocapsid IgG detection. Four (18.2%) of the 22 infected patients were treated with SARS-CoV-2-specific monoclonal antibodies. Ten (7.0%) patients had a SARS-CoV-2 infection between the two blood draw-

ings before and after the fourth vaccination. No patient reported recurrent SARS-CoV-2 infections (Figure 1B).

3.2. Immunosuppression

Immunosuppressive medication was prescribed in 16 (11.3%) patients during the observation period. Reasons for immunosuppression were history of organ transplantation in eight, cancer treatment in four, underlying kidney disease in two, and unknown causes in two other patients. Immunosuppressive agents were glucocorticoids in 14, tacrolimus in four, mycophenolate mofetil in three, and others in two patients (lenalidomide, rituximab, and reduced dose CHOP).

3.3. Impact of Four Vaccinations on Neutralization Capacity and NABs

After the fourth vaccination significantly increased serum neutralization capacities were found for both VoCs, Delta and Omicron BA.1. Infection neutralization capacity for Delta increased from a median IC50 (serum dilution factor, 1:x) of 247.0 (46.3–1560.8) to 2560.0 (1174.0–2560.0), and for Omicron BA.1 from 37.5 (20.0–198.8) to 668.5 (182.2–2560.0) (each $p < 0.001$) (Figure 2A,B). NAb levels significantly increased from 721.0 (184.5–801.0) to 801.0 (801.0–801.0, $p < 0.001$) (Figure 2C). Serum neutralization capacity after the fourth vaccination was significantly lower for Omicron BA.1 compared to Delta (668.5 [182.2–2560.0] vs. 2560.0 [1174.0–2560.0], $p < 0.001$). Similar to the overall cohort, when analyzing only NAb high-responder, we found a significant increase for the neutralization capacity for both VoCs, Delta (1172.5 [382.8–2560.0] vs. 2560.0 [2560.0–2560.0], $p < 0.001$) and Omicron BA.1 (170.5 [56.3–468.5] vs. 2553.0 [640.2–2560.0], $p < 0.001$).

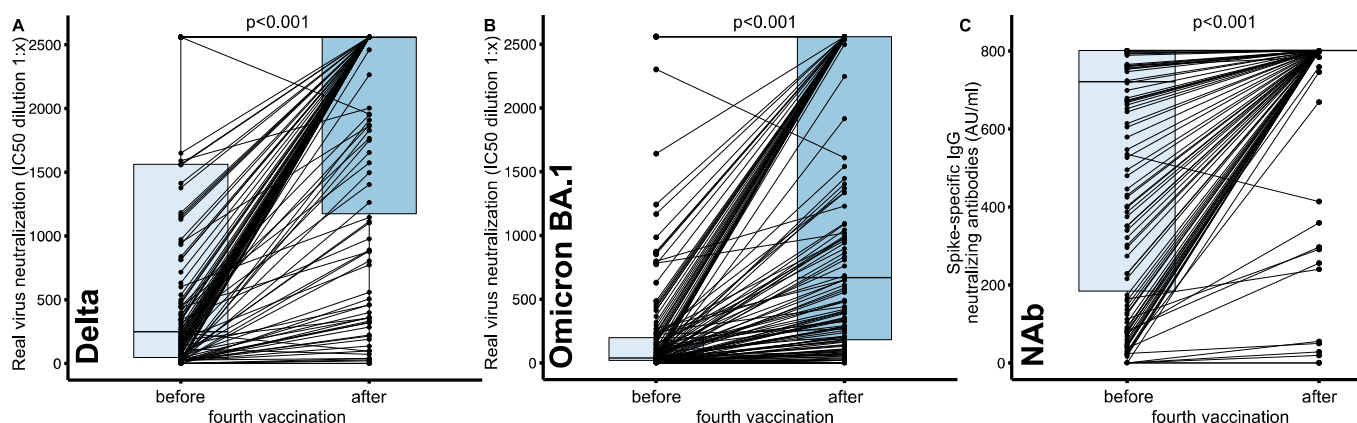


Figure 2. Changes in SARS-CoV-2 infection neutralization capacity before and after the fourth COVID-19 vaccination in hemodialysis patients. Real virus neutralization assay was performed using (A) the SARS-CoV-2 Delta (B.1.617.2) and (B) the Omicron (B.1.1.529, sub-lineage BA.1) variant of concern upon serial dilution of hemodialysis patient sera before and after the fourth vaccination. Inhibitory concentration (IC50) dilution values are given. (C) Change of spike-specific IgG neutralizing antibody (NAb) titers given in AU/mL in a surrogate neutralization assay. Dots indicate the measurement of an individual patient with lines connecting individual patient values before and after the fourth vaccination. Boxes indicate median and interquartile ranges. Statistical analysis was performed using paired-samples Wilcoxon test, p values indicate statistical significance between groups.

Patients with a serum $IC_{50} \leq 20$ were classified as low, and those with no detectable neutralization as non-responder. Regarding Delta and Omicron BA.1 infection neutralization capacity, significantly fewer patients (Delta: 30 vs. 5; Omicron BA.1: 61 vs. 12, each $p < 0.001$) were low or non-responders after the fourth vaccination. The percentage of NAb responders was already very high before the fourth vaccination and did not further increase significantly (136 [95.8%] vs. 139 [98.6%], $p = 0.13$) (Figure 3).

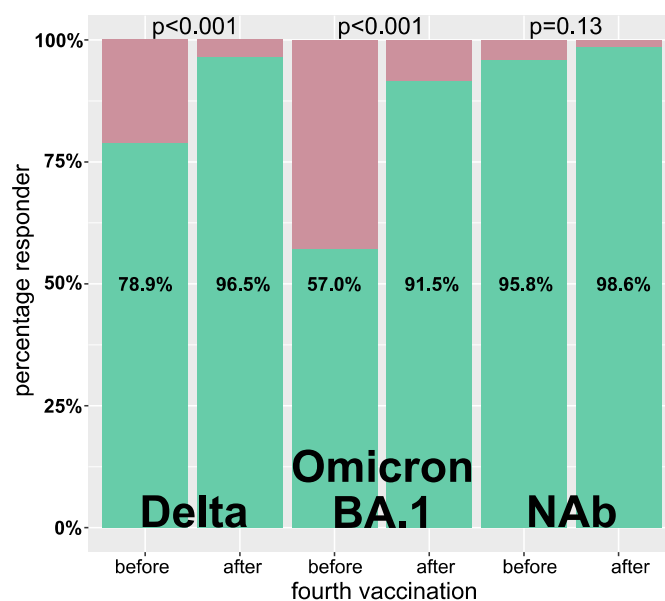


Figure 3. Percentage of responders before and after the fourth vaccination. A responder was defined by a Delta or Omicron BA.1 IC50 virus infection neutralization of >1:20 as well as neutralizing antibodies (NAb) ≥10 AU/mL. Green and red indicate the percentages classified as responder and non-responder, respectively. Statistical analysis was done using the McNemar test for paired samples.

After the fourth vaccination, infection neutralization of Delta and NAb titers were correlated highly significantly ($p < 0.0001$) but moderately ($\rho = 0.50$) positive. Similarly, the correlation of the infection neutralization capacity of Omicron BA.1 and NAb was highly significant ($p < 0.0001$) and moderately ($\rho = 0.44$) positive.

Univariate regression analysis showed significantly reduced neutralization capacity for Delta after the fourth vaccination if immunosuppressive medication ($p = 0.001$) or hepatitis B vaccination non-response ($p = 0.046$) was present (Table 2A, left column). Multivariate analysis showed a reduced Delta neutralization capacity after the fourth vaccination if immunosuppressive medication ($p < 0.001$) was taken and—by trend—if hepatitis B vaccination non-response was present ($p = 0.070$) (Table 2A, right column). For Omicron BA.1 infection neutralization, no such association was present (Table 2B). Univariate and multivariate analyses showed reduced NAb after the fourth vaccination if immunosuppressive medication was prescribed (Table 2C).

Table 2. Univariate and multivariate regression models to identify predictors of Delta (A) and Omicron BA.1 (B) neutralization capacity, respectively as well as neutralizing antibodies (C) after the fourth vaccination.

Predictor	Univariate		Multivariate	
	b (95% CI)	p	b (95% CI)	p
A. Delta				
(Intercept)	-	-	1918.2 (985.5, 2850.9)	<0.001
Age (1 year)	-2.1 (-14.1, 10.0)	0.74	2.6 (-14.5, 19.6)	0.77
Dialysis vintage (1 month)	2.1 (-0.4, 4.6)	0.10	0.05 (-0.04, 0.13)	0.27
Charlson comorbidity index	-28.4 (-102.6, 45.7)	0.45	-17.3 (-120.8, 86.1)	0.74
Immunosuppressive medication	-814.7 (-1293.8, -355.9)	0.001	-867.3 (-1356.7, -377.9)	<0.001
Hepatitis B vaccination non-response	-331.9 (-658.1, -5.6)	0.046	-290.8 (-605.3, 23.7)	0.070
B. Omicron BA.1				
(Intercept)	-	-	1167.7 (91.6, 2243.8)	0.034
Age (1 year)	-0.5 (-13.9, 12.9)	0.94	0.2 (-19.4, 19.9)	0.98
Dialysis vintage (1 month)	1.0 (-1.9, 3.8)	0.50	0.02 (-0.07, 0.12)	0.62
Charlson comorbidity index	-7.9 (-90.5, 74.8)	0.85	-0.6 (119.9, 118.7)	0.99
Immunosuppressive medication	-382.7 (-933.3, 167.9)	0.17	-457.6 (-1031.3, 116.0)	0.12
Hepatitis B vaccination non-response	-228.1 (-590.7, 134.4)	0.22	-180.7 (-568.3, 206.8)	0.36

Table 2. Cont.

Predictor	Univariate		Multivariate	
	b (95% CI)	p	b (95% CI)	p
C. Neutralizing antibodies				
(Intercept)	-	-	837.9 (661.4, 1014.4)	<0.001
Age (1 year)	-1.2 (-3.6, 1.1)	0.30	-1.3 (-4.6, 1.9)	0.41
Dialysis vintage (1 month)	0.4 (-0.1, 0.19)	0.12	0.01 (-0.01, 0.02)	0.32
Charlson comorbidity index	-7.0 (-21.3, 7.4)	0.34	2.8 (-16.7, 22.3)	0.78
Immunosuppressive medication	-209.6 (-302.1, -117.0)	<0.001	-223.0 (319.9, -126.0)	<0.001
Hepatitis B vaccination non-response	-228.1 (-590.7, 134.4)	0.22	-22.8 (-86.5, 40.9)	0.48

Abbreviations: b, regression coefficient; CI, confidence interval.

When comparing serum neutralizing capacities after the fourth vaccination between subgroups we saw significant differences in Delta infection neutralization if immunosuppression was prescribed (716.5 [176.2–2560.0] vs. 2560.0 [1678.0–2560.0], $p = 0.002$) (Figure 4A), and by trend for Omicron BA.1 (193.5 [80.0–1481.8] vs. 820.5 [214.3–2560.0], $p = 0.067$) (Figure 4B). Patients with a history of SARS-CoV-2 infection had by trend a higher IC50 value for Delta (2560.0 [2560.0–2560.0] vs. 2560.0 [955.2–2560.0], $p = 0.069$) and significantly higher values for Omicron BA.1 neutralization (1952.0 [893.2–2560.0] vs. 489.0 [157.8–2560.0], $p = 0.013$) (Figure 4C,D). If patients were classified as hepatitis B vaccine non-responder, they had significantly lower IC50 values for Delta neutralization (2460 [531.0–2560.0] vs. 2560.0 [1765.0–2560.0], $p = 0.018$) (Figure 4E), but not for Omicron BA.1 neutralization (553.0 [103.5–1762.5] vs. 760 [254.0–2560.0], $p = 0.18$) (Figure 4F).

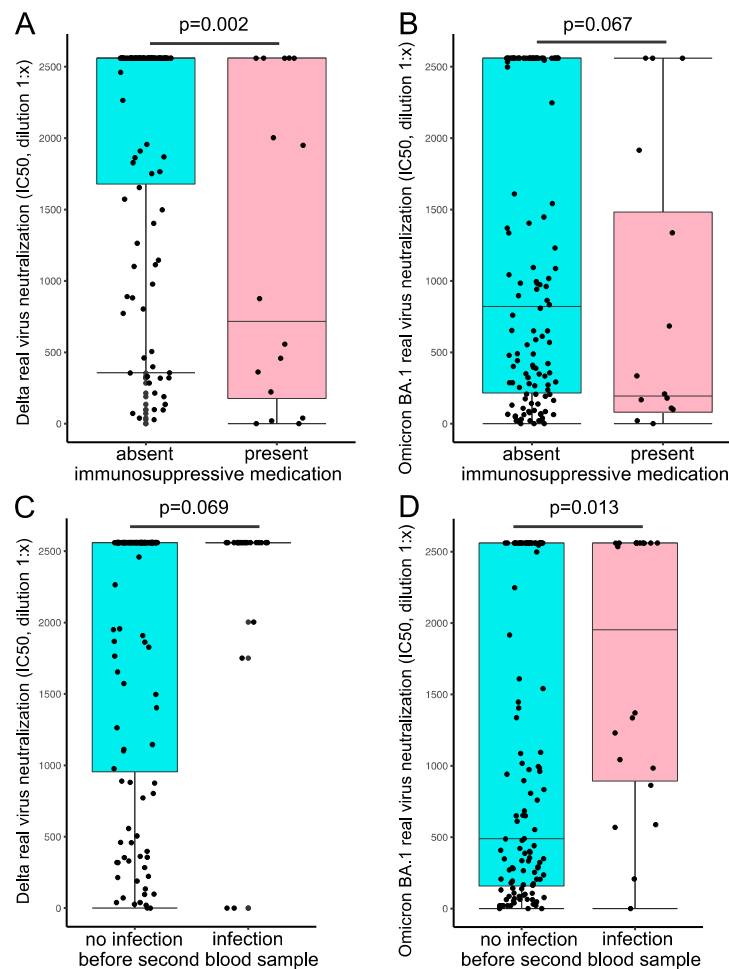


Figure 4. Cont.

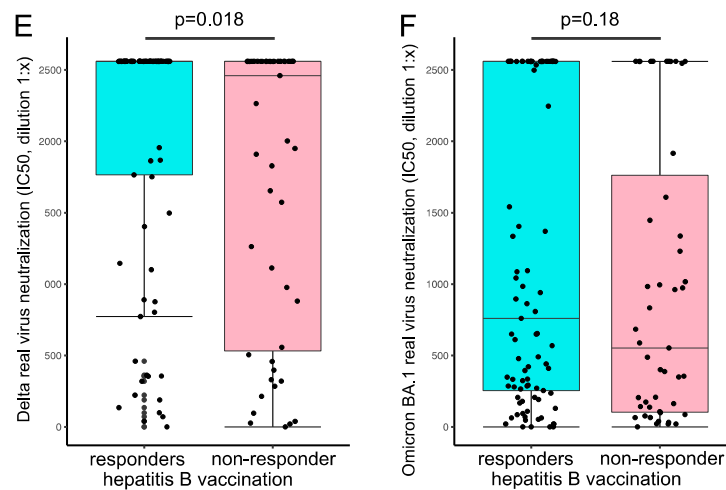


Figure 4. Influence of immunosuppressive medication, SARS-CoV-2 breakthrough infection, and hepatitis B response status on COVID-19 vaccine responses. Serum real-virus neutralization capacity for Delta (left column) and Omicron BA.1 (right column) was analyzed after the fourth vaccination in subgroups. Comparison of immunosuppressive drug treatment (A,B), the prevalence of SARS-CoV-2 infection before the second blood sampling (C,D), and hepatitis B vaccination non-response (E,F) on serum neutralization capacity. Statistical analysis was performed using the Mann-Whitney-U test, p values indicate statistical significance between groups.

3.4. Impact of NAb and Infection Neutralization Capacity on Breakthrough Infections

Finally, the ten patients with a SARS-CoV-2 breakthrough infection between the first and the second blood sampling had by trend lower serum neutralization capacity for Omicron BA.1 at the first blood sampling being almost significant (10.0 [0.0–26.8] vs. 42.5 [20.0–217.5], $p = 0.051$) (Figure 5). No difference was detected for serum neutralization capacity of Delta (189.5 [42.5–1167.0] vs. 257.5 [50.8–1583.8], $p = 0.54$). The VoC causing the SARS-CoV-2 infection was not determined. Omicron BA.1 serum neutralization capacity at the first blood sampling could not predict the COVID-19 breakthrough infection between the first and the second blood sampling ($p = 0.29$) when using univariate logistic regression.

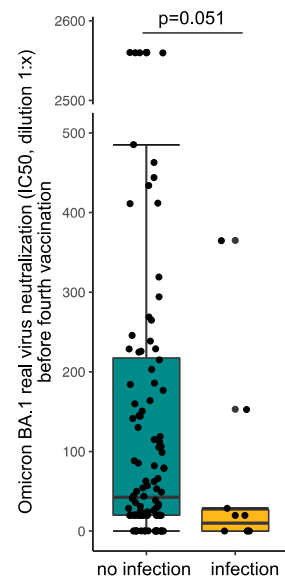


Figure 5. Serum neutralization capacity for Omicron BA.1 variant of concern before the fourth vaccination stratified by patients with SARS-CoV-2 breakthrough infections between the first and the second blood sampling. Statistical analysis was performed using the Mann-Whitney-U test, p value indicates statistical significance between groups. The y-axis is interrupted between 500 and 2500 for better visibility.

4. Discussion

This prospective observational study demonstrates that hemodialysis patients benefit from a fourth COVID-19 vaccination. Serum infection neutralization capacity increased more than 10-fold for Delta and almost 18-fold for Omicron BA.1 after a fourth vaccination indicating better protection from infection with these highly infectious SARS-CoV-2 VoCs. The strength of our study is the examination of the live-virus infection neutralization capacity of patients' sera for two of the most recent SARS-CoV-2 VoCs, Delta and Omicron BA.1. These two variants are also most distant from the original SARS-CoV-2 strain which was used to design the vaccines currently in use. Thus, the protective capacity against the new variants was hard to predict.

Our observation is highly important since hemodialysis patients show reduced immunological responses to vaccination compared to healthy controls, which may be explained in the context of uremia [5,13]. The hemodialysis patients in our study showed a significantly increased capacity to neutralize both SARS-CoV-2 VoCs, Delta and Omicron BA.1, after the fourth vaccination. Our results are consistent with previous reports of significantly increasing anti-spike antibody titers after the fourth vaccination in hemodialysis patients [14,15] but add an important quality as these antibody titers were determined against the original vaccine strain of SARS-CoV-2 but not against the currently circulating variants. Furthermore, in line with previous work with a pseudovirus assay, we found a reduced neutralization capacity for VoC Omicron BA.1 compared to Delta [16].

Patients with a breakthrough infection between the first and the second blood sampling had a lower neutralization capacity for Omicron BA.1, only slightly missing significance. This was not seen for the Delta neutralization capacity. This might be partly explained by the fact that the analysis was performed between February and March 2022, when the Omicron wave peaked in Germany. Hence, over 99.3% of the majority of COVID-19 cases were Omicron infections at that time [10]. Logistic regression could not predict a SARS-CoV-2 breakthrough infection, possibly due to the low infection rate after the first blood collection. In French hemodialysis patients, a response towards wild-type virus neutralization two weeks after the third vaccination was present in approximately 54% of patients [5]. Another study in a British cohort found response rates of 97% and 72% for Delta and Omicron, respectively, in hemodialysis patients one month after the third BNT162b2 vaccination when applying an IC₅₀ cut-off at 40 [17]. We found response rates of 57% for Omicron BA.1 and 79% for Delta four months after the third vaccination. Methodological differences in the neutralization assays [5,17] as well as time interval differences associated with reduced immune responses to vaccination [18] might explain these variations.

In line with previous reports [18–20], we identified immunosuppressive agents as a predictor for lower neutralization capacity, primarily prescribed to patients with a history of kidney transplantation. Patients on immunosuppressive medication had significantly lower neutralization capacity for Delta and, by trend, for Omicron BA.1. Other studies, however, did not identify immunosuppressive drugs as a predictor of neutralization capacity in hemodialysis patients [5]. Discrepancies might be explained due to the specific immunosuppressive agents prescribed. A previous study showed significantly reduced seroconversion rates in patients on anti-CD20 therapy regimes or mycophenolate mofetil, especially in combination with glucocorticoids [20], substances also prescribed to our patients.

Interestingly, a positive hepatitis B vaccination response was by trend associated with an improved neutralization capacity. This was, however, only seen for the Delta VoC. It thus needs to be determined by further studies if hepatitis B vaccination response might serve as a surrogate for COVID-19 vaccination response or vice versa.

In clinical routine, only NAb or anti-S antibody levels are readily and widely available. These, however, only detect the response against the original SARS-CoV-2 strains and not against the VoCs. Before the fourth vaccination, NAb was present in 96% of the study population, and response rates did not further increase after the fourth vaccination. However, when looking at the absolute change of NAb titers, NAb increased significantly after the fourth vaccination. This increase was less pronounced than the increase in IC₅₀

values in infection neutralization due to the limited range of the assay, although the SARS-CoV-2 strain used for vaccination and in the NAb assay were identical. Although NAb levels are highly predictive of immune protection [21], this further demonstrates the limitation of routinely available assays.

We do not have outcome data of our cohort after the fourth vaccination concerning infection prevention but decreased COVID-19 incidence and severity in vaccinated hemodialysis patients have been observed by others [5]. Thus, increasing NAb levels might still be a good indicator of vaccine response after the fourth vaccination and, therefore, useful in clinical routine.

In a study by Espi et al., a third vaccination did not improve the immune response in patients that had already shown a high response after the second vaccination and was associated with more side effects [5]. In our cohort, we did not record side effects. Still, we observed even in NAb high-responder a further significant increase of neutralization capacity and, more importantly, a very strong increase in infection-neutralization capacity of the two most prevalent SARS-CoV-2 VoCs. Differences worth mentioning in the work of Espi et al. might be the application of a third dose three months after the second dose. At the same time, the fourth vaccination was administered at least four months after the third dose in our cohort. Nevertheless, reports of increased side effects in high-responders may argue for an individual decision-making process depending on routinely available antibody levels.

Finally, some limitations have to be mentioned. We examined the neutralization capacity of the Omicron sub lineage BA.1. The question remains if these results are generalizable to other Omicron subvariants currently becoming predominant. Further studies have to show if improved neutralization capacity after the fourth vaccination is associated with COVID-19 incidence and severity.

5. Conclusions

In conclusion, a fourth vaccination against SARS-CoV-2 significantly improves the antibody-mediated immune response in hemodialysis patients. A routinely applied four-time vaccination regimen, therefore, seems reasonable in hemodialysis patients. NAb might be a good clinical surrogate of vaccination response. However, neutralization antibody titers above the upper limit of quantification should not hinder a fourth vaccination as this further improves and broadens live-virus infection neutralization.

Author Contributions: Conceptualization, C.-C.C., L.P., L.R., U.P. and M.C.B.; methodology, C.-C.C., L.P., C.C., M.T., V.K., R.B., B.-H.L., C.H.-L., M.W., E.S., L.R., U.P. and M.C.B.; validation, C.-C.C., L.P., C.C., M.T., V.K., R.B., B.-H.L., C.H.-L., M.W., E.S., L.R., U.P. and M.C.B.; formal analysis, L.P. and M.C.B.; investigation, L.P., M.T., V.K., M.W., E.S., E.P., P.E., L.T., C.K. and C.S.; writing—original draft preparation, C.-C.C., L.P., L.R., U.P. and M.C.B.; writing—review and editing, all authors; visualization, L.P. and M.C.B.; supervision, U.H., L.R., U.P. and M.C.B.; project administration, L.R., U.P. and M.C.B. All authors have read and agreed to the published version of the manuscript.

Funding: This study was supported by the BMBF initiative NaFoUniMedCovid19 (01KX2021), subprojects B-FAST and COVIM, the Bavarian research networks FOR-COVID and Bay-VOC, the German Center for Infection Research (DZIF) and by the project “Virological and immunological determinants of COVID-19 pathogenesis—lessons to get prepared for future pandemics (KA1-Co-02 “COVIPA”)", a grant from the Helmholtz Association’s Initiative and Networking Fund.

Institutional Review Board Statement: The study, conforming to the ethical guidelines of the Helsinki Declaration, was approved by the Medical Ethics Committee of the Klinikum rechts der Isar of the Technical University of Munich (approval number 163/21 S-SR, 19 March 2021) and registered at the Paul Ehrlich Institute (NIS592).

Informed Consent Statement: Informed consent was obtained from all subjects involved in the study.

Data Availability Statement: The datasets for this manuscript are not publicly available because written informed consent did not include wording on data sharing (German data protection laws). Reasonable requests to access the datasets should be directed to the corresponding author.

Acknowledgments: We would like to thank all patients for their participation in the study. We thank Roman Wölfel and J. Bugert (Institut für Mikrobiologie der Bundeswehr, Munich), Oliver Keppler (Max von Pettenkofer Institute, Ludwig-Maximilians University of Munich) and the Bavarian Landesamt für Gesundheit und Lebensmittel (LGL, Oberschleißheim) for sharing SARS-CoV-2 isolates.

Conflicts of Interest: The authors declare no conflict of interest. UP is receiving grants from Hoechst AG, SCG Cell Therapy and VirBio and personal fees from Abbott, Abbvie, Arbutus, Gilead, GSK, J&J, Roche, Sanofi, Sobi and Vaccitech. UP is co-founder and share-holder of SCG Cell Therapy.

References

1. El Karoui, K.; Hourmant, M.; Ayav, C.; Glowacki, F.; Couchoud, C.; Lapidus, N. Vaccination and COVID-19 Dynamics in Dialysis Patients. *Clin. J. Am. Soc. Nephrol.* **2022**, *17*, 395–402. [CrossRef]
2. Ahmed, N.; Khderat, A.H.; Sarsour, A.; Taher, A.; Hammoudi, A.; Hamdan, Z.; Nazzal, Z. The vulnerability of maintenance dialysis patients with COVID-19: Mortality and risk factors from a developing country. *Ann. Med.* **2022**, *54*, 1511–1519. [CrossRef]
3. Hilbrands, L.B.; Duivenvoorden, R.; Vart, P.; Franssen, C.F.M.; Hemmelder, M.H.; Jager, K.J.; Kieneker, L.M.; Noordzij, M.; Pena, M.J.; Vries, H.; et al. COVID-19-related mortality in kidney transplant and dialysis patients: Results of the ERACODA collaboration. *Nephrol. Dial. Transplant.* **2020**, *35*, 1973–1983. [CrossRef] [PubMed]
4. Erber, J.; Kappler, V.; Haller, B.; Mijočević, H.; Galhoz, A.; Prazeres da Costa, C.; Gebhardt, F.; Graf, N.; Hoffmann, D.; Thaler, M.; et al. Infection Control Measures and Prevalence of SARS-CoV-2 IgG among 4,554 University Hospital Employees, Munich, Germany. *Emerg. Infect. Dis.* **2022**, *28*, 572–581. [CrossRef] [PubMed]
5. Espi, M.; Charmetant, X.; Barba, T.; Mathieu, C.; Pelletier, C.; Koppe, L.; Chalencon, E.; Kalbacher, E.; Mathias, V.; Ovize, A.; et al. A prospective observational study for justification, safety, and efficacy of a third dose of mRNA vaccine in patients receiving maintenance hemodialysis. *Kidney Int.* **2022**, *101*, 390–402. [CrossRef] [PubMed]
6. Wand, O.; Nacasch, N.; Fadeela, A.; Shashar, M.; Grupper, A.; Benchetrit, S.; Erez, D.; Shitrit, P.; Cohen-Hagai, K. Humoral response and breakthrough infections with SARS-CoV-2 B.1.617.2 variant in vaccinated maintenance hemodialysis patients. *J. Nephrol.* **2022**, *35*, 1479–1487. [CrossRef]
7. Garcia-Beltran, W.F.; St Denis, K.J.; Hoelzemer, A.; Lam, E.C.; Nitido, A.D.; Sheehan, M.L.; Berrios, C.; Ofoman, O.; Chang, C.C.; Hauser, B.M.; et al. mRNA-based COVID-19 vaccine boosters induce neutralizing immunity against SARS-CoV-2 Omicron variant. *Cell* **2022**, *185*, 457–466. [CrossRef] [PubMed]
8. Wratil, P.R.; Stern, M.; Priller, A.; Willmann, A.; Almanzar, G.; Vogel, E.; Feuerherd, M.; Cheng, C.C.; Yazici, S.; Christa, C.; et al. Three exposures to the spike protein of SARS-CoV-2 by either infection or vaccination elicit superior neutralizing immunity to all variants of concern. *Nat. Med.* **2022**, *28*, 496–503. [CrossRef] [PubMed]
9. Verdier, J.F.; Boyer, S.; Chalmin, F.; Jeribi, A.; Egasse, C.; Maggi, M.F.; Auvray, P.; Yalaoui, T. Response to three doses of the Pfizer/BioNTech BNT162b2 COVID-19 vaccine: A retrospective study of a cohort of haemodialysis patients in France. *BMC Nephrol.* **2022**, *23*, 189. [CrossRef] [PubMed]
10. Robert-Koch-Institute. Wöchentlicher Lagebericht des RKI zur Coronavirus-Krankheit-2019 (COVID-19), Kalenderwoche 11, 24 March 2022. Available online: https://www.rki.de/DE/Content/InfAZ/N/Neuartiges_Coronavirus/Situationsberichte/Gesamt.html (accessed on 12 August 2022).
11. Koerber, N.; Priller, A.; Yazici, S.; Bauer, T.; Cheng, C.C.; Mijočević, H.; Wintersteller, H.; Jeske, S.; Vogel, E.; Feuerherd, M.; et al. Dynamics of spike-and nucleocapsid specific immunity during long-term follow-up and vaccination of SARS-CoV-2 convalescents. *Nat. Commun.* **2022**, *13*, 153. [CrossRef] [PubMed]
12. Chan, K.H.; Leung, K.Y.; Zhang, R.R.; Liu, D.; Fan, Y.; Chen, H.; Yuen, K.Y.; Hung, I.F. Performance of a Surrogate SARS-CoV-2-Neutralizing Antibody Assay in Natural Infection and Vaccination Samples. *Diagnostics* **2021**, *11*, 1757. [CrossRef] [PubMed]
13. Espi, M.; Koppe, L.; Fouque, D.; Thauinat, O. Chronic Kidney Disease-Associated Immune Dysfunctions: Impact of Protein-Bound Uremic Retention Solutes on Immune Cells. *Toxins* **2020**, *12*, 300. [CrossRef] [PubMed]
14. Housset, P.; Kubab, S.; Hanafi, L.; Pardon, A.; Vittoz, N.; Bozman, D.F.; Caudwell, V.; Faucon, A.L. Humoral response after a fourth “booster” dose of a coronavirus disease 2019 vaccine following a 3-dose regimen of mRNA-based vaccination in dialysis patients. *Kidney Int.* **2022**. [CrossRef] [PubMed]
15. Cinkilic, O.; Anft, M.; Blazquez-Navarro, A.; Meister, T.L.; Roch, T.; Stervbo, U.; Pfaender, S.; Westhoff, T.H.; Babel, N. Inferior humoral and sustained cellular immunity against wild-type and omicron variant of concern in hemodialysis patients immunized with 3 SARS-CoV-2 vaccine doses compared with 4 doses. *Kidney Int.* **2022**, *101*, 1287–1289. [CrossRef] [PubMed]
16. Anft, M.; Blazquez-Navarro, A.; Frahnert, M.; Fricke, L.; Meister, T.L.; Roch, T.; Stervbo, U.; Pfaender, S.; Westhoff, T.H.; Babel, N. Inferior cellular and humoral immunity against Omicron and Delta variants of concern compared with SARS-CoV-2 wild type in hemodialysis patients immunized with 4 SARS-CoV-2 vaccine doses. *Kidney Int.* **2022**. [CrossRef] [PubMed]
17. Carr, E.J.; Wu, M.; Harvey, R.; Billany, R.E.; Wall, E.C.; Kelly, G.; Howell, M.; Kassiotis, G.; Swanton, C.; Gandhi, S.; et al. Omicron neutralising antibodies after COVID-19 vaccination in haemodialysis patients. *Lancet* **2022**, *399*, 800–802. [CrossRef]

18. Quiroga, B.; Soler, M.J.; Ortiz, A.; Orero, E.; Tejedor, S.; Mantecon, C.J.J.; Gomez Perez, V.O.; Marin Franco, A.J.; Alfaro Sanchez, C.; Puerta Carretero, M.; et al. Humoral Response to Third Dose of SARS-CoV-2 Vaccines in the CKD Spectrum. *Clin. J. Am. Soc. Nephrol.* **2022**, *17*, 872–876. [[CrossRef](#)] [[PubMed](#)]
19. Quiroga, B.; Soler, M.J.; Ortiz, A.; Vaquera, S.M.; Mantecón, C.J.J.; Useche, G.; Márquez, M.G.S.; Carnerero, M.; Rodríguez, M.T.J.; Ramos, P.M.; et al. Safety and immediate humoral response of COVID-19 vaccines in chronic kidney disease patients: The SENCOVAC study. *Nephrol. Dial. Transplant.* **2021**, gfab313. [[CrossRef](#)] [[PubMed](#)]
20. Wieske, L.; van Dam, K.P.J.; Steenhuis, M.; Stalman, E.W.; Kummer, L.Y.L.; van Kempen, Z.L.E.; Killestein, J.; Volkens, A.G.; Tas, S.W.; Boekel, L.; et al. Humoral responses after second and third SARS-CoV-2 vaccination in patients with immune-mediated inflammatory disorders on immunosuppressants: A cohort study. *Lancet Rheumatol.* **2022**, *4*, e338–e350. [[CrossRef](#)]
21. Khoury, D.S.; Cromer, D.; Reynaldi, A.; Schlub, T.E.; Wheatley, A.K.; Juno, J.A.; Subbarao, K.; Kent, S.J.; Triccas, J.A.; Davenport, M.P. Neutralizing antibody levels are highly predictive of immune protection from symptomatic SARS-CoV-2 infection. *Nat. Med.* **2021**, *27*, 1205–1211. [[CrossRef](#)] [[PubMed](#)]

Targeting genomic SARS-CoV-2 RNA with siRNAs allows efficient inhibition of viral replication and spread

Shubhankar Ambike^{1,†}, Cho-Chin Cheng^{1,†}, Martin Feuerherd¹, Stoyan Velkov¹, Domizia Baldassi², Suliman Qadir Afridi¹, Diana Porras-Gonzalez³, Xin Wei³, Philipp Hagen¹, Nikolaus Kneidinger⁴, Mircea Gabriel Stoleriu⁷, Vincent Grass¹, Gerald Burgstaller³, Andreas Pichlmair^{1,5}, Olivia M. Merkel^{2,3}, Chunkyu Ko^{1,6} and Thomas Michler^{1,5,*}

¹Institute of Virology, School of Medicine, Technische Universität München / Helmholtz Zentrum München, Trogerstr. 30, 81675 Munich, Germany, ²Department of Pharmacy, Pharmaceutical Technology and Biopharmaceutics, Ludwig-Maximilians-Universität München, Butenandtstraße 5, 81377 Munich, Germany, ³Institute of Lung Biology and Disease (ILBD) and Comprehensive Pneumology Center (CPC) with the CPC-M bioArchive, Helmholtz Zentrum München, Member of the German Center for Lung Research (DZL), Munich, Germany, ⁴Department of Medicine V, University Hospital, LMU Munich, Member of the German Center for Lung Research (DZL), Munich, Germany, ⁵German Center for Infection Research (DZIF), Munich partner site, Germany, ⁶Infectious Diseases Therapeutic Research Center, Therapeutics & Biotechnology Division, Korea Research Institute of Chemical Technology (KRICT), 34114 Daejeon, Republic of Korea and ⁷Center for Thoracic Surgery Munich, Ludwig-Maximilians-University of Munich (LMU) and Asklepios Pulmonary Hospital; Marchioninistraße 15, 81377 Munich and Robert-Koch-Allee 2, 82131 Gauting, Germany

Received November 25, 2020; Revised November 10, 2021; Editorial Decision November 30, 2021; Accepted December 05, 2021

ABSTRACT

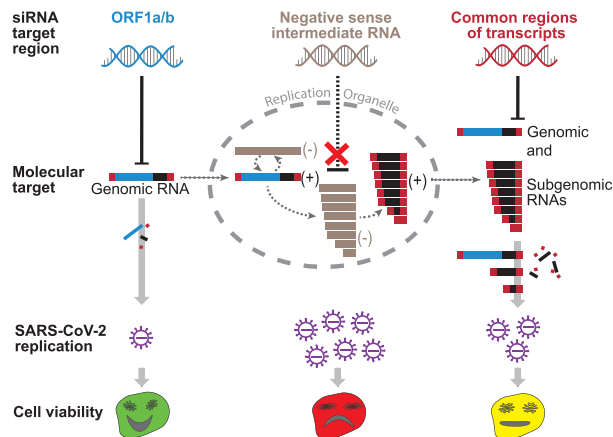
A promising approach to tackle the severe acute respiratory syndrome coronavirus-2 (SARS-CoV-2) could be small interfering (si)RNAs. So far it is unclear, which viral replication steps can be efficiently inhibited with siRNAs. Here, we report that siRNAs can target genomic RNA (gRNA) of SARS-CoV-2 after cell entry, and thereby terminate replication before start of transcription and prevent virus-induced cell death. Coronaviruses replicate via negative sense RNA intermediates using a unique discontinuous transcription process. As a result, each viral RNA contains identical sequences at the 5' and 3' end. Surprisingly, siRNAs were not active against intermediate negative sense transcripts. Targeting common sequences shared by all viral transcripts allowed simultaneous suppression of gRNA and subgenomic (sg)RNAs by a single siRNA. The most effective suppression of viral replication and

spread, however, was achieved by siRNAs that targeted open reading frame 1 (ORF1) which only exists in gRNA. In contrast, siRNAs that targeted the common regions of transcripts were outcompeted by the highly abundant sgRNAs leading to an impaired antiviral efficacy. Verifying the translational relevance of these findings, we show that a chemically modified siRNA that targets a highly conserved region of ORF1, inhibited SARS-CoV-2 replication *ex vivo* in explants of the human lung. Our work encourages the development of siRNA-based therapies for COVID-19 and suggests that early therapy start, or prophylactic application, together with specifically targeting gRNA, might be key for high antiviral efficacy.

*To whom the correspondence should be addressed. Tel: +49 89 4140 6814; Fax: +49 89 4140 6823; Email: thomas.michler@tum.de

†The authors wish it to be known that, in their opinion, the first two authors should be regarded as Joint First Authors.

Present address: Suliman Qadir Afridi, Fraunhofer Institute for Cell Therapy and Immunology, Perlickstraße 1, 04103 Leipzig, Germany.

GRAPHICAL ABSTRACT**INTRODUCTION**

Severe acute respiratory syndrome coronavirus-2 (SARS-CoV-2) is causing a pandemic with disastrous consequences on global health, politics and economy. SARS-CoV-2, like other coronaviruses affecting humans, is mainly transmitted via respiratory secretions (1), and replicates primarily in respiratory epithelial cells (2). Due to its lytic cell cycle (3), it causes severe endothelial injury and widespread microangiopathy (4), which can trigger a pathological cascade that can lead to respiratory failure and death (5). While some progress has been made by repurposing the RNA polymerase inhibitor Remdesivir (6), using monoclonal antibodies against the receptor-binding domain of the viral Spike (S) protein (7), or by ameliorating SARS-CoV-2 induced lung injury using dexamethasone (8), the impact of such therapies on lethality of coronavirus disease 19 (COVID-19) remains limited (9). Several potential new treatments are currently investigated (10). One promising approach could be to deliver small interfering (si)RNAs locally to the respiratory tract by inhalation (11), and induce degradation of viral RNAs by the RNA interference (RNAi) machinery. Studies performed with severe acute respiratory syndrome coronavirus-1 (SARS-CoV-1) or Middle East respiratory syndrome coronavirus (MERS-CoV), showed that siRNAs can silence viral RNA and relieve symptoms caused by related coronaviruses (12–15). The ongoing pandemic prompted multiple research groups to evaluate siRNA-based therapies for COVID-19. While most of the so far published studies reviewed the potential of RNAi to treat COVID-19 (16–21), describe in-silico studies (22–28), or are restricted to using reporter assays to test activity of siRNAs (29,30), initial proof-of-concept that SARS-CoV-2 can be inhibited by siRNAs, was also provided (31,32). However, until today it is unclear, which viral replication steps are accessible for RNAi and which are the determinants for an efficient suppression of viral replication. An in-depth understanding of these factors, however, would be a requirement to formulate a potent antiviral strategy.

SARS-CoV-2, as other coronaviruses, has a positive sense, single-stranded RNA genome with a length of ~30 000 nucleotides. Following binding to the cellular receptor angiotensin-converting enzyme 2 (33), the virus is taken

up via endocytosis (34). After fusion with the endosomal membrane with the help of the host protease transmembrane protease serine 2 (35), the ribonucleocapsid is released into the cytoplasm. Here, the viral genome serves as template for translation of the polyprotein 1ab (pp1ab) from open reading frame 1 (ORF1) by the cellular ribosomal machinery. Pp1ab is cleaved into 16 non-structural proteins (NSPs) of which several assemble around the viral genome to form the replication/transcription complex (RTC) (36). As for other positive sense RNA viruses, transcription does not take place in the cytosol, but exclusively within double-membrane vesicles (37). Therefore, the viral RTC associates with endoplasmic reticulum membranes to form viral replication organelles (ROs). Here, the viral genome serves as template for transcription of full-length progenitor genomic (g)RNA as well as subgenomic (sg)RNAs encoding for structural (S, envelope protein [E], membrane protein [M], Nucleocapsid [N]) as well as accessory proteins (3a, 6, 7a, 7b, 8 and 10) (38). Replication takes place via negative sense intermediate RNAs in a process called discontinuous transcription (39,40). As a result, each coronavirus RNA contains an identical 5' (the ~70 nucleotide long leader sequence [L]) as well as 3' end (N ORF and 3' untranslated region [3'UTR]) (38). Next, sgRNAs are released from ROs (41), translated into the corresponding protein and gRNA packaged by the structural proteins to assemble progeny virions.

Coronaviruses protect their RNA well. Besides the lipid bilayer envelope, nucleocapsid proteins bind directly to the viral genome. Thus, even between uncoating and incorporation into double-membraned ROs, the genome is not present as naked RNA (42). Furthermore, while sgRNAs are exported from ROs for translation, this does not seem to be the case for gRNA which remains associated with double-membraned vesicles (41). Currently, it is not clear whether and how the different viral RNA species can be targeted by an RNAi-based therapy. Furthermore, certain viral components might be essential for replication, whereas the loss of others might be tolerated by the virus. Thus, suppression of reporter constructs as often performed during siRNA development may not accurately predict the effect of siRNAs on viral replication and spread. To shed light upon these questions, we systematically analyzed which viral RNA species and steps of the SARS-CoV-2 life cycle can be targeted by siRNAs and how this would affect viral replication.

MATERIALS AND METHODS**siRNA design and synthesis**

We designed siRNAs against the SARS-CoV-2 Leader sequence, ORF1, Nucleocapsid gene (N) and 3' untranslated region (3'UTR) employing a publicly available online tools (43) using the full-length reference sequence (NCBI Accession number: NC_045512.2) from the RefSeq database as a template. For a fair comparison of target regions, siRNAs for which a similar silencing efficacy was predicted (44) were further incorporated in the study. The siRNAs were designed in two versions: (i) As symmetric siRNAs with a length of 21 or 23 nucleotides with 2 nucleotide overhangs

Table 1. Sequences of siRNAs used in the study. siRNA duplexes were designed with occasional G:U wobbles at the 5' end of the antisense strand, as indicated by small lettered 'u'. L1–3; leader-sequence specific siRNAs 1–3; O1–3, ORF1-specific siRNAs 1–3; N1–3, N-specific siRNAs 1–3; U, 3'UTR-specific siRNAs 1–3; GFP = Green Fluorescent Protein; Luc = Firefly Luciferase; A = adenine; C = cytosine; G = guanine; U = uracil; T = thymine

Name	Sense strand (5'-3')	Antisense strand (5'-3')
L1	UCUGUUCUCUAAACGAAuUTT	AGUUCGUUUAGAGAACAGAUC
L2	CCAACCAACUUUCGAUuUuTT	GAGAUCGAAAGUUGGUUGGUU
L3	AAACCAACCAACUUUCGAUTT	AUCGAAAGUUGGUUGGUUUGU
O1	CCAAAUGUGCCUUUCAACUTT	AGUUGAAAGGCACAUUUGGUU
O2	GUUACAUGCACCAUUGGATT	UCCAU AUGGUGCAUGUAACAA
O3	GGUACUUGGUAGUUUAGCUTT	AGCUAAACUACCAAGUACCAU
N1	GAAUAAGCAUuUGACG <u>u</u> ATT	UGCGUCAAUAGCUUUAUCAG
N2	CAA <u>u</u> UUGGCUACUACCGAATT	UUCGGUAGUAGCCAAUUGGU
N3	CGCUUCAGCGUUCUUCGGAAUTT	AUUCCGAAGAACGCUGAAGCGTT
N4	GGACGAUUGUUACGACGUUTT	AACGUCGUAACAAUCGUCCUA
N5	CCCUUGAAGAGACGAUuUTT	AGCGUCCUCCAUACAGGGGA
N6	CGUGGGCGUUAGGACGAUUTT	AAUCGUCCUACGCCACGGU
N7	GAUUGUUUCUGCCGUAUATT	UACUACGGCAGAAACAAUCGU
N8	GGGUGGUUGUCUCGGAUUUTT	AAAUCGAGACAACCACCCUU
N9	GUUCCUUGUUAACGGUUTT	AACCGUUUAACAAGGAACUC
N10	GACGAUUGUUAACGACGUUATT	UAACGUCGUAACAAUCGUCCU
N11	CUAGUUCAGUAAAACG <u>u</u> UTT	AGUCGUUUUACUGAACUAGAA
U1	CUUUAUCAGUGUGUAAACATT	UGUUACACACUGAUUAAAGAU
U2	CCUAAUGUGUAAA <u>u</u> AAUUTT	AUUAAUUUUACAUUAGGGC
U3	CAUGUGAUUUUUAAUAGCUUTT	AAGCUAUUUAAUACAUUGGG
siGFP	GCAGCACGACUUCUUAAGTT	CUUGAAGAAGUCGUGCUGCTT
siLuc	CGUACGCGGAUACUUCGATT	UCGAAGUAUUCGCGUACG

at the 3' ends of both strands and occasional G:U wobbles at the 5' end of the antisense strand (45) to improve specificity (43) (Table 1 and Supplementary Table S1; experiments shown in Figures 1–4 and Supplementary Figures S1–S5). (ii) To exclude a bias by the slight variations in the siRNA design (different lengths and containment of wobbles), we additionally ordered siRNAs against the same target sites that all had an identical design (symmetric 21-mers with 2 nucleotide overhangs at 3' ends of both strands [sense strand overhang consisting of dTdT] and no wobbles) (Supplementary Table S3; experiments shown in Supplementary Figure S6). Two additional siRNAs targeting GFP (siGFP) and Firefly Luciferase (siLuc) were designed as negative controls. siLuc served as control for SARS-CoV-2 infection experiments and siGFP for experiments in which Luciferase reporters were used. All chemically unmodified siRNAs were purchased in desalted form (Microsynth AG, Balgach, Switzerland), resuspended and maintained in RNase free water upon arrival.

Chemically modified versions of ORF1-targeting siRNAs and siLuc were designed in an asymmetric fashion using a previously described design and chemical modification pattern (46) as employed for Lumasiran (47). In brief, all nucleotides of the siRNA were subjected to a 2'-O-methyl modification (2'OMe) except nucleotides at positions 7, and 9–11 of the siRNA sense-, as well as positions 2, 6, 8, 9, 14 and 16 of the antisense-strand (all 5'-3' direction), which contained 2'-Fluoro modifications (2'F) instead. Additionally, two consecutive nucleotides at both ends of the siRNA antisense strand, as well as at the 5' end of the sense strand were incorporated with phosphorothioate linkages (for details see Supplementary Table S4). Chemically modified siRNAs were synthesized by Eurogentec (Liège, Belgium) at a 40 nmol scale and purified by high performance liquid chromatography (HPLC). The siRNAs

were obtained in desalted form and reconstituted in RNase free water at a concentration of 20 mM.

Conservation of siRNA target sites

To analyze the conservation of the siRNA target sites within the global SARS-CoV-2 population, we downloaded (date of retrieval: 26 October 2021) SARS-CoV-2 sequences from the GISAID EpiCoV™ Database (48) using the most stringent quality indicators (only complete sequences with high sequencing coverage). To analyze the conservation of siRNA target sites within currently circulating SARS-CoV-2 strains without bias, we retrieved the 100 000 sequences with latest submission date (ranging from 1 October until 26 October 2021) without restriction to a specific lineage. For a more in-depth analysis of the SARS-CoV-2 variants that were defined by the WHO by the day of sequence retrieval as major variants of concern (VoC) or interest (VoI), we downloaded 20 000 sequences (each time considering only the latest submission dates) of each of the four VoC (WHO labels: Alpha, Beta, Gamma, and Delta variant) and all available sequences for the two VoI (WHO labels: Lambda and Mu variant) for which less sequences were available (848 and 5889). These included lineages that were defined by the Pango nomenclature system (27) as: B.1.1.7 and Q.x (Alpha variant); B.1.351, B.1.351.2 and B.1.351.3 (Beta variant), P.1 and P.1.x (Gamma variant), B.1.617.2 and AY.x (Delta variant), C.37 and C.37.1 (Lambda variant), as well as B.1.621 and B.1.621.1 (Mu variant). For each of the 12 siRNAs, a search was performed for the presence of the siRNA target site within each of the acquired data sets using an inhouse script written in Ruby programming language (<https://www.ruby-lang.org>). Only perfect matches were counted, and the fraction of SARS-CoV-2 sequences containing the match presented in percent.

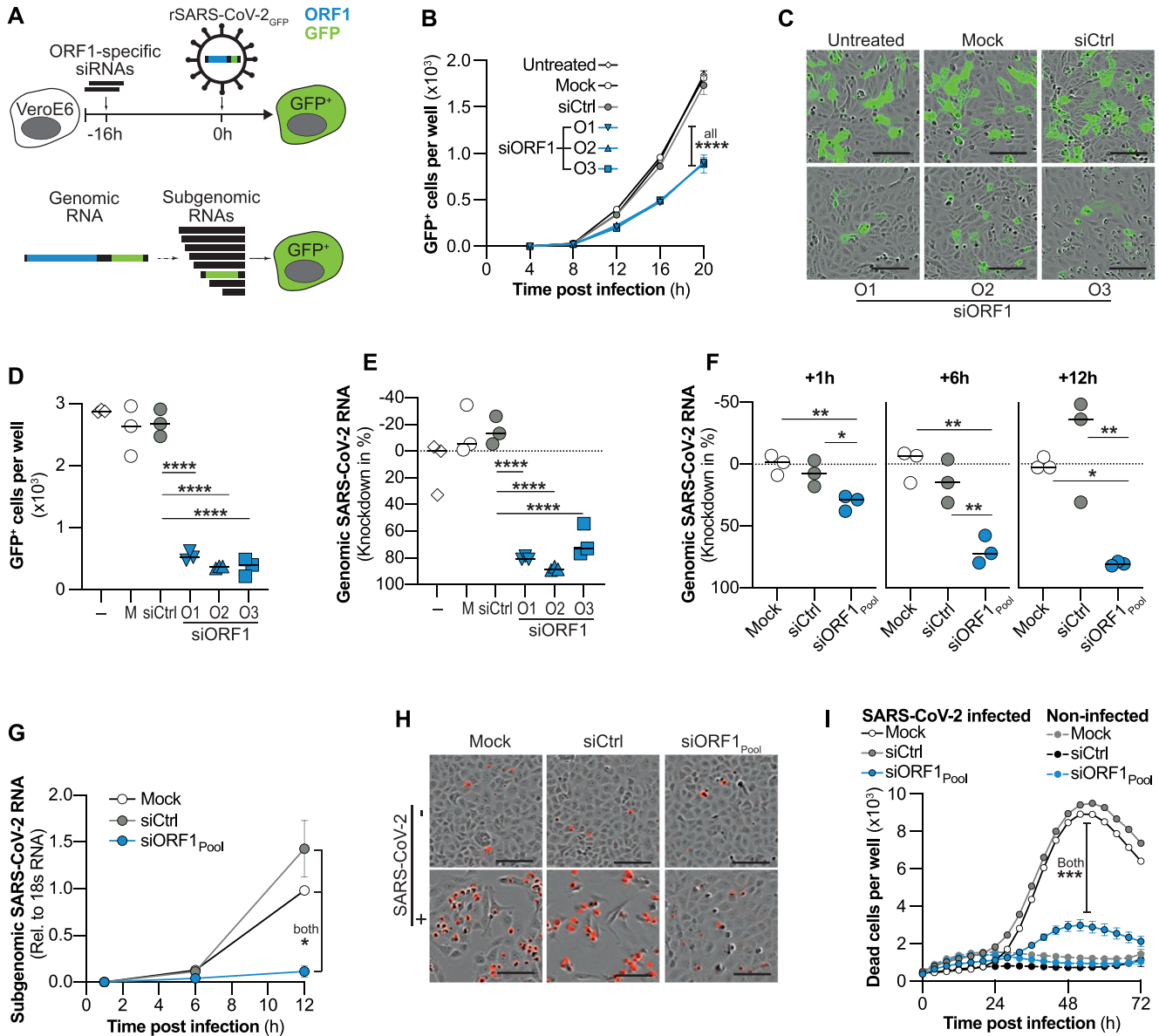


Figure 1. Effect of targeting genomic SARS-CoV-2 RNA with siRNAs on viral replication and cytopathy. (A, top) Experimental setup used in (B–D). VeroE6 cells were transfected with siRNAs targeting ORF1 (siORF1) 16h before infection with recombinant, GFP-expressing SARS-CoV-2 (rSARS-CoV-2-GFP; MOI 1) and number of GFP⁺ positive cells quantified. Cells receiving no treatment (untreated), transfection reagent only (Mock) or a control siRNA (siCtrl) served as controls. (A, bottom) Schematic representation of gRNA, as well as sgRNAs. Note that ORF1 (blue) is only part of full-length gRNA but not sgRNAs. GFP, green fluorescent protein. (B) Kinetic of viral spread showing number of GFP⁺ cells determined by automated quantification using the integrated Incucyte S3 software. (C, D) GFP expression 24h after infection with rSARS-CoV-2-GFP. (C) Exemplanary fluorescence microscopy pictures. Bar at lower right indicates 0.1 mm length and (D) quantification of GFP⁺ cells. (E) Same experimental setup as in (B–D) but cells were infected with *wildtype* SARS-CoV-2 (MOI 0.1) and lysed after 24 h to quantify genomic SARS-CoV-2 RNA from cell lysate by RT-qPCR. (F, G) siRNAs used in (B–E) were pooled and transfected into VeroE6 cells 6h before infection with *wildtype* SARS-CoV-2. Cells were lysed at different time points after infection and SARS-CoV-2 (F) gRNA as well as (G) sgRNAs quantified by RT-qPCR. (H, I) VeroE6 cells were transfected with siRNAs 6h before infection with *wildtype* SARS-CoV-2 (MOI 1) and dead cells visualized using the Incucyte[®] Cytotox Red Dye and quantified using the Incucyte S3. (H) Exemplanary fluorescent microscopy pictures taken at 56h p.i. Dead cells are shown in red. Bar at lower right indicates 100 μm length. (I) Time kinetic of dead cells quantified every 4h over a period of 3 days. (B, G, I) Mean of triplicates for each treatment group is shown, error bars indicate SEM. Bars in (D–F) show median. Statistical differences were calculated using (B, G, I) repeated measures one-way Anova or (D–F) regular one-way Anova with Dunnett's multiple comparison correction. M, Mock; –, untreated; O1-3, ORF1-specific siRNAs 1–3; **P* < 0.05; ***P* < 0.01; ****P* < 0.001; *****P* < 0.0001.

Prediction of secondary structure of siRNA target sites

The stability of RNA secondary structures of regions that were targeted by our siRNAs were analyzed by making use of data provided by Andrews et al. (49) who analyzed all possible 120-nucleotide windows (each shifted by 1 nucleotide) of the SARS-CoV-2 genome using the 'ScanFold' algorithm (50). We averaged the values of four consecutive 120-nucleotide windows that contained the respective siRNA target site in the center to calculate the mean 'native dG score' (or 'minimum free energy' [MFE]), the thermodynamic 'z-score', and the GC content for each region. The native dG score predicts the free energy value of the most stable possible structure the sequence could adopt. A more negative value represents a more stable structure, correlating with less efficient RNAi activity (51). The z-score refers to the difference of minimum free energy between a potentially folded structural RNA and a random RNA of the same dinucleotide frequency. Negative z-score indicates a window which generates a more stable structure than the sequence content would typically produce; on the contrary, positive z-score represents a less stable structure (52). The GC content positively correlates with stable secondary structures and in contrast to the other two parameters inversely with RNAi target site accessibility (53).

Cell lines and seeding

HEK293T cells were maintained in glucose-containing Dulbecco's modified Eagle's medium (DMEM), supplemented with 10% fetal bovine serum (FBS), 2 mM L-glutamine, 50 U/ml penicillin/streptomycin, 1% non-essential amino acids and 1 mM sodium pyruvate (Gibco™-Thermo Fisher Scientific GmbH; Dreieich, Germany). VeroE6 cells were maintained in glucose containing DMEM supplemented with 5% FBS. Mycoplasma contaminations were excluded in all cell lines. Cells were kept at 37°C in humidified incubators at 5% CO₂. 200 000 HEK293T cells were plated in poly-L-lysine (Sigma-Aldrich Chemie; Taufkirchen, Germany) treated 24-well plates for reporter assays, 150 000 or 20 000 VeroE6 cells were plated in 24-well or 96-well plates (Techno Plastic Products; Trasadingen, Switzerland) respectively for experiments including SARS-CoV-2 infection.

Human tissue, ethics statement and human precision-cut lung slices (hPCLS)

Human tissue was obtained from the CPC-M bioArchive at the Comprehensive Pneumology Center (CPC), from the University Hospital Großhadern of the Ludwig Maximilian University (Munich, Germany) and from the Asklepios Biobank of Lung Diseases (Gauting, Germany). Participants provided written informed consent to participate in this study, in accordance with approval by the local ethics committee of the Ludwig Maximilian University Munich, Germany (Project 19-630). PCLS were prepared as described before (54,55). Shortly, PCLS were prepared from tumor-free peri-tumor tissue. The lung tissue was inflated with 3% agarose solution and solidified at 4°C. Tissue blocks were cut in 500 µm thick slices using a vibration microtome Hyrax V50 (Karl Zeiss AG, Oberkochen,

Germany). PCLS were cultured in DMEM F-12 medium supplemented with 0.1% FBS (Thermo Fisher Scientific; Dreieich, Germany). Prior to experiments, PCLS punches of 4 mm in diameter were generated using a 4 mm biopsy puncher.

Cloning of luciferase reporters

Initial siRNA screenings, testing of siRNA strand-specific activities and the competition assay (shown in Figure 4D, E) were performed using the dual luciferase expressing psiCHECK™-2 vector (Promega GmbH; Walldorf, Germany). The siRNA target sites were cloned into a multiple cloning site present downstream of the Renilla luciferase translational stop codon via XhoI/NotI digestion (FastDigest™, Thermo Fisher Scientific; Dreieich, Germany). The binding sites of siRNAs were purchased as single-stranded DNA oligonucleotides, designed to form overhangs mimicking digested oligonucleotide fragments after annealing. Hence, equal amounts of complementary oligonucleotides were mixed and heated at 95°C for five minutes followed by gradual cooling for 2 h at 30°C to allow forming of oligonucleotide duplexes. These were directly used in a ligation reaction with the digested psiCHECK-2™ vector.

To determine strand specific siRNA activities shown in Figure 2 and Supplementary Figure S2, the full-length positive or negative sense N coding sequences were cloned into the luciferase vector. Hence, the positive sense N coding sequence was PCR amplified using primers E-N Fw BamHI and E-N Rev EcoRI from cDNA of SARS-CoV-2 infected VeroE6 cells and cloned into the pcDNA1/Amp plasmid vector. In a next step, the N-coding sequence was PCR-amplified using primers N CDS Fw XhoI and N CDS Rev NotI and cloned into the luciferase reporter. The full-length negative sense N gene was purchased as desalted, pre-annealed double-stranded DNA oligonucleotide (Eurogentec, Liège, Belgium) and used directly for the annealing reaction with digested psiCHECK™-2 vector. A list of used oligonucleotides is given in Supplementary Table S2.

Transfection

siRNAs were transfected using Lipofectamine RNAiMAX (Thermo Fisher Scientific; Dreieich, Germany) according to manufacturer's instructions at time points and concentrations provided in the figure legends of respective experiments. For transfections before SARS-CoV-2 infection, a reverse-transfection protocol was used. All transfection experiments were performed with at least three biological replicates. For the pre-selection of siRNAs, the determination of strand-specific activities of N-targeting siRNAs, and the competition assay, siRNAs were co-transfected together with respective plasmid expressing a luciferase reporter. In brief, 200 ng of reporter plasmid and 6 pmol of siRNA were mixed with 1 µl of transfection reagent (Lipofectamine 2000, Thermo Fisher Scientific; Dreieich, Germany) diluted with Opti-MEM to a final volume of 100 µl. siRNA and plasmid containing transfection complexes were added on top of confluent cells, resulting in 10 nM final concentration of siRNA per well. For the pre-screening of siRNAs and the determination of strand specific activities of N-specific

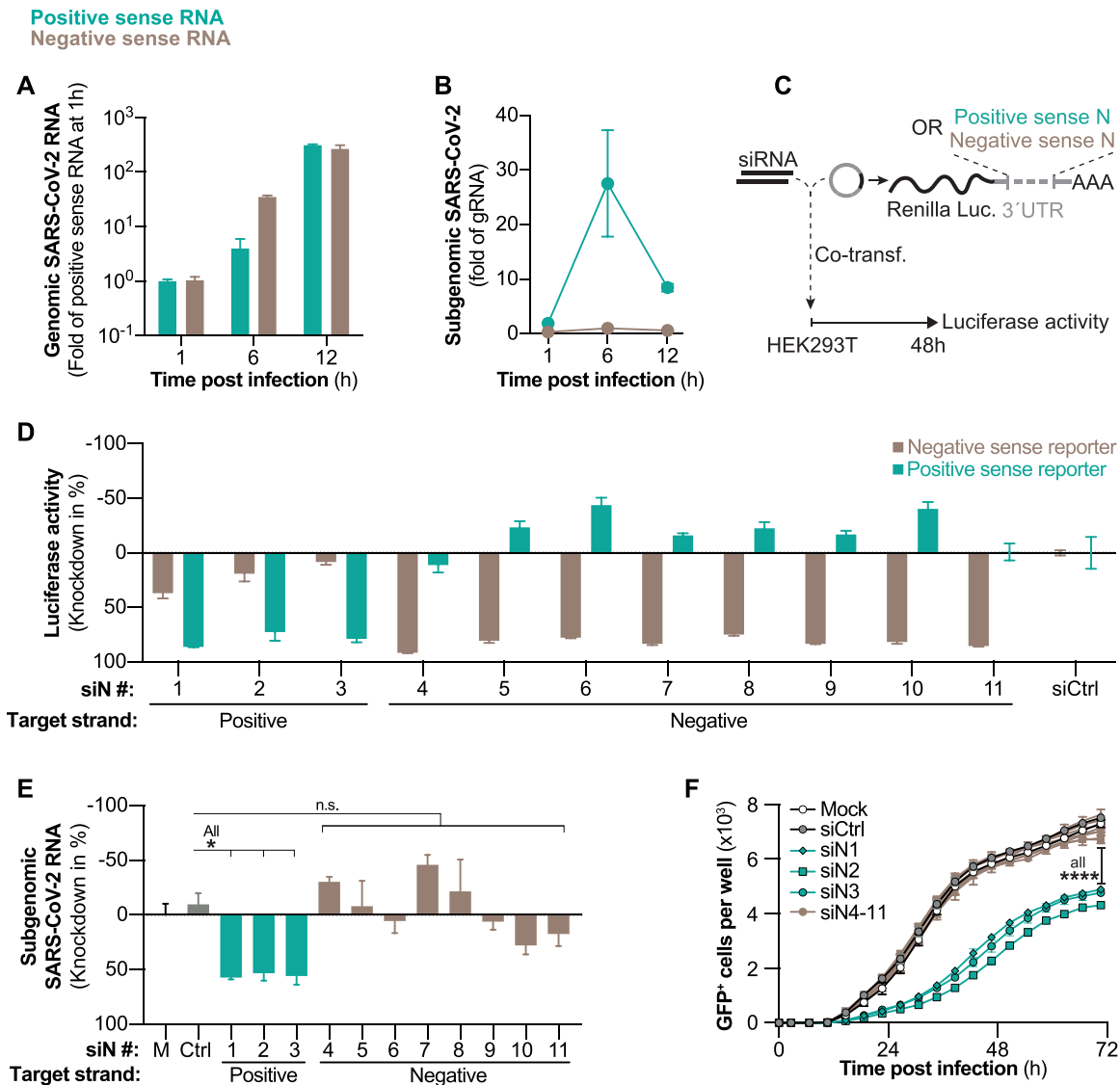


Figure 2. Evaluation of SARS-CoV-2 negative sense RNA as siRNA target. (A, B) Kinetics of negative and positive sense SARS-CoV-2 RNAs following *wildtype* SARS-CoV-2 infection (MOI 0.1) of VeroE6 cells. Negative and positive sense RNAs were individually transcribed to cDNA by using either poly A or poly T primers and (A) gRNA and (B) sgRNAs quantified by RT-qPCR. (C) Experimental setup to determine siRNA strand specific activities. Luciferase reporters with incorporated positive or negative sense N sequences in the 3'UTR of *Renilla* luciferase were co-transfected with siRNAs into HEK293T cells and (D) luciferase activity measured after 48 h (E) siRNAs were transfected into VeroE6 cells 6 h before infection with *wildtype* SARS-CoV-2 (MOI 0.1) and 24 h p.i. sgRNAs quantified from cell lysate using RT-qPCR. (F) Same setup as in (E) but VeroE6 cells were infected with rSARS-CoV-2-GFP (MOI 1.0) and GFP⁺ cells quantified every 4 h. All experiments were performed with three biological replicates. Graphs in (A, B, D, E) show mean and error bars SEM. Statistical differences were calculated using (E) Regular or (F) repeated measures one-way Anova with Dunnett's multiple comparison correction. Co-transf., co-transfection; M = mock-transfected; n.s., non-significant, **P* < 0.05; *****P* < 0.0001

siRNAs, constructs were transfected into 85–90% confluent HEK293T cells and for the competition assay into confluent VeroE6 cells.

Polymer/siRNA polyplexes for *ex vivo* lung transfections were prepared as described before (56) by first dissolving polyethylenimine 25 kDa (BASF, Ludwigshafen, Germany) in water at a concentration of 1 mg/ml, which was then filtered through a 0.22 μm filter for sterilization. Stocks of siRNA and PEI were further diluted in a sterile 5% glucose solution to reach the desired concentration. Polyplexes were prepared with a total amount of 60 pmol of siRNA. The required amount of PEI in μg (mPEI) was calculated

as follows:

$$mPEI = \frac{m(\text{siRNA})}{M(\text{siRNA})} \times 43.1 \text{ g mol}^{-1} \times N/P$$

where 43.1 is the molecular weight of the protonable unit of PEI, and N/P is the ratio of protonable amines of the polymer to phosphate groups of the siRNA backbone (56). The experiment was performed at an N/P ratio of 6. A defined volume of the polymer solution was added to an equal volume of the diluted siRNA and incubated for 20 minutes at room temperature to allow polyplex formation.

Dual-luciferase based reporter assay and competition experiment

To determine silencing activity of siRNA sequences, siRNAs were co-transfected into cells with plasmids expressing dual luciferase reporters. After co-transfecting siRNAs and plasmids (for details see paragraph above), cells were lysed after 48h (siRNA prescreening and strand specific activities) with 100 μ l passive lysis buffer (Promega GmbH; Walldorf, Germany), and luciferase activity from 10 μ l cell lysate measured using the Dual Luciferase[®] Reporter Assay System (Promega GmbH; Walldorf, Germany) according to instructions using a Tecan Infinite 200 PRO Microplate reader (Tecan Group Ltd.; Männedorf, Switzerland). Relative activity of *Renilla* luciferase (normalized to Firefly luciferase activity as an internal transfection control) was indicated as silencing efficiency of the siRNA and compared to the same luciferase reporter co-transfected with the control siRNA siGFP. For the competition experiment (shown in Figure 4D, E), siRNAs and the respective luciferase reporter plasmid were co-transfected into VeroE6 cells as described previously, which were 6 h later infected with *wildtype* SARS-CoV-2 (MOI 0.1), and 24 h later, luciferase activity and knockdown efficacy were determined.

SARS-CoV-2 infection

VeroE6 cells were seeded in 24-well format at least 6h before infection to gain ~90–95% confluency at time of inoculation. The SARS-CoV-2 stock was pre-diluted in 200 μ l growth media to achieve the desired multiplicity of infection (MOI) for the respective experiment. At time of inoculation, old growth media was removed, and the pre-diluted SARS-CoV-2 solution added to cells. After 1h incubation at 37°C, a medium exchange was performed. Experiments with *wildtype* SARS-CoV-2 were terminated at different time points ranging from 1 to 24 h post infection depending on which step of the viral replication cycle was investigated. The SARS-CoV-2 *wildtype* virus used in this study was isolated in March 2020 from a patient at the Institute of Virology, TU Munich. The full-length sequence was uploaded onto GISAID database (<https://www.gisaid.org/>) under name *hCoV-19/Germany/BAV-PL-virotum-naeq/2020* and accession ID: EPI_ISL_582134.

PCLS samples were prepared as described above and cultured with Dulbecco's Modified Eagle Medium (DMEM) F-12 supplemented with L-Glutamine, HEPES, 10,000 IE Penicillin, 10 000 IE streptomycin and 0.1% fetal bovine serum. For each biological replicate, three PCLS were placed in a 48-well plate in 500 μ l medium and transfected with 60 pmol siRNA and PEI at N/P 6 (for details see 'transfection' section) six hours before being infected with *wildtype* SARS-CoV-2. For infection, 300 000 plaque-forming units (PFU) SARS-CoV-2 were added to each well, which contained PCLS with an estimated cell number of 300 000 cells, resulting in an approximated MOI of 1.0.

Real-time monitoring of virus spread using rSARS-CoV-2-GFP and automated fluorescence analysis with the InCuCyte[®] Live-Cell Analysis

VeroE6 cells in growth media were seeded at least 6h before infection into 96-well plates to gain ~90–95% con-

fluency at time of infection. Cells were then inoculated with a recombinant SARS-CoV-2, expressing green fluorescent protein (GFP) from a sequence integrated at the ORF7 locus (rSARS-CoV-2-GFP). For this, the rSARS-CoV-2-GFP virus infection solution was pre-diluted in 50 μ l growth media to achieve the desired MOI. After adding 50 μ l of the infection solution to cells, media was exchanged after 1 h, and multi-well plates placed into InCuCyte[®] Live-Cell Analysis device for acquisition of phase contrast as well as fluorescence pictures of the entire well every 4 h for three days. Infected cell population was quantified using the GFP channel and the InCuCyte S3 software (Essen Bioscience; version 2019B Rev2).

Half maximal inhibitory concentration

Efficacy of siRNAs to inhibit luciferase reporters or SARS-CoV-2 replication was analyzed by determining half maximal inhibitory concentrations (IC₅₀). To investigate activity to suppress viral replication, siRNAs were reversely transfected into VeroE6 cells at a series of concentrations of 100, 25, 6.25, 1.56, 0.39, 0.098, 0.024 and 0.006 nM. The cells were infected with rSARS-CoV-2-GFP (MOI 1) after 6 h as described earlier. The siRNA silencing activity was determined as number of GFP⁺ cells 24 h p.i. using the InCuCyte[®] software. To determine IC₅₀ values for luciferase reporters, siRNAs were co-transfected into HEK293T cells with respective dual luciferase reporters at identical siRNA concentrations as described above and activity of firefly and *Renilla* luciferases measured after 48 h (for details see paragraph 'Dual-Luciferase based reporter assay and competition experiment'). All experiments were performed using three biological replicates. IC₅₀ values were calculated by fitting a nonlinear curve with variable slope using the nonlinear regression model in GraphPad 9.0 software.

Determination of cell death and cell viability

To evaluate the impact of siRNA-treatment on SARS-CoV-2-induced cytopathy, VeroE6 cells were reversely transfected in 96-well plate with siRNAs and 6 h later infected with *wildtype* SARS-CoV-2 (MOI 1). Number of dead cells was quantified using the InCuCyte[®] Cytotox Red Dye to monitor the loss of the cell membrane integrity (Sartorius AG, Göttingen, Germany; Cat. No. 4632). As the cyanine nucleic acid dye is unable to pass the plasma membranes of healthy cells, the dye can only bind to DNA if the integrity of cellular membranes is compromised. Fluorescence signal (maximum at 631 nM) was measured using the red channel of the InCuCyte S3 analyzing system every 4 h for 3 days after infection. As a further marker of cell viability, the metabolic rate of treated cells was determined using the CellTiter-Blue Cell Viability Assay kit (Promega GmbH, Walldorf, Germany) according to manufacturer's instructions. Accordingly, CellTiter-Blue reagent was diluted 1:5 with culture medium and applied to cells for 1 h at 37°C, 5% CO₂. Conversion from resazurin to resorufin was analyzed with fluorescence filters 550/590 nm from a Tecan Infinite F200 (Tecan Group Ltd.; Männedorf, Switzerland).

Table 2. Oligonucleotides and cycling conditions used during polymerase chain reaction. A = adenine; C = cytosine; G = guanine; T = thymine; Rev = reverse; min = minute; s = second; RDRP = RNA-dependent RNA polymerase

Primers	Sequence (5'-3')
N CDS Fw XhoI	ATCATACTCGAGATGTCTGATAACGGACCCCA
N CDS Rev NotI	ATCATTGCGGCCGCGCCTGAGTTGAGTCAGCAC
E-N fw BamHI	GGTGGTGGATCCTGAGCCTGAAGAACATGTCC
E-N Rev EcoRI	GGTGGTGAATTCAGCTCTCCCTAGCATTGTTC
Oligo(dT) ₂₀	TTTTTTTTTTTTTTTTTTTTTTTTTTTTTTTT
Oligo(dA) ₂₀	AAAAAAAAAAAAAAAAAAAAAAAAAAAA
18S cDNA 1	CCTCCGCAGGTTACCTAC
18S cDNA 2	CCTCCAATGGATCCTCGT
18S cDNA 3	TAATCATGGCCTCAGTTCCG
18S qPCR	Fw: AAACGGCTACCACATCCA Rev: CCTCCAATGGATCCTCGT
N qPCR	Fw: GACCCCAAAAATCAGCGAAAT Rev: TCTGGTACTGCCAGTTGAATCTG
RDRP qPCR	Fw: CGTCTGCGGTATGTGGAAAG Rev: TAAGACGGGCTGCACTTACA
PCR cycling conditions:	Initial Denaturation: 95°C 5 Min (Ramp rate 4.4) 45 Cycles: 95°C - 15 seconds (Ramp rate 4.4) 55°C - 10 seconds (Ramp rate 2.2) 72°C - 25 seconds (Ramp rate 4.4)

Nucleic acid extraction and qPCR

RNA from cultured cells was extracted with the NucleoSpin RNA kit (Macherey-Nagel; Düren, Germany), and cDNA synthesized with the Superscript™ III First-Strand Synthesis System (Thermo Fisher Scientific; Dreieich, Germany) according to manufacturer's instructions. SARS-CoV-2 transcripts were amplified in subsequent qPCR using primers specific for the N region, essentially covering all the viral transcripts or the RNA dependent RNA polymerase (Rdrp) region, as a measure of gRNA. For quantification of viral RNAs, a standard curve was constructed using plasmids with integrated Rdrp or N sequences. Amount of sgRNAs was calculated by subtracting the number of Rdrp containing transcripts (as a marker of gRNA) from the N-containing transcripts as full-length gRNA is also detected by the N primers. 18S rRNA was used as a reference gene for relative quantification. All quantitative PCRs were performed on a LightCycler® 480 (Roche Holding AG; Basel, Switzerland) using primers and cycling conditions shown in Table 2.

Strand-specific cDNA synthesis

To individually determine negative or positive sense SARS-CoV-2 RNA, we specifically transcribed RNA of a certain polarity to cDNA. Hence, first strand synthesis was performed from total RNA extracts using the Superscript™ IV First-Strand Synthesis System (Thermo Fisher Scientific; Dreieich, Germany) with primers specific either for positive sense mRNA (Oligo(dT)₂₀ primers) or negative sense mRNA (Oligo(dA)₂₀ primers). To allow transcription of a house keeping gene also in the reaction transcribing negative sense RNA, primers specific for the 18S rRNA gene (18S cDNA1-3; Table 2) were added to the reaction. A final concentration of 50 μM for all primers combined were used for first strand synthesis reaction and viral RNAs quantified by qPCR as described above.

Statistical analysis

Statistical analysis was performed with GraphPad Prism (version 8.4.3) for Mac. Normally distributed samples were analyzed using the Student T-test for independent samples when comparing two groups and with One-way Anova with Dunnett's multiple comparison correction when comparing three or more groups. Statistical differences of non-normally distributed data were calculated for two groups using Mann-Whitney *U* or Kruskal-Wallis with Dunn's multiple comparison correction tests when comparing three or more groups. *P*-values <0.05 were considered significant.

RESULTS

Targeting the genome of SARS-CoV-2 with siRNAs terminates replication before start of transcription and prevents virus-induced cell death

Following the events in the viral replication cycle, first, we investigated whether siRNAs can directly target the incoming genome of SARS-CoV-2 after cell entry. We chose ORF1 as target region, as it is only contained in full-length genomic, but not sgRNAs. We individually transfected three siRNAs which were active in previous luciferase reporter screens (Supplementary Figure S1A) into VeroE6 cells. After 16 h, cells were infected with a recombinant SARS-CoV-2 (rSARS-CoV-2-GFP), which expresses GFP from an integrate at the ORF7 locus. Viral infection and spread were monitored by quantifying GFP⁺ cells every 4h over the course of three days (Figure 1A, top). As the ORF1-specific siRNAs do not target the transcript from which GFP is expressed, a suppression of GFP expression would indicate that siRNAs targeted full-length gRNA (Figure 1A, bottom). Indeed, we found the number of GFP⁺ cells reduced to ~50% by each of the tested siRNAs (Figure 1B-D; Supplementary Figure S1B). Importantly, this difference was already present at the earliest time point (12 h post infection [p.i.]) with detectable GFP signal (Figure 1B), indicating that genomes of incom-

ing virus were successfully targeted. We confirmed this by repeating the experiment using *wildtype* SARS-CoV-2 but lysed the cells 24 h p.i. and quantified SARS-CoV-2 gRNA by RT-qPCR. As indicated by our previous experiment, gRNA was reduced in groups pre-treated with the ORF1-specific siRNAs (Figure 1E). To further confirm that indeed genomes of incoming virus were degraded, we transfected cells with a pool of three ORF1-specific siRNAs 6 h before infection with *wildtype* SARS-CoV-2 and quantified intracellular viral RNAs at different time points. Viral RNAs were further differentiated into full-length gRNA and sgRNAs (see Materials and Methods for details). We found that gRNA was reduced as early as 1 h p.i. (Figure 1F), before sgRNAs were synthesized (Figure 1G). Treatment with ORF1-specific siRNAs prevented sgRNA expression (Figure 1G), improved cell viability (Supplementary Figure S1C) and prevented cell death (Figure 1H, I). Taken together, our data demonstrates that siRNAs can target the genome of SARS-CoV-2 and terminate viral replication at an early replication step and by this prevent cytopathy.

Negative sense SARS-CoV-2 RNAs are not accessible for siRNA therapy

Currently it is unclear if both, negative and positive sense coronavirus RNA, or only RNA with a certain polarity is accessible for RNAi silencing. This question is particularly interesting when designing therapeutic siRNAs, as potentially both strands of the siRNA could convey antiviral activity. To gain a more detailed understanding on the kinetic of RNA synthesis during SARS-CoV-2 replication, we lysed *wildtype* SARS-CoV-2-infected VeroE6 cells at different time points. Positive and negative sense viral RNAs were individually quantified by strand-specific first strand synthesis (see Materials and Methods). Negative sense gRNA was detected in low quantities already 1 h p.i., but strongly increased at 6 h p.i. when it was more abundant than positive sense gRNA (Figure 2A). In contrast, sgRNAs started to appear only at 6 h p.i. (Figure 2B). Consistent with other coronaviruses, lower amounts of negative sense sgRNAs were detected as compared to their positive sense counterparts (57). We then investigated whether negative sense SARS-CoV-2 RNA is accessible for RNAi-mediated silencing. We developed siRNAs that specifically targeted either negative or positive sense SARS-CoV-2 RNA. We chose the N ORF as target region, as it is also part of sgRNAs which are – in contrast to gRNA—exported from ROs (41), and should therefore be easily accessible for siRNAs. siRNA strand-specific activity was validated by co-transfecting siRNAs with reporter plasmids that either carried the positive or negative sense N coding sequence in the 3'UTR of the *Renilla* luciferase gene (see scheme in Figure 2C and methods section). The majority of siRNAs presented a selectivity for the RNA strand they were designed against (Supplementary Figure S2). We chose siRNAs with almost exclusive activity against either the positive or negative sense reporter (Figure 2D) and tested their antiviral activity. To our surprise, only siRNAs active against positive sense N ORF reduced sgRNAs during *wildtype* SARS-

CoV-2 infection (Figure 2E), and inhibited viral spread in the rSARS-CoV-2-GFP model (Figure 2F). In summary, our data proves that negative sense SARS-CoV-2 RNAs are inaccessible for RNAi.

siRNA-targeting of the common regions of SARS-CoV-2 transcripts allows simultaneous suppression of gRNA and sgRNAs, but leads to reduced antiviral efficacy

We further went on to investigate whether targeting the common regions shared by all SARS-CoV-2 transcripts (L, N ORF and 3'UTR; see scheme in Figure 3A) would allow simultaneous suppression of gRNA as well as sgRNAs, and how this would affect antiviral efficacy. To achieve a fair comparison between target regions, we selected three siRNAs for each target region for which a similar efficacy was predicted by the design tool (Supplementary Figure S3A) and which suppressed luciferase reporters to comparable degrees (Supplementary Figure S3B), with only siRNAs against the leader sequence showing slightly lower scores, as the small size of the target limited options for siRNA design. To not interfere with incoming SARS-CoV-2 genomes of input virus, we first infected VeroE6 cells with *wildtype* SARS-CoV-2 and transfected the siRNAs 3h later. To compensate for the differences of the activities of individual siRNAs, we pooled three siRNAs for each target region and tested their effect on SARS-CoV-2 RNA expression (Figure 3B). As expected, ORF1-specific siRNAs suppressed only gRNA, whereas siRNAs targeting common regions of transcripts suppressed gRNA and sgRNAs. We next investigated how targeting sgRNAs in addition to gRNA would affect antiviral efficacy of siRNAs. To this end, we infected cells with rSARS-CoV-2-GFP and this time transfected the three siRNAs per target region individually. All siRNAs significantly inhibited viral replication and viral dissemination as evidence by lower frequency of GFP-expressing cells as compared to controls (Supplementary Figure S3C). To our surprise, however, SARS-CoV-2 spread significantly slower in groups treated with siRNAs that solely targeted gRNA (target region ORF1), illustrated by increased doubling times of GFP⁺ cells (Figure 3C). While both groups of siRNAs (targeting only gRNA or additionally sgRNAs) suppressed luciferase reporters to a similar extent, the siRNAs that targeted exclusively gRNA significantly stronger suppressed replicating virus (Figure 3D). This finding was further confirmed in an experiment using *wildtype* SARS-CoV-2, which showed an improved knockdown of SARS-CoV-2 gRNA (Figure 3E) leading to enhanced suppression of sgRNAs by ORF1-specific siRNAs (Supplementary Figure S3D). The enhanced viral suppression led to improvements of the metabolic rate of infected cells (Supplementary Figure S3E) and reduced cell death (Figure 3F,G; Supplementary Figure S3F).

In summary, our data showed a concurrent suppression of genomic and subgenomic viral RNAs by siRNAs that targeted the common regions of viral transcripts. On the other hand, the ORF1-specific siRNAs, which solely targeted SARS-CoV-2 gRNA, subdued viral replication and spread more efficiently as compared to siRNAs that additionally targeted sgRNAs.

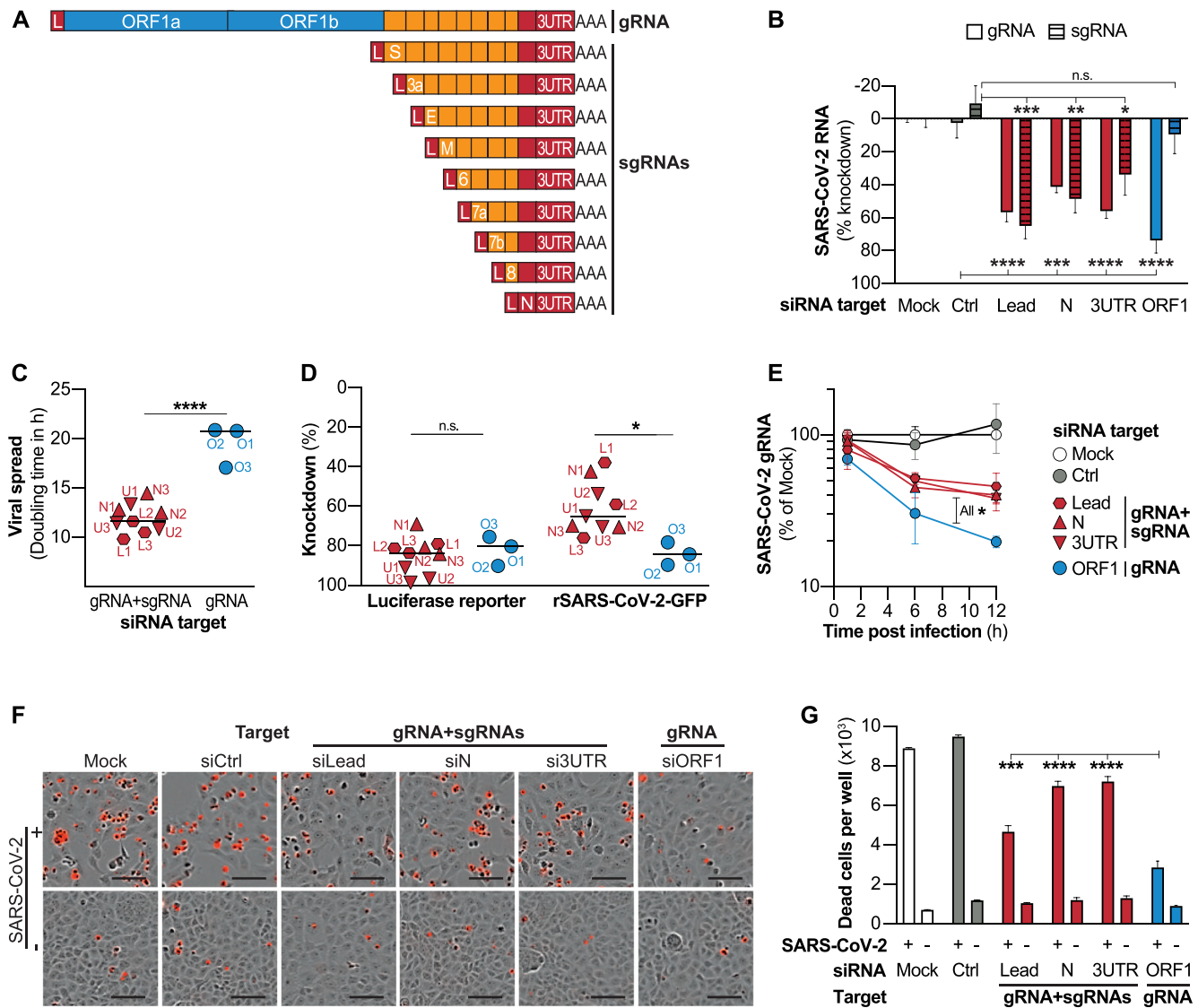


Figure 3. Targeting common regions of SARS-CoV-2 transcripts allows simultaneous suppression of gRNA and sgRNAs, but leads to impaired antiviral activity. (A) Schematic presentation of SARS-CoV-2 transcripts with sequences that are found in several transcripts shown in orange or red, and sequences that are exclusively part of viral gRNA shown in blue. (B) Effect of siRNAs targeting ORF1 which is only part of full-length SARS-CoV-2 gRNA or targeting sequences common within gRNA and sgRNAs. VeroE6 cells were infected with *wildtype* SARS-CoV-2 (MOI 0.1) and 3 h p.i. transfected with siRNA pools (containing three siRNAs each) specific for indicated genomic regions of SARS-CoV-2. At 24 h p.i., viral gRNA and sgRNAs were quantified by RT-qPCR. gRNA levels are shown relative to 18S rRNA and sgRNA relative to gRNA. (C) VeroE6 cells were infected with rSARS-CoV-2-GFP (MOI 1) and 3 h later transfected with individual siRNAs targeting indicated genomic regions of SARS-CoV-2. GFP⁺ cells were quantified every 4h (for full data see Supplementary Figure S3C) and virus spread quantified by fitting an exponential curve and calculating the doubling time. Dots represent median of three biological replicates each. Name of siRNA is given by red and blue labeling; L1–3; Leader-sequence specific siRNAs 1–3; N1–3, N-specific siRNAs 1–3; U, 3'UTR-specific siRNAs 1–3; O1–3, ORF1-specific siRNAs 1–3. (D) Comparison of siRNA efficacy against luciferase reporters or SARS-CoV-2 infection. To determine activity against luciferase reporters, each siRNA was transfected together with the respective luciferase reporter into HEK293T cells and luciferase activity measure after 48 h. To measure antiviral activity, experimental setup as described under (C) was used, and GFP⁺ cells quantified at final time point (68 h). Each dot represents median of three biological replicates. (E) VeroE6 cells were transfected with siRNA pools and infected with *wildtype* SARS-CoV-2 (MOI 0.1) after 6 h. Viral gRNA was quantified relative to 18srRNA at given time points using RT-qPCR (F, G). Effect of siRNA treatment on SARS-CoV-2 induced cytolysis. VeroE6 cells were transfected with siRNA pools and infected with *wildtype* SARS-CoV-2 (MOI 1) after 6 h. Virus-induced cell death was analysed using the Incucyte[®] Cytotox Red Dye at 56 h p.i. (F) Exemplary fluorescence microscope images showing dead cells in red. Bars in lower right of images represent 100 μ m. (G) Number of dead cells were quantified using the Incucyte S3 analyzing system. Bar in (C, D) shows median. (B, E, G) show mean \pm SEM. Statistical differences were calculated using (B, G) one-way Anova, or (E) repeated measures Anova with Dunette's multiple comparison correction and in (C, D) using Student's *t*-test for independent samples. All experiments were performed using three biological replicates. n.s., non-significant; * $P < 0.05$; ** $P < 0.01$; *** $P < 0.001$; **** $P < 0.0001$.

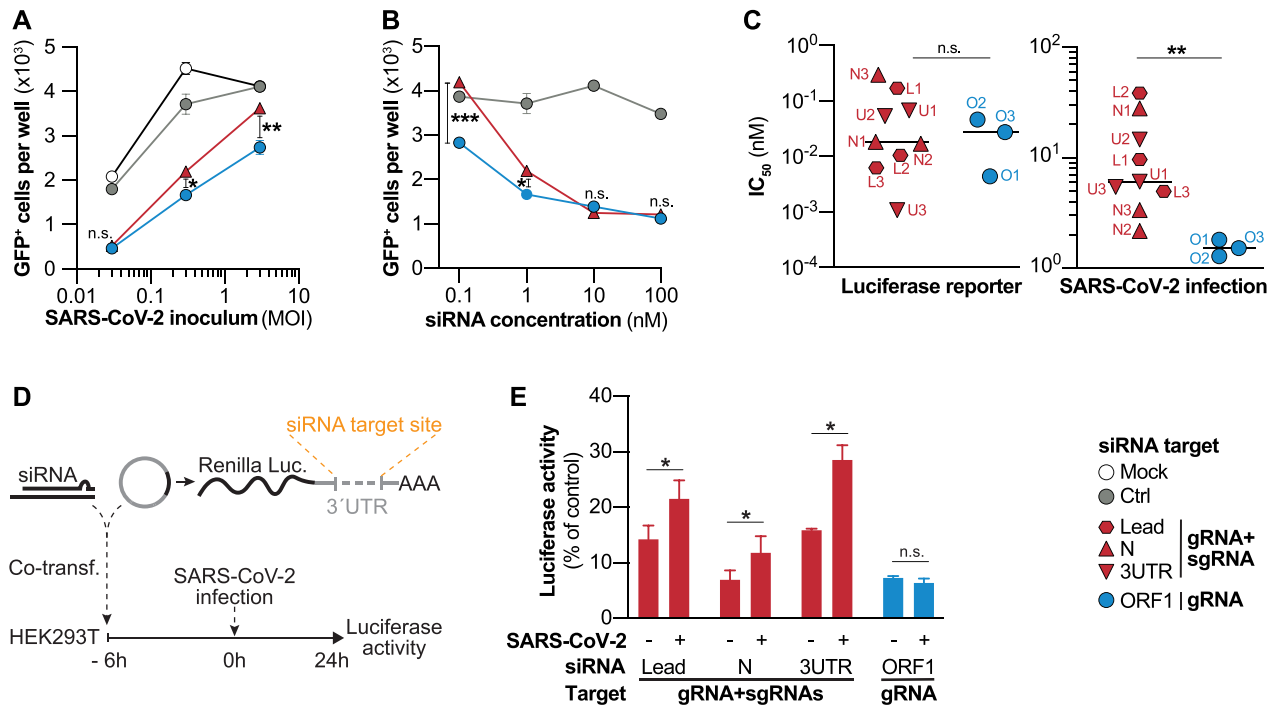


Figure 4. Subgenomic RNAs out-compete and impair antiviral activity of siRNAs. (A, B) VeroE6 cells were transfected with siRNAs targeting sgRNA and gRNA (N2) or exclusively gRNA (O2), infected 6h later with rSARS-CoV-2-GFP and the number of GFP⁺ cells was determined 24 h p.i. (A) siRNAs were transfected at a concentration of 1 nM, and cells were infected with MOIs of 0.03, 0.3 and 3. (B) siRNAs were transfected at varying concentrations ranging from 0.1 to 100 nM and VeroE6 were infected with a MOI of 0.3. (C) Comparison of mean inhibitory concentrations (IC₅₀) of siRNAs determined using luciferase reporters (left graph) or rSARS-CoV-2-GFP (right graph). Full data is shown in Supplementary Figures S4 and S5. For experimental details see Materials and Methods section. (D, E) Competition experiment to determine effect of SARS-CoV-2 replication on RNAi silencing efficacy. (D) HEK293T cells were co-transfected with siRNAs against different target region as well as luciferase reporters with incorporated binding sites for the co-transfected siRNA. After 6h, cells were infected with *wildtype* SARS-CoV-2 (MOI 0.1) and (E) luciferase activity determined from cell lysate 24 h p.i.. Statistical differences were calculated using Student's *t*-test for independent samples; n.s., non-significant, **P* < 0.05; ***P* < 0.01.

Subgenomic RNAs out-compete siRNAs that target the common regions of transcripts leading to a reduced antiviral efficacy

We hypothesized, that the reason for the decreased efficacy of siRNAs that targeted gRNA and sgRNAs could be that they were outnumbered by the highly abundant sgRNAs. In a first approximation, we asked how the level of viral replication would affect knockdown efficacy of siRNAs. We transfected a relatively low concentration (1 nM) of an siRNA that either targeted both, gRNA and sgRNA (N2) or exclusively gRNA (O2) into VeroE6 cells and infected cells with increasing amounts of rSARS-CoV-2-GFP. Interestingly, we found that both siRNAs reduced viral replication to the same extent when cells were infected with a relatively low amount of virus (MOI 0.03). With increasing viral inoculum, however, the sgRNA-targeting siRNA more prominently lost antiviral efficacy than the exclusively gRNA-targeting siRNA (Figure 4A). This was a first indication that out-competition of siRNAs by sgRNAs could indeed be responsible for the reduced antiviral efficacy of siRNAs that target the common regions of transcripts. To substantiate this finding, we asked if increasing siRNA dosages could compensate for this effect. Cells were thus transfected with increasing siRNA concentrations of the same siRNAs and infected with rSARS-CoV-2-GFP. In line with the previous experiment, both siRNAs inhibited viral

replication to similar extent when transfected at very high concentrations of 100 nM. With decreasing concentrations, likewise, the sgRNA-targeting siRNA showed a substantial loss of antiviral efficacy which was significantly less distinct for the siRNA that targeted only gRNA (Figure 4B). This added further evidence that competition with sgRNAs impaired antiviral efficacy of siRNAs that target the common regions of transcripts.

The above observations prompted us to acquire a more thorough picture of how SARS-CoV-2 replication impacts the antiviral efficacy of siRNAs at different concentrations. We thus determined the IC₅₀ for each siRNA using both, luciferase reporters (Supplementary Figure S4), as well as the SARS-CoV-2 infection model (Supplementary Figure S5). If indeed common region siRNAs would be out-competed by sgRNAs, we would expect higher IC₅₀ compared to siRNAs that solely target gRNA. This phenomenon, however, should only appear in the SARS-CoV-2 model as the luciferase reporters do not express sgRNAs. In general, IC₅₀ determined using luciferase reporters were considerably lower than those determined in the infection model, most likely as due to the co-transfection of siRNA and reporter plasmid, the majority of cells that expressed luciferase had also received an siRNA. However, this was probably not the case in the infection model, where SARS-CoV-2-infected and siRNA-transfected cells did not necessarily overlap to such a large extent. On the same lines of

Table 3. Conservation of siRNA target sites in circulating SARS-CoV-2 strains. Full-length, high-quality SARS-CoV-2 sequencing results were retrieved from the GISAID EpiCoV™ Database (www.gisaid.org) and analyzed for the presence of the siRNA target sites. To estimate conservation within all currently circulating strains ('Any variant'), the 100,000 latest submissions until October 26th 2021 were included without restricting to a specific variant. Lineages defined by WHO as Variants of Concern (VoC) or Variants of Interest (VoI) were separately downloaded and analyzed accordingly. For VoC, only the latest 20,000 submissions, and for VoI, all available sequences were considered. VoC and VoI are labeled according to WHO nomenclature, for details regarding the included lineages according to the Pango nomenclature system see materials & methods. n, number of analyzed full-length SARS-CoV-2 sequences

Variant	Any variant	Variants of concern				Variants of interest	
		Alpha	Beta	Gamma	Delta	Lambda	Mu
Sequences (n)	100 000	20 000	20 000	20 000	20 000	848	5889
siRNA		Conservation of target site (Only perfect matches in %)					
L1	94.92	95.10	91.15	96.65	93.43	98.23	92.96
L2	39.53	37.34	36.16	29.81	47.39	22.40	28.76
L3	24.11	23.32	26.06	17.43	15.95	16.98	13.04
O1	99.55	99.33	99.83	99.42	99.51	99.76	99.59
O2	99.65	99.46	99.45	99.66	99.33	99.88	99.54
O3	99.90	99.95	99.88	99.93	99.91	100	99.83
N1	99.54	99.60	99.71	99.71	99.55	99.64	99.88
N2	99.68	99.79	99.90	99.89	99.50	99.52	99.06
N3	99.50	99.69	99.77	98.70	99.67	99.29	99.52
U1	96.49	96.89	97.20	91.16	93.78	92.57	90.25
U2	86.64	84.74	86.05	59.20	82.78	89.62	81.28
U3	24.53	38.39	33.49	25.95	35.98	38.44	28.83

similar relative knockdown extents (Figure 3D, Supplementary Figure S3B), we also found comparable IC_{50} values for ORF1- or common region siRNAs when tested against luciferase reporters (left graph of Figure 4C). In the infection model, however, common region siRNAs presented significantly higher IC_{50} than ORF1-specific siRNAs (right graph of Figure 4C), as higher siRNA concentrations were necessary to suppress viral replication. In summary, our data show that SARS-CoV-2 replication negatively affected the efficacy of siRNAs which targeted sgRNAs, but not the ones which exclusively targeted gRNA.

To finally prove that the silencing capacity of common region siRNAs was indeed impaired by SARS-CoV-2 replication, we designed a competition experiment. We co-transfected siRNAs targeting the different SARS-CoV-2 regions together with their respective luciferase reporters. After 6h, we infected cells with *wildtype* SARS-CoV-2 and analyzed how SARS-CoV-2 replication would affect silencing of the luciferase reporter (Figure 4D). Of note, in this experimental setting, both SARS-CoV-2 RNAs and mRNA transcribed from a luciferase reporter plasmid can be targeted by the respective siRNAs. Indeed, we found that silencing of luciferase reporters by siRNAs which targeted the common region of transcripts was significantly impaired by SARS-CoV-2 replication. This was not observed for the ORF1-specific siRNA which suppressed the luciferase reporter with same efficacy in both, infected as well as non-infected cells (Figure 4E). We furthermore examined possible confounding factors, such as the siRNA design (Supplementary Table S3 and Figure S6A,B), or the secondary structure of the target region (Supplementary Figure S6C–E), none of which explained the better antiviral activities of siRNAs that targeted solely gRNA.

In summary, our data proves that an impaired RNAi silencing affects siRNAs that targeted sgRNAs leading to a reduced antiviral efficacy.

Ex vivo human lung model confirms the antiviral activity of an ORF1-targeting siRNA therapy

An important factor to consider especially while devising a siRNA-based therapy against RNA viruses is the conservation of the target sites, to enable a broad applicability and minimize the risk of resistance mutations occurring. When analyzing publicly available SARS-CoV-2 sequencing results, we found that the conservation of target sites of our siRNAs varied largely. Interestingly, ORF1-targeting siRNAs showed a significantly higher conservation than siRNAs against the common regions of transcripts (Supplementary Figure S7). The target sites of all three analyzed ORF1-specific siRNAs were conserved to at least 99.55% within all currently circulating strains and within >99.30% of each of the VoC and VoI. The best-performing siRNA, O3, even presented an overall conservation of 99.90% and at least 99.83% within all VoC and VoI (Table 3).

As non-modified siRNAs are prone to nuclease digestion, we tested chemically stabilized versions of our ORF1-targeting siRNAs using a modification pattern (46), that is also employed by the recently approved Lumasiran (47). While the silencing activity of O1 and O2 were negatively affected by the introduction of these chemical modifications, the modified version of O3 (O3*) presented even an enhanced activity against the luciferase reporter (Figure 5A). In combination with the finding that O3 targeted also the most conserved viral target of all analyzed siRNAs, it prompted us to select O3* for further experiments. In line with the expected increased stability, the modified version of O3 revealed an even stronger pronounced benefit at later time points (Figure 5B). Consequently, O3* also inhibited SARS-CoV-2 replication significantly stronger than the non-modified siRNA (Figure 5C).

To test the relevance of our findings, we aimed to validate O3* in a more realistic model of the human lung and opted for human precision cut lung slices (hPCLS). PCLS

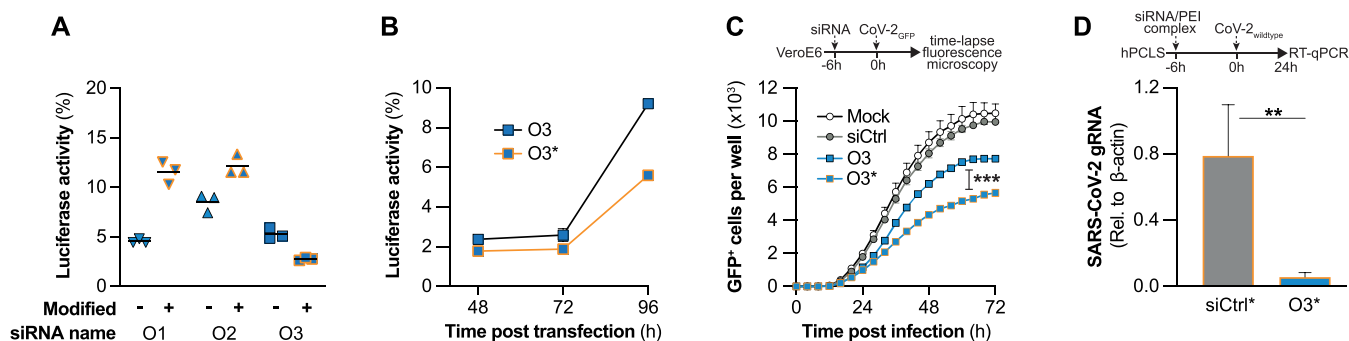


Figure 5. Chemically modified siRNA inhibits SARS-CoV-2 replication *ex vivo* in the human lung. (A) ORF1-targeting siRNAs were chemically modified using a clinically validated chemistry (for details, see Material and Methods and Supplementary Table S4) and the activity compared to chemically non-modified versions of the siRNAs using luciferase reporters. For this, siRNAs and luciferase reporter plasmids were co-transfected into HEK293T cells and after 24 h luciferase activities determined. Values were normalized to a control group transfected with the respective luciferase reporter and the control siRNA with identical chemistry. (B) Effect of chemical modifications on the duration of RNAi-silencing by siRNA O3 was compared using the same experimental setup as in (A), and luciferase activity was determined at indicated time points. (C) Antiviral activity of the modified and non-modified version of siRNA O3 were compared using the rSARS-CoV-2-GFP model. siRNAs were transfected into VeroE6 at a concentration of 50nM. 6h later, cells were infected with rSARS-CoV-2-GFP (MOI1), and GFP⁺ cells were quantified using the Incucyte S3 system. (D) To validate the approach in a highly relevant model of the human lung, the chemically modified siRNA O3 was complexed with polyethylenimine (PEI), and transfected into human precision cut lung slices (hPCLS; 100nM), which were infected with *wildtype* SARS-CoV-2 (MOI 1) 6h later. RNA was extracted from hPCLS harvested 24h p.i. and viral replication quantified by RT-qPCR for SARS-CoV-2 gRNA (normalized to β -actin expression). Experiments shown in (A–C) were performed using three biological replicates, (D) using five replicates. Horizontal bars in (A, D) indicate mean, error bars in (B–D) S.E.M. n.s., non-significant; ** $P < 0.01$; *** $P < 0.001$.

are a complex *ex vivo* 3D tissue culture model of primary human lung cells and thus constitute a highly physiological model to evaluate siRNA delivery to the human lung and to study human respiratory viruses (58). Also, we delivered our siRNAs using PEI this time, which has a well characterized toxicity profile allowing *in vivo* application (56) and can better be nebulized than liposomal formulations (59), an important characteristic for a lung-directed therapy. hPCLS were infected with wildtype SARS-CoV-2 6h after siRNA application, and effects on viral replication were assessed after 24 h by RT-qPCR. Indeed, also in this highly realistic model of the human lung, siRNA O3* significantly inhibited SARS-CoV-2 replication by 92.8% compared to the control siRNA-treated group (Figure 5D).

In summary, we show that factors which might prove crucial for clinical translation can be applied to ORF1-targeting siRNAs, including a high conservation of the target site, the stabilization via chemical modifications, as well as a formulation which supports application by inhalation. The resulting therapy strongly inhibited SARS-CoV-2 replication *ex vivo* in explants of the human lung, underlining the relevance of our findings.

DISCUSSION

A promising approach to develop antiviral therapies against SARS-CoV-2 constitute siRNAs, which is pursued by several academic and industry groups. First proof-of-concept studies presented that SARS-CoV-2 can be targeted with siRNAs. Until today, however, there is no in-depth investigation which coronaviral replication steps can be targeted with siRNAs, which is not even available for other positive sense RNA viruses. By systematically analyzing the individual replication steps following cell entry, we found that siRNAs, when given in a prophylactic setting, can target the genome of SARS-CoV-2 at an early replication step

and halt replication before start of transcription, preventing virus-induced cell death. To our surprise, targeting solely gRNA resulted in a stronger antiviral efficacy than a simultaneous targeting of gRNA and sgRNA. We show that the impaired RNAi silencing affecting siRNAs that target gRNA and sgRNAs results from an out-competition by the highly abundant sgRNAs. This notion appears especially plausible as Kim *et al.* showed that roughly 2/3rd of the transcriptome of infected cells are made up of SARS-CoV-2 RNAs of which almost all contain the targeted sequences (38).

Our findings on a first look might contradict a previous report which described that targeting the leader sequence of SARS-CoV-1 with siRNAs would be more efficacious than targeting the S ORF (12). Several factors could explain differences found in our study. First of all, SARS-CoV-1, which—while being the closest related virus—has an amino acid sequence homology of only between 40 and 94% depending on the ORF (60), thus findings might not be applicable to SARS-CoV-2. Also, Li *et al.* compared an siRNA targeting the Leader sequence to siRNAs targeting the S gene, which does not only exist in gRNA, but also in at least a fraction of sgRNAs. Third, Li *et al.* compared only a single Leader-specific siRNA to two S-specific siRNAs questioning if the finding can be generalized to the target region or if intra-individual differences of siRNA activity were responsible for the observed differences.

Along these lines, the question arises if differences between siRNA activities, in contrast to general differences between target regions, could also explain why ORF1-siRNAs were most efficient in our study. Given that ORF1 constitutes roughly 2/3rd of the viral genome, the bigger genomic space compared to the common regions might have allowed to select more efficient siRNAs. This explanation, however, appears unlikely as during the design and preselection of the siRNAs, we prioritized to acquire siRNAs

with similar activity for each target region over selecting the most efficient siRNAs. As a result, we chose siRNAs for which a similar efficacy was predicted and which additionally showed comparable knockdown of luciferase reporters. While ORF1-specific siRNAs suppressed luciferase reporters to a similar degree as the common region siRNAs, they were superior in inhibiting replicating virus. This proves that a virological factor, rather than more efficient siRNA sequences, was responsible for the better antiviral efficacy of ORF1-specific siRNAs. Nonetheless, activities of different siRNA sequences can differ strongly. Thus, we cannot exclude that an siRNA against any SARS-CoV-2 genomic region might prove highly efficacious in inhibiting viral replication. Also, as we did not investigate any other target region beside the leader sequence, ORF1, N, or the 3'UTR, we cannot exclude that targeting another genomic region of SARS-CoV-2 could prove to be superior to targeting ORF1.

Another factor which might influence the antiviral activity of siRNAs could be the accessibility of the viral RNA. On the one side, certain replication steps might occur within cellular compartments, which we believe is the most plausible explanation why negative sense RNA was not accessible for siRNA silencing. As negative sense RNAs do not encode for proteins, there is no need to export them to the cytosol. However, as probably no RISC complexes are present within the ROs, activity of siRNA is restricted to viral RNAs which have either not yet entered ROs (gRNA of incoming virus), or positive sense sgRNAs that are exported from ROs for translation. Another factor which can influence the accessibility of RNAs are secondary structures (61), which are especially important characteristics of viral RNAs. While we found no correlation of predicted secondary structures with the higher antiviral activity of ORF1-targeting siRNAs, further factors, such as the coverage of specific genomic regions by viral or host accessory proteins, could potentially also have an impact.

It furthermore needs to be mentioned, that our study did not employ *in vivo* experiments. While we used two different cell culture infection models with varying conditions such as time points of siRNA application, siRNAs dosages or viral inoculum sizes, we still cannot exclude, that factors play out crucial during *in vivo* application which could not be addressed in these models. Nonetheless, by verifying the antiviral activity of our lead siRNA in hPCLS, we validated our approach in a model system which in certain aspects can be considered as even more relevant for translational aspects than the available animal models. As hPCLS are explants of human lungs, they contain all cell types (including resident immune cells) and the physiologic structural architecture that is characteristic for the human lung. This comprises several factors with potential influence on efficacy of a siRNA therapy, such as the cell polarization, mucus production, or the innate immune system.

For clinical translation of siRNA-based therapies, several additional factors need to be considered. One issue is the possible occurrence of escape mutations that render the virus resistant to therapy. Here, it is assumed that a high conservation of the specific genomic region goes along with an essential function for the virus, limiting the likelihood of such mutations occurring. While during the design of

our siRNAs, we originally did not take the conservation of target sites into account, the targets of our ORF1-specific siRNAs were significantly more conserved than siRNAs that targeted sgRNAs, which is supported by the fact that ORF1 shows a relatively high conservation compared to other regions of the SARS-CoV-2 genome (62). The target site of our most efficient siRNA, O3, even showed a conservation of 99.9% in currently circulating SARS-CoV-2 strains. These findings strongly support the assumption that an ORF1-specific siRNA drug candidate with a broad applicability and a high resistance barrier could be developed.

Another important factor is the resistance of the siRNA to nucleases, which are found throughout different body compartments and can minimize siRNA activity especially *in vivo*. Using a clinically validated chemical modification pattern, we show that our most promising siRNA candidate O3 gained a higher and more durable RNAi activity by introducing these modifications, leading to an enhanced antiviral efficacy. Moreover, the chemically modified siRNA could successfully be complexed with PEI, which most likely constitutes a further protection from nucleases.

Clinical application of siRNA-based approaches furthermore crucially depends on siRNA delivery (63–66). Especially the identification of the optimal carrier and administration route is an important factor. While pulmonary delivery can be achieved by intranasal (i.n.) or inhalation administration, i.n. administration was chosen as the delivery route in Alnylam's early attempts of delivering siRNA against RSV (67). The big advantage of i.n. delivery is the possibility of administering a liquid formulation as nose drops without the need of nebulizing the formulation. This is particularly of impact for liposomal formulations as they do not withstand shear forces and temperature-related stress during nebulization (59). The biggest disadvantage of i.n. administration, however, is the low pulmonary bioavailability of the administered dose, while a large proportion is swallowed and degraded (68). Inhalation delivery, in contrast, requires aerosol development of a mist or dry powder. For nebulization of macromolecules such as siRNA, vibrating mesh nebulizers are preferred for decreased effects on biomolecule stability (64). Dry powder inhalation offers the advantages of long shelf-lives and enhanced stability of nucleic acid formulations against chemical, physical and microbial factors (65) but faces engineering challenges when nucleic acids nanoformulations need to be transferred into dry powders (69). Such nanoformulations are, however, particularly important for pulmonary delivery where free nucleic acids do not efficiently diffuse through the mucus barrier for subsequent uptake into the epithelium (70). Numerous siRNA nanoformulations exist based on polymers, lipids, peptides and inorganic materials (71), each of which can be improved in efficiency and specificity with different surface modifications such as targeting ligands or membrane-active substances (66). PEI polymer has widely been investigated as delivery system for siRNA (56). Thanks to its positive surface charge it can be used to complex negatively charged nucleic acids. PEI ensures high encapsulation efficiency of siRNA even at low N/P ratio, it protects the cargo against degradation by RNases and confers higher transfection efficiency in comparison to free siRNA (72). In

this study, siRNA O3*/PEI polyplexes confirmed the activity of the siRNA against SARS-CoV-2 in a relevant *ex vivo* model, the hPCLS, which closely mimic the anatomy of the respiratory tract.

To our knowledge, there is so far no equally detailed analysis of RNAi-targetable replication steps and RNA species for any positive sense RNA virus. Thus, our results might also be of relevance beyond SARS-CoV-2. The reduction of cytopathic effects achieved by antiviral siRNAs could be crucial, as endothelial injury has been proposed to trigger pathology in lethal COVID-19 cases (4). Along this line, early therapy starts, or possibly even prophylactic application of siRNAs appears as major benefit. Exclusive targeting of gRNA was advantageous over targeting sgRNAs additionally which could be a valuable information for designing siRNAs and treatment regimens in clinical studies. Taken together, our study confirms that siRNA-based strategies could allow to develop potent antivirals to reduce pathology of COVID-19, encouraging academia and industry to proceed with ongoing efforts.

DATA AVAILABILITY

All data supporting the findings of this study are available within the article and the supplementary information files. The SARS-CoV-2 reference sequence used as a template for siRNA design is available at the NCBI RefSeq database under the accession number: NC.045512.2. The sequence of the SARS-CoV-2 variant used for infection experiments with *wildtype* virus is available on the GISAID database (<https://www.gisaid.org/>) under the accession ID: EPI_ISL_582134.

SUPPLEMENTARY DATA

Supplementary Data are available at NAR Online.

ACKNOWLEDGEMENTS

We thank Prof. Dr Volker Thiel for providing the recombinant, GFP-expressing SARS-CoV-2 virus, Theresa Asen for help with cell culture and Prof. Dr Ulrike Protzer for general support such as providing the *wildtype* SARS-CoV-2 virus. We gratefully acknowledge the provision of human biomaterial and clinical data from the CPC-M bioArchive and its partners at the Asklepios Biobank Gauting, the Klinikum der Universität München and the Ludwig-Maximilians-Universität München.

FUNDING

Bavarian State Government by the Förderprogramm Corona-Forschung; Else Kroener-Research College 'Microbial triggers as cause of disease' (to T.M.); Volkswagen Foundation (to O.M.M., T.M., G.B.); D.B. and O.M.M. received support from an ERC starting grant [ERC-StG 637830]; A.P. from an ERC consolidator grant [ERC-CoG ProDAP, 817798]; German Research Foundation [PI1084/5, TRR178/TP11, TRR 237/A07]; German Federal Ministry of Education and Research (COVINET); S.A. received a stipend from the German Academic Exchange Service (DAAD).

Conflict of interest statement. T.M. is an ad hoc advisor for VIR Biotechnology and received research grants by Alnylam Pharmaceuticals and Gilead Sciences. M.F. is a consultant for Dr Hönle AG.

REFERENCES

- Wölfel, R., Corman, V.M., Guggemos, W., Seilmaier, M., Zange, S., Müller, M.A., Niemeyer, D., Jones, T.C., Vollmar, P., Rothe, C. *et al.* (2020) Virological assessment of hospitalized patients with COVID-2019. *Nature*, **581**, 465–469.
- Sungnak, W., Huang, N., Bécavin, C., Berg, M., Queen, R., Litvinukova, M., Talavera-López, C., Maatz, H., Reichart, D., Sampaziotis, F. *et al.* (2020) SARS-CoV-2 entry factors are highly expressed in nasal epithelial cells together with innate immune genes. *Nat. Med.*, **26**, 681–687.
- Chu, H., Chan, J.F.W., Yuen, T.T.T., Shuai, H., Yuan, S., Wang, Y., Hu, B., Yip, C.C.Y., Tsang, J.O.L., Huang, X. *et al.* (2020) Comparative tropism, replication kinetics, and cell damage profiling of SARS-CoV-2 and SARS-CoV with implications for clinical manifestations, transmissibility, and laboratory studies of COVID-19: an observational study. *Lancet Microbe*, **1**, e14–e23.
- Ackermann, M., Verleden, S.E., Kuehnel, M., Haverich, A., Welte, T., Laenger, F., Vanstapel, A., Werlein, C., Stark, H., Tzankov, A. *et al.* (2020) Pulmonary vascular endothelialitis, thrombosis, and angiogenesis in Covid-19. *N. Engl. J. Med.*, **383**, 120–128.
- Guan, W.J., Ni, Z.Y., Hu, Y., Liang, W.H., Ou, C.Q., He, J.X., Liu, L., Shan, H., Lei, C.L., Hui, D.S.C. *et al.* (2020) Clinical characteristics of coronavirus disease 2019 in China. *N. Engl. J. Med.*, **382**, 1708–1720.
- Beigel, J.H., Tomashek, K.M., Dodd, L.E., Mehta, A.K., Zingman, B.S., Kalil, A.C., Hohmann, E., Chu, H.Y., Luetkemeyer, A., Kline, S. *et al.* (2020) Remdesivir for the treatment of Covid-19 - final report. *N. Engl. J. Med.*, **383**, 1813–1826.
- Taylor, P.C., Adams, A.C., Hufford, M.M., de la Torre, I., Winthrop, K. and Gottlieb, R.L. (2021) Neutralizing monoclonal antibodies for treatment of COVID-19. *Nat. Rev. Immunol.*, **21**, 382–393.
- Horby, P., Lim, W.S., Emberson, J., Mafham, M., Bell, J., Linsell, L., Staplin, N., Brightling, C., Ustianowski, A., Elmahi, E. *et al.* (2020) Effect of dexamethasone in hospitalized patients with COVID-19: preliminary report. medRxiv doi: <https://doi.org/10.1101/2020.06.22.20137273>, 22 June 2020, preprint: not peer reviewed.
- WHO_Solidarity_trial_consortium, Pan, H., Peto, R., Karim, Q.A., Alejandria, M., Restrepo, A.M.H., Garcia, C.H., Kieny, M.P., Malekzadeh, R., Murthy, S. *et al.* (2020) Repurposed antiviral drugs for COVID-19; interim WHO SOLIDARITY trial results.
- Zhou, Y.W., Xie, Y., Tang, L.S., Pu, D., Zhu, Y.J., Liu, J.Y. and Ma, X.L. (2021) Therapeutic targets and interventional strategies in COVID-19: mechanisms and clinical studies. *Signal Transduct. Target Ther.*, **6**, 317.
- Chow, M.Y.T., Qiu, Y. and Lam, J.K.W. (2020) Inhaled RNA therapy: from promise to reality. *Trends Pharmacol. Sci.*, **41**, 715–729.
- Li, T., Zhang, Y., Fu, L., Yu, C., Li, X., Li, Y., Zhang, X., Rong, Z., Wang, Y., Ning, H. *et al.* (2005) siRNA targeting the leader sequence of SARS-CoV inhibits virus replication. *Gene Ther.*, **12**, 751–761.
- Shi, Y., Yang, D.H., Xiong, J., Jia, J., Huang, B. and Jin, Y.X. (2005) Inhibition of genes expression of SARS coronavirus by synthetic small interfering RNAs. *Cell Res.*, **15**, 193–200.
- Nur, S.M., Hasan, M.A., Amin, M.A., Hossain, M. and Sharmin, T. (2015) Design of potential RNAi (miRNA and siRNA) molecules for Middle East respiratory syndrome coronavirus (MERS-CoV) gene silencing by computational method. *Interdiscip. Sci.*, **7**, 257–265.
- Tang, Q., Li, B., Woodle, M. and Lu, P.Y. (2008) Application of siRNA against SARS in the rhesus macaque model. *Methods Mol. Biol.*, **442**, 139–158.
- Berber, B., Aydin, C., Kocabas, F., Guney-Esken, G., Yilancioglu, K., Karadag-Alpaslan, M., Caliseki, M., Yuce, M., Demir, S. and Tastan, C. (2021) Gene editing and RNAi approaches for COVID-19 diagnostics and therapeutics. *Gene Ther.*, **28**, 290–305.
- Uludag, H., Parent, K., Aliabadi, H.M. and Haddadi, A. (2020) Prospects for RNAi Therapy of COVID-19. *Front. Bioeng. Biotechnol.*, **8**, 916.

18. Naqvi, R.A., Shukla, D. and Naqvi, A.R. (2021) SARS-CoV-2 targeting by RNAi and host complement inhibition: a two-pronged subterfuge for COVID-19 treatment. *Immun. Inflamm. Dis.*, **10**, 22–24.
19. Talukder, P. and Chanda, S. (2021) RNAi technology and investigation on possible vaccines to combat SARS-CoV-2 infection. *Appl. Biochem. Biotechnol.*, **193**, 1744–1756.
20. Pashkov, E.A., Korchevaya, E.R., Faizuloev, E.B., Svitich, O.A., Pashkov, E.P., Nechaev, D.N. and Zverev, V.V. (2021) Potential of application of the RNA interference phenomenon in the treatment of new coronavirus infection COVID-19. *Vopr. Virusol.*, **66**, 241–251.
21. Mehta, A., Michler, T. and Merkel, O.M. (2021) siRNA Therapeutics against Respiratory Viral Infections—What Have We Learned for Potential COVID-19 Therapies? *Adv. Healthc. Mater.*, **10**, e2001650.
22. Baldassarre, A., Paolini, A., Bruno, S.P., Felli, C., Tozzi, A.E. and Masotti, A. (2020) Potential use of noncoding RNAs and innovative therapeutic strategies to target the 5'UTR of SARS-CoV-2. *Epigenomics*, **12**, 1349–1361.
23. Rohani, N., Ahmadi Moughari, F. and Eslahchi, C. (2021) DisCoVering potential candidates of RNAi-based therapy for COVID-19 using computational methods. *PeerJ*, **9**, e10505.
24. Shawan, M., Sharma, A.R., Bhattacharya, M., Mallik, B., Akhter, F., Shakil, M.S., Hossain, M.M., Banik, S., Lee, S.S., Hasan, M.A. *et al.* (2021) Designing an effective therapeutic siRNA to silence RdRp gene of SARS-CoV-2. *Infect. Genet. Evol.*, **93**, 104951.
25. Chowdhury, U.F., Sharif Shohan, M.U., Hoque, K.I., Beg, M.A., Sharif Siam, M.K. and Moni, M.A. (2021) A computational approach to design potential siRNA molecules as a prospective tool for silencing nucleocapsid phosphoprotein and surface glycoprotein gene of SARS-CoV-2. *Genomics*, **113**, 331–343.
26. Pandey, A.K. and Verma, S. (2021) An in silico analysis of effective siRNAs against COVID-19 by targeting the leader sequence of SARS-CoV-2. *Adv. Cell Gene Ther.*, **4**, e107.
27. Hasan, M., Ashik, A.I., Chowdhury, M.B., Tasnim, A.T., Nishat, Z.S., Hossain, T. and Ahmed, S. (2021) Computational prediction of potential siRNA and human miRNA sequences to silence orf1ab associated genes for future therapeutics against SARS-CoV-2. *Inform. Med. Unlocked*, **24**, 100569.
28. Medeiros, I.G., Khayat, A.S., Stransky, B., Santos, S., Assumpcao, P. and de Souza, J.E.S. (2021) A small interfering RNA (siRNA) database for SARS-CoV-2. *Sci. Rep.*, **11**, 8849.
29. Ahn, S.H., Gu, D., Koh, Y., Lee, H.S. and Chi, S.W. (2021) AGO CLIP-based imputation of potent siRNA sequences targeting SARS-CoV-2 with antifibrotic miRNA-like activity. *Sci. Rep.*, **11**, 19161.
30. Wu, R. and Luo, K.Q. (2021) Developing effective siRNAs to reduce the expression of key viral genes of COVID-19. *Int. J. Biol. Sci.*, **17**, 1521–1529.
31. Idris, A., Davis, A., Supramaniam, A., Acharya, D., Kelly, G., Tayyar, Y., West, N., Zhang, P., McMillan, C.L.D., Soemardy, C. *et al.* (2021) A SARS-CoV-2 targeted siRNA-nanoparticle therapy for COVID-19. *Mol. Ther.*, **29**, 2219–2226.
32. Khaitov, M., Nikonova, A., Shilovskiy, I., Kozhikhova, K., Kofiadi, I., Vishnyakova, L., Nikolskii, A., Gattinger, P., Kovchina, V., Barvinskaia, E. *et al.* (2021) Silencing of SARS-CoV-2 with modified siRNA-peptide dendrimer formulation. *Allergy*.
33. Hoffmann, M., Kleine-Weber, H., Schroeder, S., Krüger, N., Herrler, T., Erichsen, S., Schiergens, T.S., Herrler, G., Wu, N.H., Nitsche, A. *et al.* (2020) SARS-CoV-2 cell entry depends on ACE2 and TMPRSS2 and is blocked by a clinically proven protease inhibitor. *Cell*, **181**, 271–280.
34. Burkard, C., Verheije, M.H., Wicht, O., van Kasteren, S.I., van Kuppeveld, F.J., Haagmans, B.L., Pelkmans, L., Rottier, P.J., Bosch, B.J. and de Haan, C.A. (2014) Coronavirus cell entry occurs through the endo-/lysosomal pathway in a proteolysis-dependent manner. *PLoS Pathog.*, **10**, e1004502.
35. Shang, J., Wan, Y., Luo, C., Ye, G., Geng, Q., Auerbach, A. and Li, F. (2020) Cell entry mechanisms of SARS-CoV-2. *Proc. Natl. Acad. Sci. U.S.A.*, **117**, 11727–11734.
36. Fehr, A.R. and Perlman, S. (2015) Coronaviruses: an overview of their replication and pathogenesis. *Methods Mol. Biol.*, **1282**, 1–23.
37. Snijder, E.J., Limpens, R.W.A.L., de Wilde, A.H., de Jong, A.W.M., Zevenhoven-Dobbe, J.C., Maier, H.J., Faas, F.F.G.A., Koster, A.J. and Bárcena, M. (2020) A unifying structural and functional model of the coronavirus replication organelle: tracking down RNA synthesis. *PLoS Biol.*, **18**, e3000715.
38. Kim, D., Lee, J.Y., Yang, J.S., Kim, J.W., Kim, V.N. and Chang, H. (2020) The architecture of SARS-CoV-2 transcriptome. *Cell*, **181**, 914–921.
39. Sola, I., Almazan, F., Zuniga, S. and Enjuanes, L. (2015) Continuous and discontinuous RNA synthesis in coronaviruses. *Annu. Rev. Virol.*, **2**, 265–288.
40. Enjuanes, L., Almazan, F., Sola, I. and Zuniga, S. (2006) Biochemical aspects of coronavirus replication and virus-host interaction. *Annu. Rev. Microbiol.*, **60**, 211–230.
41. van Hemert, M.J., van den Worm, S.H., Knoops, K., Mommaas, A.M., Gorbalenya, A.E. and Snijder, E.J. (2008) SARS-coronavirus replication/transcription complexes are membrane-protected and need a host factor for activity in vitro. *PLoS Pathog.*, **4**, e1000054.
42. Chang, C.K., Hou, M.H., Chang, C.F., Hsiao, C.D. and Huang, T.H. (2014) The SARS coronavirus nucleocapsid protein—forms and functions. *Antiviral Res.*, **103**, 39–50.
43. Boudreau, R.L., Spengler, R.M., Hylock, R.H., Kusenda, B.J., Davis, H.A., Eichmann, D.A. and Davidson, B.L. (2013) siSPOTR: a tool for designing highly specific and potent siRNAs for human and mouse. *Nucleic Acids Res.*, **41**, e9.
44. Pan, W.J., Chen, C.W. and Chu, Y.W. (2011) siPRED: predicting siRNA efficacy using various characteristic methods. *PLoS One*, **6**, e27602.
45. Holen, T., Moe, S.E., Sørbø, J.G., Meza, T.J., Ottersen, O.P. and Klungland, A. (2005) Tolerated wobble mutations in siRNAs decrease specificity, but can enhance activity in vivo. *Nucleic Acids Res.*, **33**, 4704–4710.
46. Foster, D.J., Brown, C.R., Shaikh, S., Trapp, C., Schlegel, M.K., Qian, K., Sehgal, A., Rajeev, K.G., Jadhav, V., Manoharan, M. *et al.* (2018) Advanced siRNA designs further improve in vivo performance of GalNAc-siRNA conjugates. *Mol. Ther.*, **26**, 708–717.
47. Crasto, A.M. (2020) In: *2020 Approvals: Lumasiran*. newdrugsapprovals.org, Vol. **2021**.
48. Elbe, S. and Buckland-Merrett, G. (2017) Data, disease and diplomacy: GISAIID's innovative contribution to global health. *Glob. Chall.*, **1**, 33–46.
49. Andrews, R.J., O'Leary, C.A., Tompkins, V.S., Peterson, J.M., Haniff, H.S., Williams, C., Disney, M.D. and Moss, W.N. (2021) A map of the SARS-CoV-2 RNA structure. *NAR Genom. Bioinform.*, **3**, lqab043.
50. Andrews, R.J., Roche, J. and Moss, W.N. (2018) ScanFold: an approach for genome-wide discovery of local RNA structural elements—applications to Zika virus and HIV. *PeerJ*, **6**, e6136.
51. Westerhout, E.M. and Berkhout, B. (2007) A systematic analysis of the effect of target RNA structure on RNA interference. *Nucleic Acids Res.*, **35**, 4322–4330.
52. Clote, P., Ferre, F., Kranakis, E. and Krizanc, D. (2005) Structural RNA has lower folding energy than random RNA of the same dinucleotide frequency. *RNA*, **11**, 578–591.
53. Chan, C.Y., Carmack, C.S., Long, D.D., Maliyakkal, A., Shao, Y., Roninson, I.B. and Ding, Y. (2009) A structural interpretation of the effect of GC-content on efficiency of RNA interference. *BMC Bioinformatics*, **10**, S33.
54. Gerckens, M., Alsafadi, H.N., Wagner, D.E., Lindner, M., Burgstaller, G. and Königshoff, M. (2019) Generation of Human 3D Lung Tissue Cultures (3D-LTCs) for Disease Modeling. *J. Vis. Exp.*, <https://doi.org/10.3791/58437>.
55. Alsafadi, H.N., Staab-Weijnitz, C.A., Lehmann, M., Lindner, M., Peschel, B., Königshoff, M. and Wagner, D.E. (2017) An ex vivo model to induce early fibrosis-like changes in human precision-cut lung slices. *Am. J. Physiol. Lung Cell Mol. Physiol.*, **312**, L896–L902.
56. Merkel, O.M., Beyerle, A., Librizzi, D., Pfestroff, A., Behr, T.M., Sproat, B., Barth, P.J. and Kissel, T. (2009) Nonviral siRNA delivery to the lung: investigation of PEG-PEI polyplexes and their in vivo performance. *Mol. Pharm.*, **6**, 1246–1260.
57. Hagemeyer, M.C., Vonk, A.M., Monastyrska, I., Rottier, P.J. and de Haan, C.A. (2012) Visualizing coronavirus RNA synthesis in time by using click chemistry. *J. Virol.*, **86**, 5808–5816.
58. Liu, G., Betts, C., Cunoosamy, D.M., Aberg, P.M., Hornberg, J.J., Sivars, K.B. and Cohen, T.S. (2019) Use of precision cut lung slices as a translational model for the study of lung biology. *Respir. Res.*, **20**, 162.
59. Weber, S., Zimmer, A. and Pardeike, J. (2014) Solid Lipid Nanoparticles (SLN) and Nanostructured Lipid Carriers (NLC) for

- pulmonary application: a review of the state of the art. *Eur. J. Pharm. Biopharm.*, **86**, 7–22.
60. Grifoni, A., Sidney, J., Zhang, Y., Scheuermann, R.H., Peters, B. and Sette, A. (2020) A Sequence Homology and Bioinformatic Approach Can Predict Candidate Targets for Immune Responses to SARS-CoV-2. *Cell Host Microbe*, **27**, 671–680.
 61. Shao, Y., Chan, C.Y., Maliyekkel, A., Lawrence, C.E., Roninson, I.B. and Ding, Y. (2007) Effect of target secondary structure on RNAi efficiency. *RNA*, **13**, 1631–1640.
 62. Abbott, T.R., Dhamdhere, G., Liu, Y., Lin, X., Goudy, L., Zeng, L., Chemparathy, A., Chmura, S., Heaton, N.S., Debs, R. *et al.* (2020) Development of CRISPR as an antiviral strategy to combat SARS-CoV-2 and influenza. *Cell*, **181**, 865–876.
 63. Weber, S., Zimmer, A. and Pardeike, J. (2014) Solid lipid nanoparticles (SLN) and nanostructured lipid carriers (NLC) for pulmonary application: a review of the state of the art. *Eur. J. Pharm. Biopharm.*, **86**, 7–22.
 64. de Kruijff, W. and Ehrhardt, C. (2017) Inhalation delivery of complex drugs—the next steps. *Curr. Opin. Pharmacol.*, **36**, 52–57.
 65. Feldmann, D.P. and Merkel, O.M. (2015) The advantages of pulmonary delivery of therapeutic siRNA. *Ther. Deliv.*, **6**, 407–409.
 66. Kandil, R. and Merkel, M. (2016) Therapeutic delivery of RNA effectors: diseases affecting the respiratory system. *Pharmazie*, **71**, 21–26.
 67. DeVincenzo, J., Lambkin-Williams, R., Wilkinson, T., Cehelsky, J., Nochur, S., Walsh, E., Meyers, R., Gollob, J. and Vaishnav, A. (2010) A randomized, double-blind, placebo-controlled study of an RNAi-based therapy directed against respiratory syncytial virus. *Proc. Natl. Acad. Sci. U.S.A.*, **107**, 8800–8805.
 68. Merkel, O.M. and Kissel, T. (2012) Nonviral pulmonary delivery of siRNA. *Acc. Chem. Res.*, **45**, 961–970.
 69. Keil, T.W.M., Feldmann, D.P., Costabile, G., Zhong, Q., da Rocha, S. and Merkel, O.M. (2019) Characterization of spray dried powders with nucleic acid-containing PEI nanoparticles. *Eur. J. Pharm. Biopharm.*, **143**, 61–69.
 70. Sanders, N., Rudolph, C., Braeckmans, K., De Smedt, S.C. and Demeester, J. (2009) Extracellular barriers in respiratory gene therapy. *Adv. Drug. Deliv. Rev.*, **61**, 115–127.
 71. Merkel, O.M., Rubinstein, I. and Kissel, T. (2014) siRNA delivery to the lung: what's new? *Adv. Drug Deliv. Rev.*, **75**, 112–128.
 72. Merkel, O.M. and Kissel, T. (2012) Nonviral pulmonary delivery of siRNA. *Acc. Chem. Res.*, **45**, 961–970.